Mainz, den 27. April 2018

Antje Richter
geboren in Karl-Marx-Stadt

On-Surface Reactions of Alkyne Molecules on Calcite (10.4)

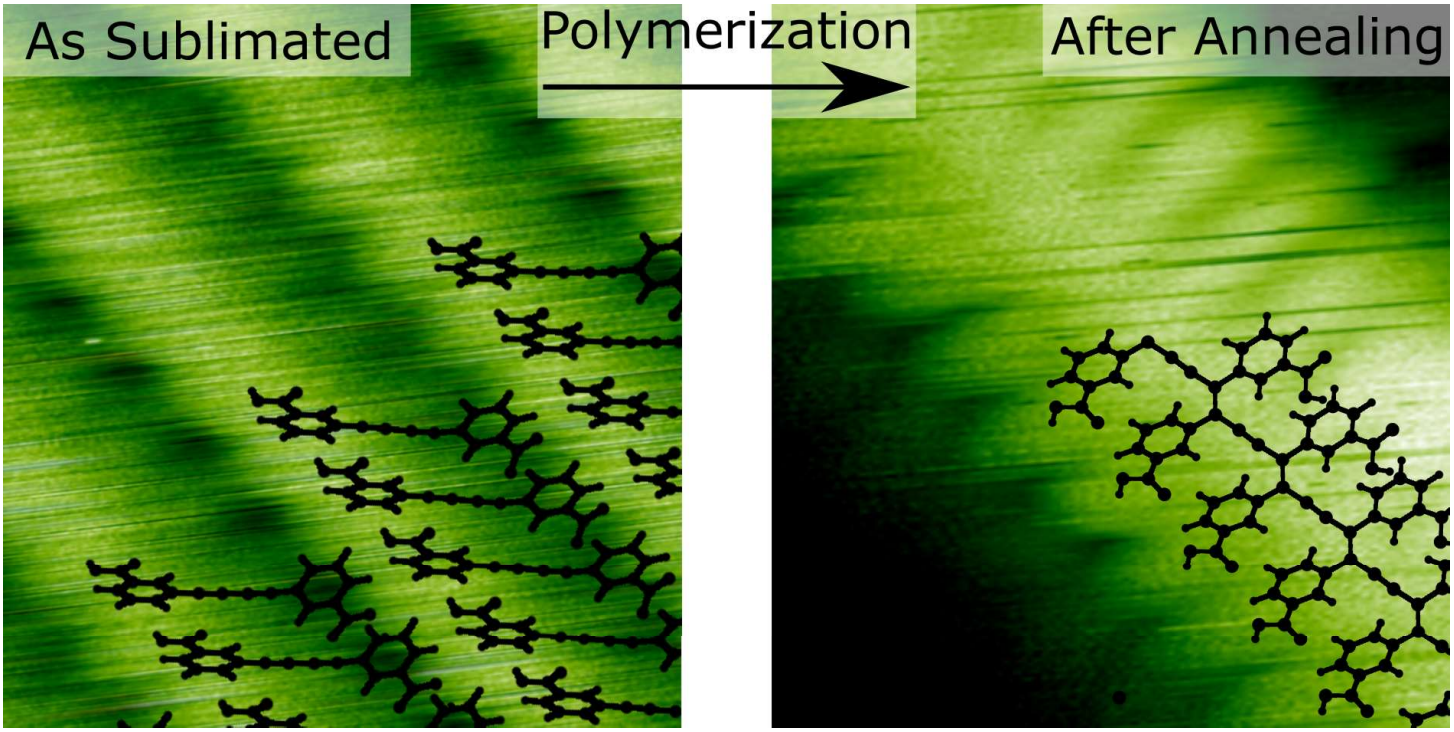

Dissertation zur Erlangung des Grades
„Doktor der Naturwissenschaften"
im Promotionsfach Chemie am Fachbereich
Chemie, Pharmazie und Geowissenschaften der
Johannes Gutenberg-Universität in Mainz

This thesis was supervised by [redacted] and was carried out at the Johannes Gutenberg University Mainz from January 2015 to June 2018.

D77 (Dissertation Johannes Gutenberg-Universität Mainz)

Dean of the Faculty	[redacted]
1st report	[redacted] Universität Bielefeld
2nd report	[redacted] Max-Planck-Institut für Polymerforschung
Submitted:	27th April 2018
Oral examination:	4th June 2018

Contents

1 Introduction

On-Surface Synthesis of Alkyne Molecules... ... towards π-conjugated Structures on Calcite (10.4)

The continuous miniaturization of electronic devices by state-of-the-art fabrication methods will reach its fundamental limits sometime in the near future. Therefore, new concepts beyond silicon-based semiconductor technology have been developed in the recent decades. One promising route is the so-called bottom-up approach. This concept starts with small single building blocks and arrives at the desired highly ordered structures *via* their combination directly on a surface.[1]

For the purpose of fabrication of electronic nanoscale devices, suitable building block units have to be identified. A promising approach is the so-called molecular electronics, which suggests single molecules or molecular groups as substitute for electronic components.[2] Theoretical and experimental studies give evidence that molecules can indeed be used as *e.g.* rectifiers,[3] transistors[4] or switches.[5–7] Nevertheless, for the creation of electronic circuits, conductive wire-like molecular arrangements are necessary to connect these functional units.

To create well-defined aggregates in a fast and serial manner at the molecular level, self-assembly has proven to be a promising approach.[8, 9] This process is based on noncovalent bonds, *e.g.* $\pi - \pi$ stacking, hydrogen bonds and van der Waals interaction. It takes place spontaneously and leads to the formation of molecular equilibrium structures.[10] Furthermore, it can be tuned by the choice of the substrate and the structure of the molecular precursors. Nevertheless, since self-assembly relies on reversible interactions, the obtained structures are somewhat fragile.

To stabilize molecular structures, on-surface synthesis has been proven to be a highly versatile tool.[11] The stabilization is obtained by the formation of covalent bonds directly on an appropriate substrate surface. In many cases, the traditional organic synthesis inspired the field of on-surface synthesis. However, the transfer to a two-dimensional surface is not trivial. Nevertheless, an enormous number of different reactions has been transferred successfully from solution synthesis to diverse substrates.[12–14]

In the view of molecular electronics, the on-surface created molecular structures need to be conductive. Therefore, conjugated molecular structures have been suggested as promising candidates. Additional, it is mandatory to decouple the formed molecular devices from the support surface. However, the majority of the present studies concerning the creation of molecular nanoscale devices, focus on conducting and semiconducting surfaces. Therefore, it is highly interesting to explore on-surface-reactions on insulating surfaces.

Therefore, the aim of this thesis is to create wire-like conjugated molecular structures on a bulk insulator surface. To reach this goal, molecular precursors equipped with terminal alkyne and diyne functionalities were chosen. These functional entities are known to form conjugated structures upon diacetylene polymerization, acetylene polymerizations, linear homocoupling and enyne formation. To provide the decoupling of the molecular structures, the bulk insulator calcite was chosen, which is the thermodynamically most stable polymorph of calcium carbonate ($CaCO_3$).

In particular, this thesis provides a detailed study of the self-assembly and on-surface reactions of three terminal alkyne and one diyne species on the (10.4) calcite surface. The experiments were performed in ultra-high vacuum (UHV) using frequency-modulated atomic force microscopy (FM-AFM). This technique has been proven to be a versatile tool for real space imaging of molecular arrangements with atomic precision.
For all investigated molecules, first the structure formation of the as deposited monomer precursors was characterized at the nanoscopic scale. Secondly, the initiation of the reaction was performed upon thermal, photochemical and sometimes even combined stimulation experiments. For two molecular precursors, density functional theory (DFT) calculation were done. The optimizations provide insights into the molecular arrangement after deposition and the structure formation of the precursors after reaction initiation. Additional, detailed parameter variations of *e.g.*, time, wavelengths and temperature were performed to investigate the influence of these parameters on the structure formation. The results present insights into the complex interplay of chosen reaction parameters, structure of the molecular precursors and substrate surface, necessary for successful on-surface synthesis. Finally, this thesis provides, for the first time, evidence for a successful diacetylene polymerization, an acetylene polymerization and a homocoupling reaction on a bulk insulator surface. For the two first named reactions, molecular wire-like structures were obtained, which are interesting as molecular wires for future molecular electronics.

Thesis Structure

In this thesis, the self-assembly and on-surface synthesis of four different precursor molecules were investigated on the calcite (10.4) cleavage plane. The experiments were performed in ultra-high vacuum (UHV) using frequency-modulation atomic force microscopy (FM-AFM). In chapter 2, the theoretical foundations of FM-AFM will be briefly outlined. Subsequently, the used substrate calcite will be introduced in chapter 3. In chapter 4, a short introduction is given to the actual status of on-surface synthesis on metals, semiconductors and insulators, while chapter 5 provides a description of the used experimental set-up.

In chapters 6 and 7, the results of my thesis will be presented.
First, the experiments on the 3,3′-(1,3-butadiyne-1,4-diyl)bisbenzoic acid (3-BBA) monomer will be discussed in chapter 6. The molecule is equipped with a diyne moiety, allowing for an on-surface diacetylene polymerization. A detailed analysis of the self-assembly is given. Furthermore, thermal, photochemical and combined initiation experiments were performed to induce a reaction. Additional, performed DFT calculations provide insights into the arrangement of the molecules before and after reaction stimulation. The experimental data together with the DFT calculations provide strong evidence for a successful initiation of a diacetylene polymerization on calcite (10.4).

In chapter 7, three molecules equipped with terminal alkyne groups will be presented, namely 3-ethynylbenzoic acid (3-EBA), 4-ethynylbenzoic acid (4-EBA) and 4,4″-diethynyl-[1,1′:4′,1″-terphenyl]-2′,5′-dicarboxylic acid (DETDCA).
First, the self-assembly, as well as photochemical and thermal initiation experiments of 3-EBA will be presented. The formation of well-ordered striped structures on the calcite (10.4) substrate after annealing will be discussed in detail. In combination with DFT calculations evidence is given for a successful acetylene polymerization on a bulk insulator surface.
Next, the formation of well-ordered elongated molecular islands of 4-EBA on the calcite (10.4) is presented. A detailed analysis of the stripe-to-stripe distance distribution discloses the interplay between short-range attraction and long-range repulsion. Further, the results of thermal and photochemical initiation will be presented.
The analysis of the self-assembly is presented. Finally, the observed changes upon thermal and photochemical initiation of DETDCA will be discussed. The results indicate that DETDCA undergoes a dimerization by homocoupling of the terminal alkyne moiety on the (10.4) surface of the bulk insulator calcite.

2 Atomic Force Microscopy (AFM)

2.1 Introduction

The dawn of the scanning probe microscopy (SPM) can be dated to the year 1981, when Gerd Binnig and Heinrich Rohrer succeeded in conducting the first real surface study using scanning tunneling microscopy (STM).[15] For this development, they were awarded the Nobel Prize in 1986.[16] The measuring principle of this method is based on the exponential distance dependence of the tunneling current between a conductive tip and a conductive surface. The disadvantage of this method, however, is that only conductive samples can be examined. Therefore, further efforts have been made to overcome this limitation. Already in 1986 G. Binnig, C. Quate and C. Gerber were able to solve this issue *via* the invention of the atomic force microscope (AFM), which allows for investigations of arbitrary surfaces, including non-conducting materials, since the distance dependency of the tip-sample force is used to record the surface properties.[17] Despite the efforts of the next years, it was not until 1995 before the first true atomic resolution could be achieved.[18] Two changes were essentially contributing this: first, the use of better sensors and second, the development of the dynamic mode by Albrecht in 1991.[19] The subsequent improvements of the dynamic AFM with its associated enhanced resolution has recently enabled investigations in molecular electronics,[13, 20, 21] elucidation of bonds[22–24] and improvements in the filed of on-surface synthesis as the here presented investigations on the bulk insulator calcite.[25, 26]

Besides AFM and STM also other methods belong to SPM, like *e.g.* magnetic force microscopy (MFM), Kelvin probe force microscopy (KPFM) and near-field scanning optical microscopy (NSOM), etc. Common to all these methods is that a tip is positioned close to (or sometimes even at) the surface of interest and scanned in a line-by-line fashion, as illustrated by the arrows on the "sample" in Fig. 2.1. In many AFMs, this tip, which is ideally atomically sharp, is positioned on the free end of the so-called cantilever. Depending on the forces acting on the tip, the cantilever gets deflected (Fig. 2.1). These forces can be both attractive and/or repulsive with short- as well as long-range distance dependencies. Furthermore, they are usually subdivided into the following main contributions, the van-der-Waals forces, electrostatic forces (Coulomb forces) and chemical forces containing chemical bonding (exchange interactions) and the Pauli repulsion. In a very popular method, the resulting deflection of the cantilever is detected *via* a laser beam, which is positioned

on the backside of the tip and is reflected to a four-quadrant photo-diode also named position-sensitive detector (PSD) (Fig. 2.1).[27] The signal is then forwarded to the data processing components for detection and analysis. Depending on the scanning mode, the electronic pass an signal to the scanner, typically consisting of a piezo tube (Fig. 2.1), which converts the received signal into a movement even down to a sub-nanometer range.[17] Finally, a defined area of the sample can be investigated, providing the information of the tip-sample force at each scanned spatial position *via* the detection and analysis of the resulting deflection of the cantilever.

2.2 Dynamic AFM

As already indicated in the text above, an AFM can be operated in different modes. The simplest mode, which also usually provides the least good resolution, is the *static mode*. Here, the cantilever is at rest, meaning that the cantilever is not excited to oscillate, but is scanned over the surface. Therefore, the measuring tip is always in contact with the surface, meaning that the measurement is conducted in the Pauli repulsion regime. Due to the consequently high mechanical load of the measuring tip and their concomitant broadening, the lateral resolution is severely limited. Hence, the *dynamic mode* has been invented. In contrast to the *static mode*, in the *dynamic mode*, the cantilever is not at rest but excited to oscillate at a certain frequency. In general, the movement of the cantilever can be expressed by its deflection q over time t. If assuming that the cantilever behaves as a harmonic oscillator and first neglecting the damping and influence of the surface, this relation can be expressed as follows (eq. 2.1).

$$q(t) = A \cdot \cos(2\pi\nu_e t + \varphi) \tag{2.1}$$

There A is the amplitude, ν_e the eigen frequency and φ the phase shift. The eigen frequency is an intrinsic property of the cantilever, defined by the effective mass m^* and the spring constant k (eq. 2.2).

$$\nu_e = \frac{1}{2\pi}\sqrt{\frac{k}{m^*}} \tag{2.2}$$

To fully characterize the cantilever, another parameter has to be determined, besides k and ν_e, which is the so-called quality factor Q (eq. 2.3) and γ is the damping constant.

$$Q = \frac{\sqrt{\frac{k}{m^*}}}{\gamma} \tag{2.3}$$

To cause the cantilever to oscillate, an external force F_{exc} is needed (eq. 2.4), which is practically transferred to the cantilever *e.g. via* a shaking piezo implemented in the piezo tube (Fig. 2.1).

$$F_{exc} = F_0 \cdot \cos(2\pi\nu_{exc}t) \tag{2.4}$$

F_0 represents the excitation force amplitude and ν_{exc} the excitation frequency. Far away from the surface, the excitation frequency ν_{exc} is set to be equivalent to the eigen frequency ν_e. By approaching the tip to the surface, besides a contribution of the damping, also a tip-surface interaction comes into play, which leads to a shift of the eigen frequency of the cantilever.

$$\Delta\nu = \nu_{exc} - \nu_e \tag{2.5}$$

The tip-sample interaction therefore also influences the movement of the excited cantilever, which can now be written as follows,

$$q(t) = q_s + A \cdot \cos(2\pi\nu_{exc}t + \varphi) \tag{2.6}$$

still assuming the harmonic approximation. There q_s represents the static deflection. If further assuming that at all times the oscillating cantilever is in steady state, meaning that the velocity of the cantilever can be written as

$$\dot{q} = \dot{z}_{ts} \tag{2.7}$$

and all observables A, φ, q_s as well as the excitation parameters F_0 and ν_{exc} are constant in time. Then the tip-sample distance z_{ts} can be further expressed as follows

$$z_{ts} = z_c + A \cdot \cos(2\pi\nu_e t + \varphi) \tag{2.8}$$

with z_c being the center position of the cantilever (Fig. 2.1). Therefore, upon the detection of the deflection $q(t)$ of the cantilever, the observables A, q_s and φ can be obtained. Reverse, the movement of the cantilever can be described with this three observables only.[28] The AFM experiment can be also fully characterized by the excitation parameters F_0 and ν_{exc} and the observables A, q_s and φ. By keeping two parameters constant while two are staying variable, the different AFM modi can be distinguished (Tab. 2.1). Since the herein presented results have been conducted in ultra-high vacuum (UHV), the modulation of A would have the disadvantage that the response time of the cantilever would be tremendously slow, since the response time is connected to the quality factor (eq. 2.9).[29]

$$\tau_{AM} \approx \frac{2Q}{\nu_e} \tag{2.9}$$

Tab. 2.1: Overview of the four modes of the dynamic AFM, defined by four parameters where two are kept constant and two are variable. There F_0 represents the excitation amplitude, ν_{exc} the excitation frequency, A the amplitude and φ the phase shift.

name	excitation	oscillation of the cantilever
amplitude modulation (AM)	F_0 =constant	A =variable
(intermittent mode/tapping mode)	ν_{exc} =constant	φ =variable
phase modulation (PM)	F_0 =variable	A =constant
	ν_{exc} =constant	φ =variable
constant excitation frequency	F_0 =constant	A =variable
modulation (CE-FM)	ν_{exc} =variable	φ =constant
frequency modulation (FM)	F_0 =variable	A =constant
	ν_{exc} =variable	φ =constant

Due to the fact that the damping factor γ is very low in UHV, the quality factors are high, which would lead in the end to slow scanning rates. Therefore, the frequency modulation (FM) technique has been used.[19]

2.3 Frequency Modulation AFM (FM-AFM)

In a frequency modulation AFM (FM-AFM) experiment the cantilever is oscillating at its eigen frequency ν_e, while keeping the amplitude A and the phase shift φ constant (Tab. 2.1), which is achieved *via* two feedback loops. To further guarantee stable measurement conditions even though the sample can be tilted or rough, the tip-sample distance is regulated, *via* changing the z-piezo displacement z_p with a third the so-called z-feedback loop.

This distance regulation is achieved upon the *constant frequency shift mode*. The general setup of a FM-AFM is illustrated in Fig. 2.1. First, the cantilever is excited with a predefined amplitude F_0 and at its eigen frequency ν_e far away from the substrate surface. *Via* approaching the oscillating cantilever near to the surface, at some point the tip-sample interaction comes into play and affects the oscillation properties. The deflection q is detected using the signal of the laser beam on the PSD. Each of the four quadrants (A, B, C and D) of the PSD converts the incident light into a voltage proportional to the light intensity. This voltage signal of the four quadrants delivers, after simple arithmetic, a sinusoidal signal, which is a function of the current force. This signal is then fed into feedback loops, namely the phase-locked loop (PLL) and the amplitude feedback loop.

The amplitude feedback loop determines the amplitude A of the oscillation and compares it with an amplitude setpoint $A_{setpoint}$ which is given by the experimentalist. If $A_{setpoint}$ and A are different, the amplitude feedback loop adjusts the excitation force amplitude F_0. Hence, the amplitude feedback loop is used to keep the amplitude constant. The adjusted signal of F_0 is further transferred to the shaking piezo, which translates the electronic signal into a movement and therefore an oscillation.

The PLL detects the phase shift φ of the oscillation and compares it with a phase

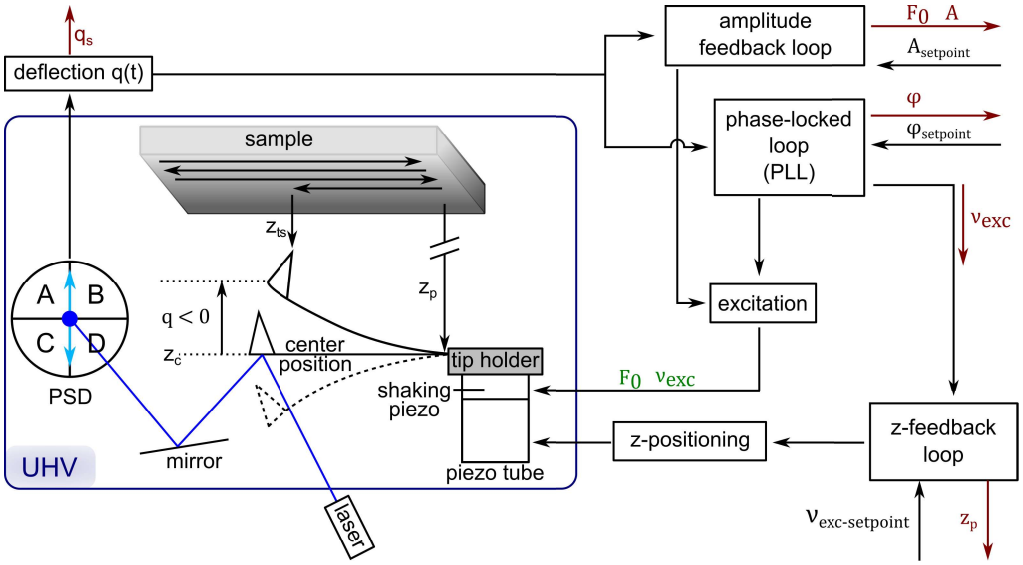

Fig. 2.1: Basic setup scheme of an FM-AFM experiment. The blue rimmed parts are situated inside the UHV-chamber. The measurement signals q_s, F_0, A, φ and z_p are displayed in red. The setpoint values $\varphi_{setpoint}$, $A_{setpoint}$ and $\nu_{exc-setpoint}$, which are given as reference, are shown in black. Inspired by Nalbach and Lindner.[30, 31]

shift setpoint $\varphi_{setpoint}$, which is usually set to $-\frac{\pi}{2}$.[28] If the phase shift setpoint $\varphi_{setpoint}$ is not equivalent to the measured phase shift φ, the PLL adjusts the excitation frequency ν_{exc} according to this difference. Hence, the PLL, as the name already suggests, is responsible for keeping the phase shift constant. The adjusted excitation frequency ν_{exc} is on the one hand passed to the z-feedback loop and on the other hand it is used to excite the cantilever *via* the shaking piezo.

If it is measured in the constant $\Delta\nu$ mode, then the following procedure is executed. The z-feedback loop compares a defined frequency shift setpoint $\nu_{exc-setpoint}$, which is given by the experimentalist, with the measured frequency shift $\Delta\nu$ (eq. 2.5), and adjust the tip-sample distance z_{ts} *via* adjusting the z-piezo distance z_p according to this difference.

3 The Bulk Insulator Calcite

3.1 Calcium Carbonate and its Modification

Calcium carbonate ($CaCO_3$) is one of about 60 known carbonate minerals on earth.[32] Together with dolomite ($CaMg(CO_3)_2$) it is accounting for more than 90% of rock-forming carbonates on earth.[33] Calcium carbonate is polymorphous and exists in at least seven modification whereof three natural ones are known, calcite (Fig. 3.1a), aragonite and vaterite.[34] The two latter ones are metastable and convert to calcite over time. With approximately 100 different forms and more than 1000 combinations, calcite is not only the mineral with the most richness in forms[35], but also the most thermodynamically stable and most common polymorph of calcium carbonate. The most prominent sources of this rock-forming mineral is limestone, which is the main component of, for example, the Swabian Jura, the Franconian Jura, parts of the Alps[32] (Fig. 3.1b) and the Mainzer Becken[36]. Furthermore, it occurs in chalk, marble and caverns as stalactites and stalagmites. Besides these pure inorganic sources, it also plays an important role for the biologically active world as skeleton or shells, for example of bivalves, snails, calcareous sponges, corals and calcareous algae.

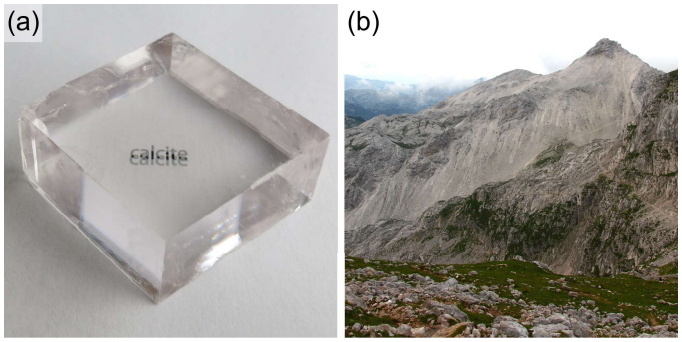

Fig. 3.1: (a) Calcite crystal with rhombohedral shape and birefringence. (b) Photographic image of the Southern Limestone Alps. (Photographic image of calcite crystal kindly provided by H. Adam)

Because of its properties and wide spread distribution across the earth, calcite was already used in ancient times as ashlar for construction of buildings and sculptures or as raw material for cement and concrete as found in old cisterns. Today, it is additionally used for the chemical glass and cellulose industry, during the metallurgical process of iron production and as raw material for soda, stone paper and

fertilizers.[37, 38] In case of very pure occurrence, calcite can be used for the optical industry, as, *e.g.*, polarizing prisms[39–41] because of its transparency and notable birefringence.[42] Besides that, it has a density of 2.71 $\frac{g}{cm^2}$[43] and a defined Mohs hardness of 3,[44] for which it is the reference value.
Calcite crystallizes in the trigonal-rhombohedral crystal system and is described by the space group R$\bar{3}$c. It can be represented by both hexagonal and rhombohedral unit cells as shown in Figs. 3.2a,b. Furthermore, being a bulk insulator, it has a band gap of 6.0 eV.[45] In contrast to usual bulk insulators like *e.g.* KBr, NaCl or CaF_2[46–53] it has a notable high surface energy of $\gamma_s(1x1) = 510\frac{mJ}{m^2}$ and $\gamma_s(2x1) = 520\frac{mJ}{m^2}$,[54], with the (1x1) and (2x1) reconstructions respectively. In combination with its excellent cleavability properties, which allows for an easy handling, it represents a promising substrate for future molecular electronic devices, because of the potential electronic decoupling between nanoelectronics and substrate. An additional beneficial property is the birefringent nature of calcite, which leads to the split-up of light perpendicular to the (10.4) surface along the [42$\bar{1}$] direction.[55] Hence, an easy determination of the absolute orientation outside the UHV chamber is possible.

3.2 The Calcite (10.4) Surface

The thermodynamically most stable cleavage plane of calcite is the (10.4) surface,[56] shown in Fig. 3.2c. It has a rectangular unit cell with dimensions of 0.5x0.81nm^2. The unit cell consists of two calcium ions and two carbonate groups. As can be seen by the marked orange rectangle in Fig. 3.2b, the carbonate groups are not in plane to the (10.4) surface, but form an angle of 44.63°.[32, 57] Hence, one oxygen atom

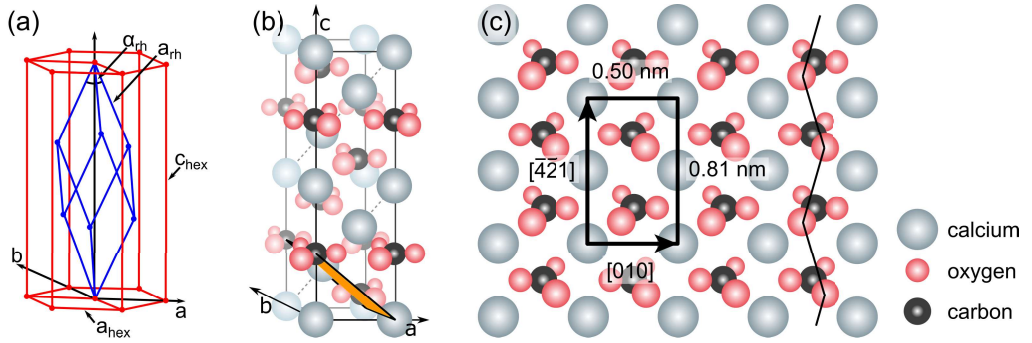

Fig. 3.2: (a) Structure of calcite represented by both, hexagonal (red) and rhombohedral (blue) unit cells. The rhombohedral unit cell is defined by the axes a_{rh} = 6.375 Å, and the angle α_{rh} = 46.08°. The hexagonal unit cell is defined by the axes a_{hex} = 4.9896 Åand c_{hex} = 17.0610 Å. (b) The hexagonal unit cell of bulk calcite with marked (10.4) cleavage plane. (c) Model of the bulk-truncated (10.4) surface. Adapted from Ref.[55]

of the carbonate group protrudes the plane of the calcium atoms, while another is in plane and the third one beneath it. Additionally, the two carbonate groups

in between one unit cell are rotated with respect to each other. Therefore, one protruding oxygen atom either points to the left or to the right, which leads to a zigzag pattern, indicated by the black line in Fig. 3.2c. Moreover, the tilt of the carbonate groups lowers the symmetry of the surface and makes it a member of the plane symmetry group *pg*. This means that a glide reflection is the only symmetry operation for the calcite (10.4) surface.

4 On-Surface Synthesis

This chapter is partly adapted from the article "On-Surface Synthesis on a Bulk Insulator Surface" by A. Richter, A. Floris, R. Bechstein, L. Kantorovich and A. Kühnle published as Topical Review in Journal of Physics: Condensed Matter, 30, (2018), 133001-133015.[26] Parts of the article is reproduced verbatim. The discussion has been extended when necessary.

4.1 Introduction

For successful downsizing of semiconductors and other electronic devices at simultaneous gain of higher computing capacities, various factors have to mesh, to met the challenges of future demands in electronic data processing. Nowadays the desired nanostructuring is reached upon defined step-wise removal of material from large macroscopic units, *e.g. via* etching, until the required structure is created (*top-down* approach). Even though tremendous improvements in the conventional way of fabrication has been achieved, this way of miniaturization will reach their fundamental limits sometime in the near future. Therefore, the *bottom-up* approach, as a promising route to create nanodevices directly on the surface has been explored, in particular since 1960 Feynmans inspiring talk: "There's plenty of room at the bottom".[58] This concept starts with small single building blocks and derives to the desired structure *via* their combination directly on the support surface.[1] The bottom-up approach is further a basis of the so called molecular electronics, which can be defined as "technology utilizing single molecules, small groups of molecules, carbon nanotubes, or nanoscale metallic or semiconductor wires to perform electronic functions".[2] Because of its broad definition the molecular electronics can be subdivided into two main fields according to the size of building blocks used for the nanodevices. The research focusing on larger components is *e.g.* identified with developments like organic light-emitting diodes (OLED), organic photovoltaic cells (OPVC) and organic field-effect transistors (OFET).[59–61] This prominent inventions are based on the fundamental experimental work of Alan J. Heeger, Alan G. MacDiarmid und Hideki Shirakawa in the late seventies, when they discovered the first intrinsically conducting polymers (ICPs).[62–64] For this research, they were awarded the Nobel Prize in Chemistry in 2000.[65–67] Additionally, conducting and semiconducting π-conjugated polymers not only allow for tuning their electrical and optical properties *via* including of special

functional groups or elements, but also exhibit outstanding mechanical properties and easy processability. The following development of the diversity of conducting polymers (exemplary shown in (Fig. 4.1)) has given new impetus to various fields in

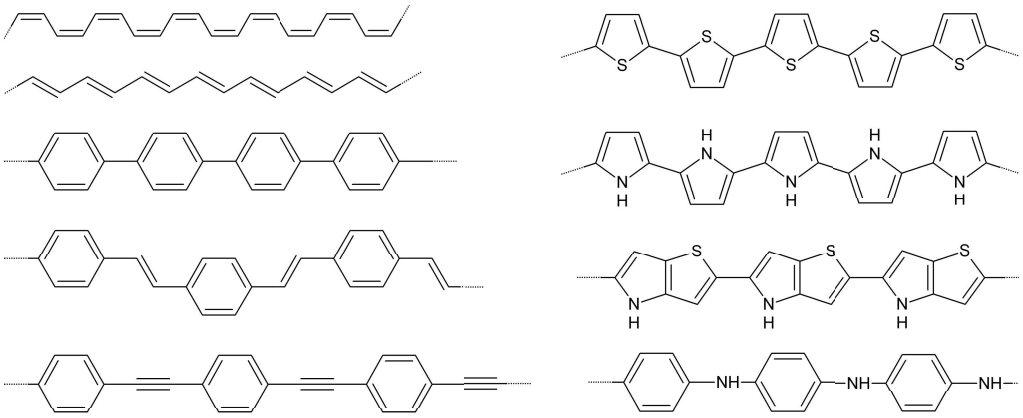

Fig. 4.1: Overview of typical conducting polymer structures in the undoped form.[68, 69]

chemistry and physics. This has further influenced the second main field of molecular electronic, which focuses on the maximal miniaturization of electrical circuits *via* using the smallest possible building blocks, *i.e.*, single molecules and small groups of molecules. The fact that molecules are indeed usable to process electronic functions was first postulated in the theoretical work by Aviram and Ratner in 1974.[70] Later experimental studies have presented that individual molecules can also act, *e.g.*, as transistors,[4] rectifiers,[3] switches,[5–7] resistance,[71] or data storage devices.[72] Furthermore, to create electrical circuitry a contacting of these functional units and also a connection between these nanodevices and the macroscopic world, upon wires is necessary. For realization such kind of contacts two main approaches are adaptable, the self-assembly or the on-surface syntheses. The first describes the spontaneous creation of well-ordered structures on the atomic level under equilibrium conditions. It further relies on the formation of reversible bonds,[10] based *e.g.* on noncovalent intermolecular forces such as hydrogen bonding,[73] $\pi - \pi$ stacking,[74] dipolar,[75] van der Waals,[76] or metal-ligand[77] interactions. Furthermore, the final arrangement of the molecules relies on the interplay between intermolecular and molecule-surface interactions and can be therefore tuned as has been shown in various publications.[78, 79] Nevertheless, since the self-assembly relies only on reversible interactions, the resulting structures can be fragile. Hence, on-surface synthesis has emerged as a very promising approach,[11, 26, 80–83] since the creation of chemical bonds provides long-term stable structures[84] and facilitates efficient charge transport in molecular wire junctions.[85] Additional, on-surface synthesis enables the creation of large planar and conjugated systems, which would not be possible in conventional chemistry, due to solubility issues. Even if these large structures can be synthesized, the transfer from beaker to surface easily leads to a formation of conglomerates or the bending or possible breaking of the components. Additionally,

no solvents are needed for on-surface synthesis. Therefore, no negatively influence of solvents on the system results and no need for the introduction of solubilizing groups exists, which often negatively affect the conductivity or other properties. Most importantly, on-surface synthesis can provide well controllable properties, due to a surface-assisted linking reaction. Nevertheless, it should be considered, that the transfer of known conventional synthesis routes to a two-dimensional surface is not trivial and sometimes this is even not possible. Furthermore, also challenging difficulties like, *e.g.* a defined positioning of the molecular precursors and their chemical stability during depositing have to be overcome.
Moreover, it has to be mentioned that on-surface synthesis can not only be used for applications in molecular electronics, but also *e.g.* for the creation of quantum boxes[86] or in the field of surface functionalization for later on catalytical[87] or maybe even membrane applications.[81]

4.2 On-Surface Synthesis

It has been shown that the challenging task of transferring classical solvent chemistry onto a 2D surface is indeed possible in 2000 by a research group around K.-H. Rieder who demonstrated that all steps of a chemical reaction can be performed on a surface.[88] In this pivotal work, the classical Ullmann coupling reaction[89] of iodobenzene has been induced using the tip of a STM on a Cu(111) surface. Another key example using the STM tip to initiate an on-surface reaction has been a diacetylene polymerization on graphite, which results in conjugated structures[90, 91] that are highly interesting for creating electrically conductive contacts on a surface. Recently, even triangulene, which has not been isolated before due to its reactivity, has been synthesized upon tip-induced dehydrogenation of a precursor molecule.[23] However, using the STM tip to initiate a reaction is very time-consuming and, thus, likely to be limited to fundamental studies. In contrast, when using photochemical or thermal initiation, on-surface synthesis can be performed in a parallel manner. One of the first examples demonstrating the thermal initiation of an on-surface covalent linking has been presented by L. Grill and coworkers in 2007.[80] In this study, an Ullmann-like reaction has been performed using bromine substituted porphyrin molecules on Au(111). Depending on the number of substitutions, dimers, linear chains or extended networks have been obtained. Later, the same group has extended their strategy by inducing a hierarchical approach, which makes use of the different aryl-halogen bond strength when comparing bromine and iodine substituted porphyrins.[92] This idea allows for a controlled step-by-step linkage of the molecular precursors, which greatly enriches the library of the resulting structures. By now, ten years after Grill′s seminal work, a multitude of different reactions have been proven possible on various conducting substrates, including Ullmann-

like coupling,[80, 92–95] cyclodehydrogenation,[96] Glaser-like coupling of terminal alkynes,[12, 97–100] condensation reactions - *e.g.*, boronic acid-based chemistry[101–103] and imine[104] as well as polyimide[105] and polyamide[106] network formation - cycloaddition[107] as well as click[108] and deoxygenation reactions.[22, 109] Both, the promising potential of on-surface synthesis in future applications and the gain in fundamental understanding alike have stimulated an impressive number of studies in the field of on-surface synthesis as can be seen in Tab. 4.1- 4.3. This immense number of reactions can be categorized according to the hybridization of the reacting carbon or to other elements acting as linking part. Furthermore, a classification of the general reaction type is useful, which also includes the name of the classical solvent analogue reaction. These classical names of the solvent reactions are often used in on-surface reaction publications, since the conventional synthesis often inspired the on-surface experiments and are therefore very helpful for the literature research. Nevertheless, these classical reaction names should not be used for the on-surface reactions, since the mechanism differs significantly.

Tab. 4.1: Overview of on-surface synthesis reactions. Δ corresponds to a thermally induced, $*$ to photochemically induced and $\downarrow$ to tip-induced reaction. Table inspired by Shen *et al.*[87] and Lindner *et al.*[13]

categ.	reaction type (classical analogue)	reaction scheme	substrate, stimulus, references
sp^0-C	N-heterocyclic dimerization (Wanzlick-type dimerization)	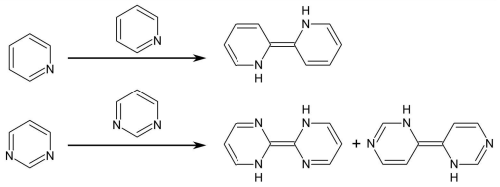	Cu$^{\Delta}$[110–113]
sp^1-C	diacetylene polymerization	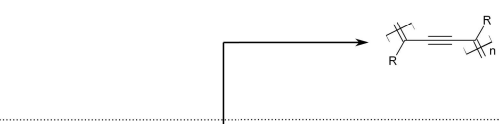	$CaCO_3$,$^{\Delta *}$[114] graphite$*$[91, 115] HOPG,$*$ $\downarrow$[90, 116–120] h-BN$^{\Delta *}$[20] graphene@SiC$*$[21] Au$*$[121, 122] MoS_2,$^{\Delta *}$ $\downarrow$[118, 119, 123]
	reactions of terminal alkynes: homocoupling (Glaser coupling)	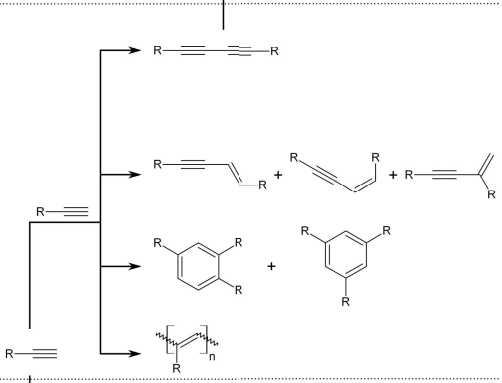	Au,$^{\Delta}$[97, 98, 124] Cu$^{\Delta *}$[97–99, 125] Ag$^{\Delta *}$[97–99, 126–130] HOPG,$^{\Delta *}$[100, 131] $CaCO_3$$^{\Delta *}$[132]
	reactions of terminal alkynes: dimerization		Au,$^{\Delta}$[97, 98] Cu$^{\Delta}$[97, 98, 125] Ag$^{\Delta}$[97, 98, 126, 133]
	reactions of terminal alkynes: cyclotrimerization/ [2+2+2] reaction		Au$^{\Delta}$[134, 135] Cu$^{\Delta}$[125]
	reactions of terminal alkynes: acetylene polymerization		Au,$^{\Delta}$[136] $CaCO_3$$^{\Delta *}$[??]
	reactions of terminal alkynes: coupling with aryl halides (Sonogashira coupl.)	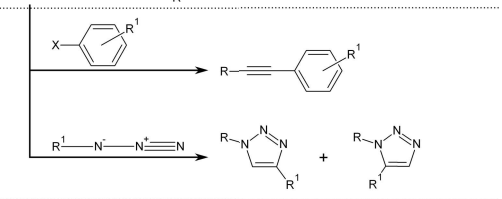	Au,$^{\Delta}$[137, 138] Ag$^{\Delta}$[139]
	reactions of terminal alkynes: azide-alkyne cycloaddition (click reaction/ Huisgen-cycloadd.)		Au,$^{\Delta}$[107] Cu$^{\Delta *}$[108]
	Bergman cyclization	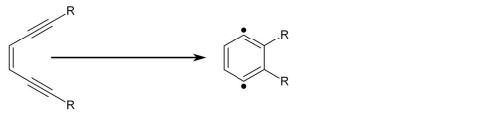	Au,$^{\Delta}$[140] Cu$^{\Delta *}$[141] Ag$^{\Delta}$[142, 143]
	coupling of halogenated terminal alkyne aryls	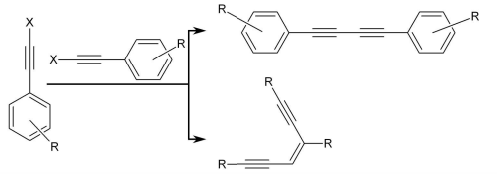	Au$^{\Delta}$[144] Ag$^{\Delta}$[133]
sp^2-C	reactions of alkenes: dimerization/ dehydrogenative coupling	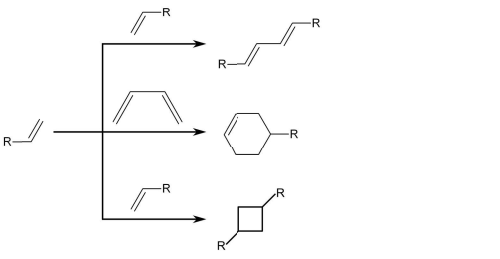	Cu$^{\Delta}$[145, 146]
	reactions of alkenes: [4+2] cycloaddition/Diels-Alder reaction		Au$^{\downarrow}$[147]
	reactions of alkenes: [2+2] cycloadd. dehydrogenative coupling		Au$^{\Delta}$[148] graphite$*$[149]
	dehalogenative homocoupling of terminal alkenyl halides	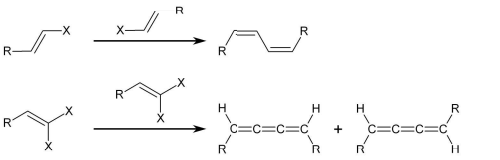	Cu$^{\Delta}$[145] Au$^{\Delta}$[150]

Tab. 4.2: Overview of on-surface synthesis reactions. Δ corresponds to a thermally induced, $*$ to photochemically induced and $\downarrow$ to tip-induced reaction. Table inspired by Shen *et al.*[87] and Lindner *et al.*[13]

categ.	reaction type (classical analogue)	reaction scheme	substrate, stimulus, references
sp^2-C	coupling of aryl halides (Ulmann coupling)	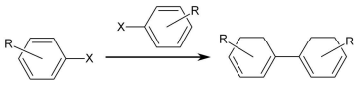	Au$^{\Delta,*}$[80, 92, 94, 95, 103, 151–153] Cu$^{\Delta,\downarrow}$[88, 93, 151, 154–158] Ag$^{\Delta}$[93, 95, 151, 152, 156, 159, 160] h-BN@Ni$^{\Delta}$[161, 162] Al_2O_3*[163] Ge:H,$^{\Delta}$[164] Cu/Pd@Au$^{\Delta}$[165, 166] mica,$^{\Delta,*}$[167] NaCl@Au$^{\Delta}$[168] $CaCO_3$,$^{\Delta}$[25, 169–171] Pt@Ag$^{\Delta}$[166]
	dehydrogenation coupling of aryls (Scholl reaction)	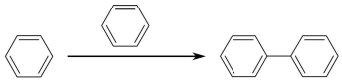	Pt,$^{\Delta}$[172] Cu$^{\Delta}$[96, 173–175] Au,$^{\Delta}$[176–180] Ag$^{\Delta}$[176, 181, 182]
	[2+2] cycloaddition/ dehalogenation coupling	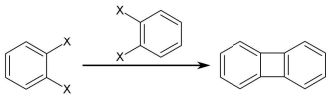	Au,$^{\Delta}$[183] Cu$^{\Delta}$[183]
	[2+2] cycloaddition	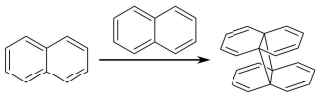	Au,$^{\Delta}$[184] $CaCO_3$*[185]
	dimerization and cyclotrimerization of acetyls	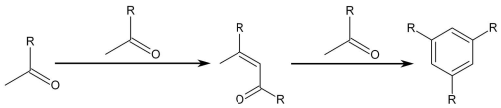	Ag$^{\Delta}$[186]
	decarboxylative polymerization	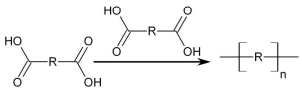	Ag,$^{\Delta}$[187] Cu$^{\Delta}$[187, 188]
	desulfurization	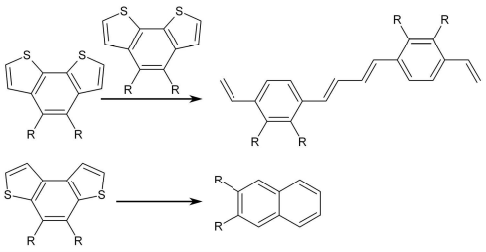	Ni$^{\Delta}$[189–191]
sp^3-C	MCMurry reaction	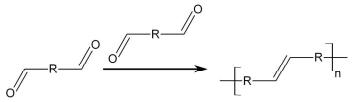	Au$^{\Delta}$[192]
	coupling of aliphatic halogenes (Wurtz coupling)		Cu$^{\Delta}$[193]
	linear alkane coupling	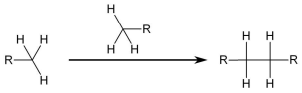	Au,$^{\Delta}$[194, 195] Cu$^{\Delta}$[196, 197]
others	dehydrogenation	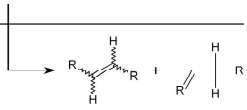	Au,$^{\Delta}$[198, 199] Cu$^{\Delta}$[23, 200] NaCl@Cu[23] Xe@Cu[23]
	carbonyl analogue reaction	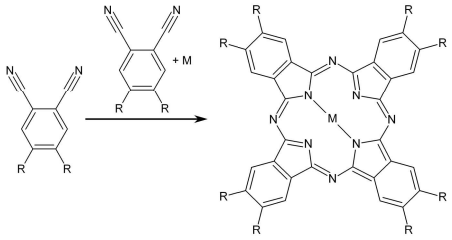	Au,$^{\Delta}$[201, 202] Ag$^{\Delta}$[201] NaCl@Ag$^{\Delta}$[201]

Tab. 4.3: Overview of on-surface synthesis reactions. Δ corresponds to a thermally induced, $*$ to photochemically induced and $\downarrow$ to tip-induced reaction. Table inspired by Shen *et al.*[87] and Lindner *et al.*[13]

categ.	reaction type (classical analogue)	reaction scheme	substrate, stimulus, references
others	condensatin reaction: boronic acid condensation	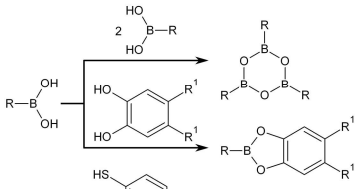	Au,$^{\Delta}$[203, 204] graphite$^{\Delta}$[205] Ag$^{\Delta\downarrow}$[203, 206] Pt$^{\Delta}$[203] HOPG$^{\Delta}$[207, 208] Cu$^{\Delta}$[203]
	condensatin reaction: thiazole formation (aminothiophenole + aldehyde)	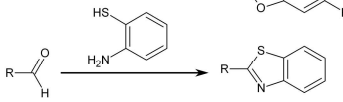	Ag,$^{\Delta}$[101] HOPG$^{\Delta}$[209]
	condensatin reaction: ester formation (acyl halide + alcohol)	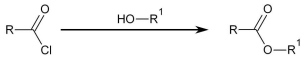	HOPG$^{\Delta}$[210]
	condensatin reaction: imine formation (Schiff-base reaction) (amine+aldehyde) (amine+ketone)	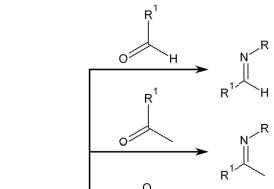	Au$^{\Delta}$[211]
	condensatin reaction: amide formation (amine+acyl halide)	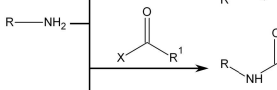	Au,$^{\Delta}$[104, 212–214] HOPG$^{\Delta}$[207, 215–220]
	condensatin reaction: imide formation (amine+anhydride)	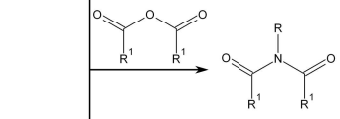	Ag$^{\Delta}$[221]
	condensatin reaction: urea derivative formation (amin+isocyanate)	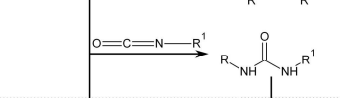	Ag$^{\Delta}$[106, 222, 223]
	azide formation	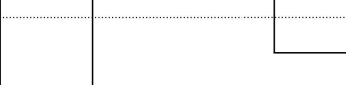	Au$^{\Delta}$[105]
	amine coupling		Au,$^{\Delta}$[224] Cu$^{\Delta}$[225]
	ring-opening-reaction	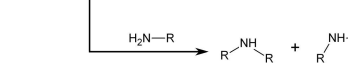	Cu$^{\Delta}$[225] Ag$^{\Delta}$[225]
	anillin polymerization	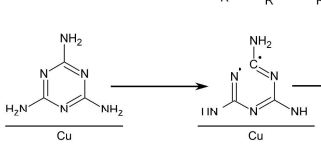	Ag,$^{\Delta*}$[226] Cu$^{\Delta}$[227]
	oxidative homocoupling	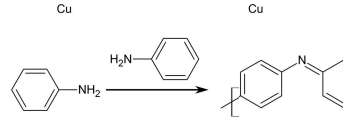	Cu$^{\Delta}$[228]
	thioether formation	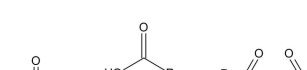	Au$^{\Delta}$[229]
	deoxygenation reaction	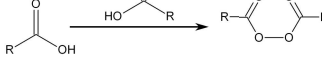	Au$^{\Delta}$[124]
		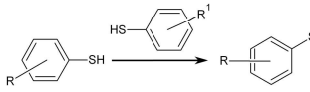	Au$^{\Delta}$[230]
		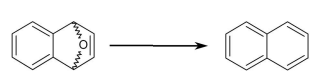	Au[109] Cu[22]

4.2.1 Transfer of On-Surface Synthesis to a Bulk Insulator Surface

The vast majority of the above-mentioned studies has been carried out on metal surfaces, with only few exceptions being highly oriented pyrolytic graphite (HOPG)[93, 100] and semiconductor surfaces.[20, 164] This limitation to metal substrates is mainly due to the fact that STM is frequently used for imaging the resulting structures. Moreover, also many other complementary surface science characterization methods rely on the use of an electrically conductive sample, so metal substrates have been a natural choice from an experimental point of view. In the context of on-surface synthesis, another, perhaps even more important, aspect needs to be considered: many of the above-mentioned reactions that have been transferred from solution chemistry, such as Ullmann or Glaser coupling, are known to be catalyzed by the presence of metal atoms. Thus, also from this fundamental point of view, metal substrates have shown superior performance in on-surface synthesis and it is proven that the choice of the specific substrate has a significant impact on the reaction.[93] However, especially in the context of applications in future molecular electronic devices, electrically non-conducting substrates are interesting as they allow for decoupling of the molecules′ electronic structure from the underlying support surface. This is mandatory for avoiding leakage currents, *e.g.*, in molecular wires, when synthesizing a conjugated molecular structure directly on a surface. A very successful solution is using thin insulator films for bond formation,[24, 168, 201, 231, 232] as they still allow using the STM for imaging, but, at the same time, greatly reduce - or even eliminate - possible leakage currents. However, this approach requires an additional step of preparing the thin film and it has so far been restricted to a rather limited class of insulator materials. In fact, a vast majority of the above-mentioned studies has been conducted on thin films of sodium chloride, with only very few exceptions such as xenon.[23] Besides, also thin flakes of an insulator like h-BN(0001) onto SiO_2/Si substrate has been fabricated.[20] However this includes further preparation and cleaning steps and is limited to a certain flake size. Thus, it remains highly interesting to extend the existing insights to bulk insulator substrates. With the advent of scanning force microscopy, it has become possible to collect atomically resolved images of bulk insulator surface, providing the option to explore on-surface synthesis on bulk insulators as well. So far, however, transferring the developed on-surface synthesis strategies to bulk insulator surfaces has posed great experimental challenges. Besides the above-mentioned fundamental limitations in initiating the reaction in the absence of a catalytically active metal, yet another practical limitation has proven to pose substantial hurdle, which is the weak interaction of the precursor molecules with prototypical insulator surfaces[233, 234] as compared to metal surfaces. Because of this weak interaction many molecules are prone to desorption at temperatures lower than those needed to initiate an on-surface reaction.

This critical issue of the comparatively weak binding between molecular precursors and substrate when exploring on-surface synthesis on a bulk insulator surface can be rationalized by considering the respective surface energies. Compared to metal surfaces having typical surface energies in the range of 1-2 $\frac{J}{m^2}$ prototypical insulators such as alkali halides have an order of magnitude smaller surface energies.[233] In this respect, calcite (10.4) is different from other ionic crystal surfaces, as it exhibits a surface energy of 0.59 $\frac{J}{m^2}$ when considering the bulk-truncated surface in UHV.[235] Besides, calcite is a cheap and a widespread material, which can be easily cleaved yielding comparatively huge flat surface terraces. Furthermore, substantial effort has been put into designing precursors that, besides possessing a reactive site for on-surface linkage, also feature a functional group that can act as an anchor towards the surface. Since the calcite (10.4) surface is ionic, the surface offers the possibility of electrostatically anchoring molecules to the calcium cations or carbonate anions. In addition to this, the protruding oxygen atoms of the carbonate groups offer the possibility of hydrogen bonding. Therefore, the carboxylic acid group has been identified to offer a suitable anchor functionality, where the negatively charged carbonyl oxygen interacts electrostatically with a surface calcium atom while the hydroxy group forms a hydrogen bond towards the protruding oxygen atom of a neighboring carbonate group[236] (Fig. 4.2).

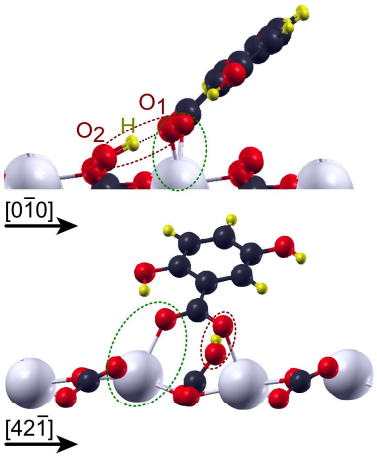

Fig. 4.2: Binding configuration of a carboxylic acid group onto calcite (10.4) of the 2,5-dihydroxybenzoic acid (DHBA) molecule, based on DFT calculations as published in.[236] Adapted from Ref.[236]

Density functional theory (DFT) calculations[236] have shown that the formation of this hydrogen bond is associated with the hydrogen atom of the carboxylic acid group moving closer toward the protruding oxygen atom of the surface as perhaps expected from the fact that calcite, being the salt of a weak acid, acts as a base. To illustrate the impact of the carboxylic acid group, we can compare desorption experiments of benzene and iodobenzoic acid: while benzene is known to desorb already at about 190 K,[237] benzoic acid and iodobenzoic acid are stable on the surface held at room temperature. Furthermore, systematic theoretical calculations of molecules containing different functional groups such as carboxyl, hydroxyl, aldehyde, thiol, amine and nitrile groups interacting with the calcite (10.4) surface, have been performed yielding an overview of adsorption

energies.[238, 239] This allows for a direct comparison of molecules with and without carboxylic acid groups. Exemplarily, acetic acid and benzoic acid yield adsorption energies of 0.98 eV and 1.03 eV, while ethane and benzene result in significantly lower values of 0.17 eV and 0.31 eV respectively.[238] Besides, also other functional groups have been identified to act as suitable anchor on calcite such as ester[240] and amide or amine[241] groups. Even C_{60} having none carboxylic acid group has found to be an appropriate molecule, since its size and, consequently, its polarizability appears to be large enough to allow for sufficiently strong van-der-Waals interactions.[185, 234] Therefore, a multitude of groups and their combination for further tuning the molecular surface interactions and influence of the self-assembly and subsequent reaction pathways await their discovery.

Proof-of-Principle: Demonstration of Aryl-Halide Coupling on Calcite (10.4)

Since the on-surface synthesis of molecular wires requires electronically decoupling of the molecular electronic structure from the support surface, the C-C coupling of aryl-halides on the (10.4) surface of the bulk insulator calcite has been explored.[25] To this end, among others, simple benzoic acid derivatives have been studied, namely 2,5-diiodobenzoic acid (DIBA), 3,5-diiodosalicylic acid (DISA), and 4-iodobenzoic acid (IBA), as they allow for a systematic change of both the number and the position of halogen atom substitutions (Fig. 4.3). Depending on the used molecular precursors either dimers, linear stripes or zigzag rows can be obtained. Moreover,

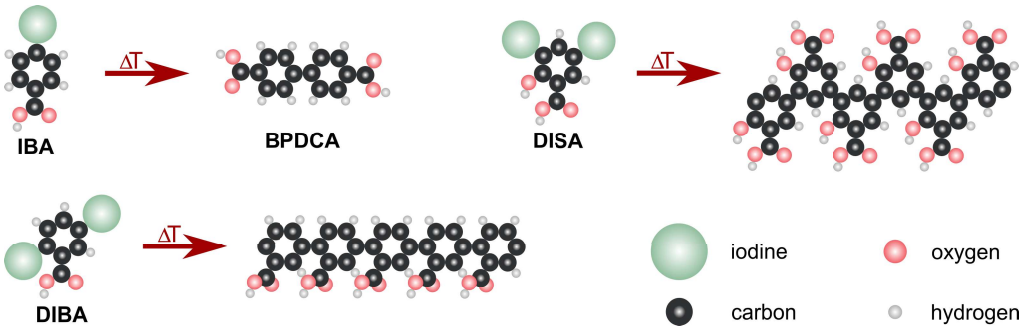

Fig. 4.3: Benzoic acid derivatives as a simple building block for on-surface C-C coupling. Depending on the number and position of the halogen atom substitutions, dimers, linear as well as zigzag rows of the molecules can be created. Adapted from Ref.[242]

it has also been shown that by changing from iodine to bromine and chlorine, the binding strength can be tuned.[169] Additionally, the C-C coupling of IBA has been intensively studied in a theoretical investigation to elucidate the details of the reaction pathway.[170]

Dimerization and Extended Row Formation When using IBA, having one iodine substitution in para position, the on-surface synthesis of the respective dimer,

biphenyl-4,4'-dicarboxylic acid (BPDCA), is expected upon C-C coupling. IBA deposited onto calcite (10.4) held at room temperature (RT) exhibits highly mobile species, which cluster at step edges (Fig. 4.4a).[171] Upon annealing to 580 K rows composed by side-by-side aligned entities exist on the surface, as can be seen in Fig. 4.4b showing the high-resolution image of a single row simultaneously with the atomically resolved calcite surface. From this image it becomes apparent that the calcite substrate is decisive for the alignment of the rows, which are oriented along the $[42\bar{1}]$ substrate direction. Interestingly, this side-by-side aligned structure can also be found when depositing BPDCA on the surface directly,[243] supporting the concept, that the observed rows are composed by the C-C coupled reaction product. To give further evidence for the coupling of aryl-halides, the number and position of

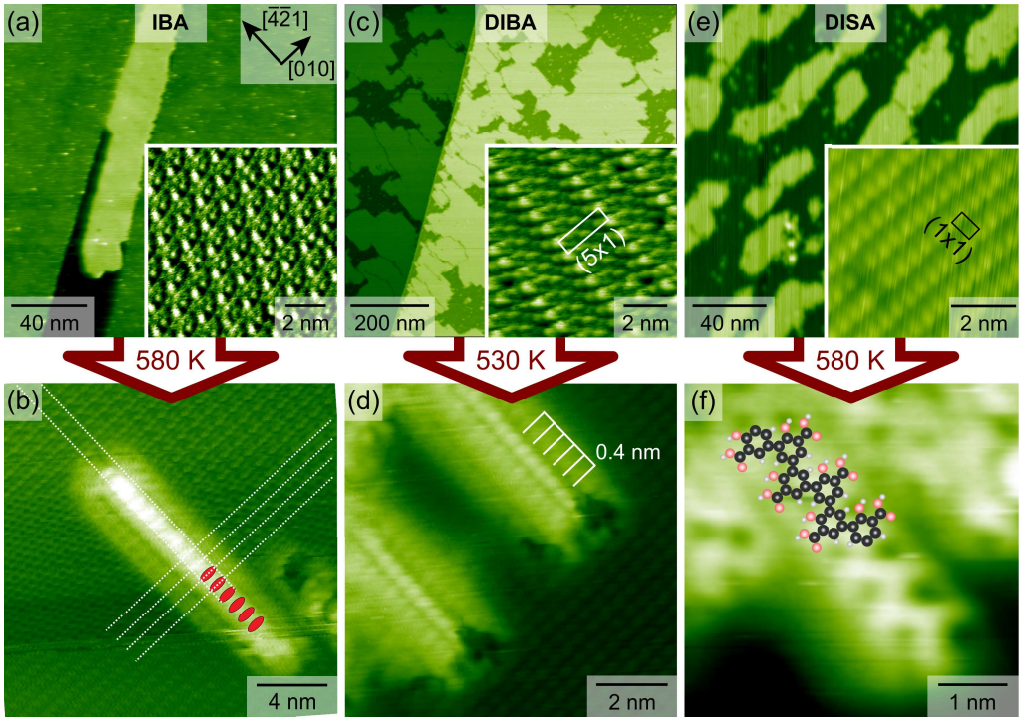

Fig. 4.4: Deposited iodine substituted benzoic acid derivatives onto calcite (10.4) held at room temperature and subsequent structural changes obtained upon annealing of the substrate. (a) Self-assembly of IBA. Adapted from Ref.[171] (b) High-resolution image obtained after annealing the sample to 580 K, showing a molecular row and the atomic structure of the surface simultaneously. BPDCA molecules are superimposed as ellipses to illustrate the envisioned side-by-side alignment of the dimerized IBA molecules. (c) After deposition of DIBA an ordered wetting layer is formed, with a (5x1) superstructure as shown in the inset. (d) Upon annealing above 530 K, the high-resolution image shows rows with an internal periodic structure of 0.4 nm along the $[42\bar{1}]$ direction. (e) Highly ordered wetting layer obtained after depositing DISA. The inset shows a zoom into the (1x1) superstructure. (f) Upon annealing to 580 K, a structural change is revealed. A zoom reveals a zigzag structure. The superimposed model illustrates the perfect size match with the expected covalently linked structure. Adapted from Ref.[25]

the halogen substitution has been changed *via* using DIBA and DISA, since this influences the shape of the resulting products as can be seen in Fig. 4.3.

Depositing DIBA on the calcite (10.4) surface held at RT results in the formation of

an ordered wetting layer (Fig. 4.4c). A substantial structural change can be induced by annealing the substrate above 530 K. Now, rows are formed that are aligned along the [42$\bar{1}$] substrate direction. The zoom on these rows reveals an internal structure with a repeat distance of 0.4 nm (Fig. 4.4d), which fits to the expected repeat distance of the C-C coupled reaction product of the DIBA precursor.
When depositing DISA onto calcite (10.4) held at RT, a highly ordered wetting layer is obtained (Fig. 4.4e). Annealing the sample to 580 K induces a significant structural change. Now, besides irregular-shaped islands a zoom on also reveals a zigzag structure (Fig. 4.4f), which fits excellently in its dimensions with the expected structure as illustrated by the superimposed model. The rather irregular structure can be understood from the fact that several linking geometries are possible, yielding rings or mixtures of ring and zigzag structures.[25]

Detailed Reaction Mechanism: Why Does It Work in the Absence of Metals? In the classical Ullmann coupling reaction,[89] first, an iodine is cleaved off from a phenyl ring, creating a phenyl radical. The cleavage of the bond having a strength of about 270 $\frac{kJ}{mol}$ and is catalyzed by the presence of copper atoms. In the second step, two phenyl radicals combine to form a biphenyl. Nevertheless, this reaction has been successfully transferred to the calcite (10.4) surface without providing metal atoms for catalysis. Furthermore, the herein reported temperatures required to induce the radial formation are by far too low to allow for cleavage of a C-halogene bond with a strength in the order of 300-400 $\frac{kJ}{mol}$.[244]Further, a single IBA dehalogenation in the gas phase has been calculated to be 306 $\frac{kJ}{mol}$.[170] Therefore, a specific reaction mechanism has to be at play, which facilitates bond cleavage even at relatively moderate temperatures. To address this, geometry optimization and Nudged Elastic Band calculations have been carried out using IBA as a model molecule.[170] A detailed description of the used computational methods and programs can be found elsewhere.[170] In total, two exothermic reaction mechanisms have been found, with strongly reduced energy barriers: the first, realized by a sequence of independent dehalogenations, and the second, where two molecules dehalogenate in a cooperative way. The DFT relaxed dimer configuration is the final product of both reactions and is shown in Fig. 4.5a.
First Mechanism (Fig. 4.5b) A flat molecule undergoes a single dehalogenation on the surface with a barrier of 169 $\frac{kJ}{mol}$.[170] This strong barrier reduction is due to the IBA chemisorption upon dehalogenation and the concomitant single iodine adsorption on the substrate. The most stable structure of the dehalogenated molecule on the surface is a flat phenyl radical, which is chemically bound to a calcite O atom.[170] Upon subsequent molecular diffusion of two dehalogenated IBA molecules a dimerization takes place, which is in turn facilitated by the recombinative desorption of I_2 molecules. The recombination makes the whole process thermodynamically favorable thanks to the large entropic contribution of the I_2 gas. Importantly, due

to the molecular chemisorption, the insulating substrate clearly plays a catalytic role by reducing the energy barrier in the total absence of a metallic catalyst.

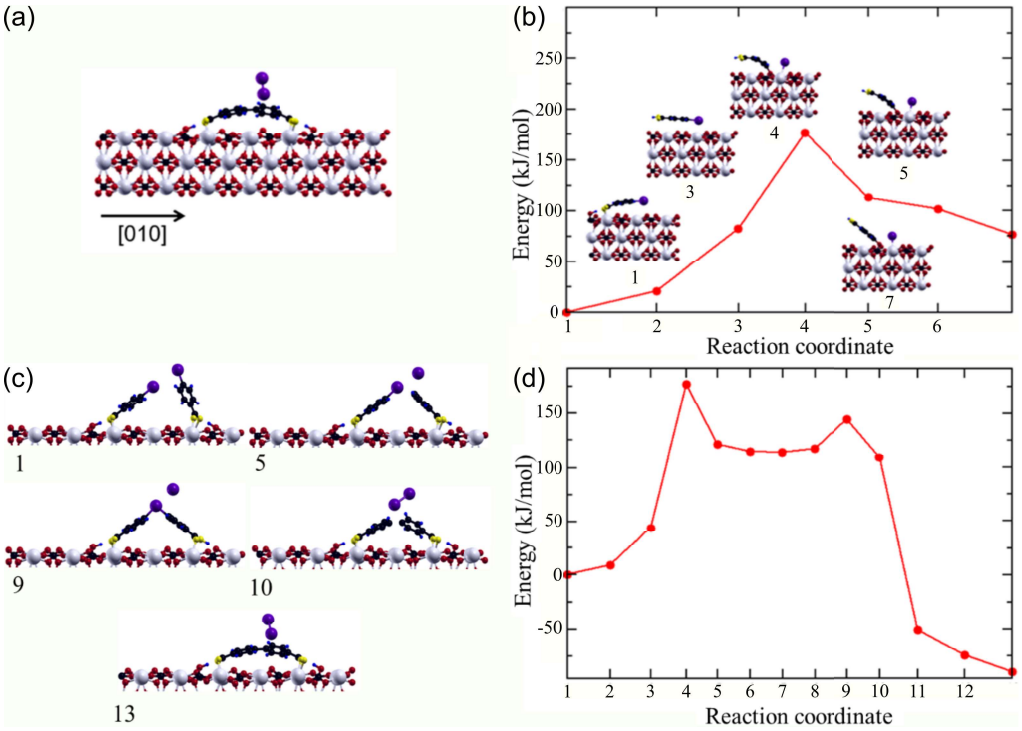

Fig. 4.5: (a) IBA dimer configuration, final product after a dehalogenation reaction. (b-d) Minimum paths and energy barriers of two main mechanisms of IBA dehalogenation on calcite (10.4).[170] (a) Independent mechanism: single molecules dehalogenate and chemisorb on the substrate before dimerization. The iodine adsorption is also visible. (c,d) Cooperative mechanism of double dehalogenation, as described in the text. In this case, the key factors facilitating the reaction are the two asynchronous dehalogenations, the exchange and sharing of the iodine atoms during the detachments from the molecules, and the I_2 recombination. Reaction coordinate numbers correspond to the intermediate molecular configurations shown. Adapted from Ref.[170]

Second Mechanism (Fig. 4.5c,d) Two molecules face each other in an upright configuration. The double dehalogenation is facilitated thanks to the following mechanism:[170] the cost of the first deionization is reduced, as the second iodine is first "exchanged" ((Fig. 4.5c), panel 5) and then "shared" between the two molecules (panel 9). The subsequent iodine detachment is instead facilitated by the I_2 molecule recombination in the gas phase (panel 10), while the dehalogenated IBAs dimerize *via* the covalent linking between phenyls (panels 10, 13). The energy barrier of this nontrivial process is 178 $\frac{kJ}{mol}$ (Fig. 4.5d),[170] comparable to the one of the first mechanism. This barrier is far less than the sum of barriers associated to individual/independent dehalogenations in gas-phase, as each detachment is somehow "assisted" by the presence of the other iodine, in a cooperative mechanism to lower the barrier. In this second case, however, there is no surface chemisorption. However, the substrate serves as a two-dimensional support to guarantee the molecular confinement, thereby providing the necessary conditions for the reaction to occur. The latter

would be hardly met in a three-dimensional environment, again emphasizing the crucial role of the insulating surface. In both cases the found mechanism on calcite differs significantly from the original one in solution.[245] This discrepancy between classical synthesis and on-surface reaction has also been found upon theoretical calculations on gold, silver and copper.[151, 155, 157] Therefore, as a consequence this on surface reaction is not named Ullmann or Ullmann-like coupling, but coupling of aryl halides to avoid misunderstandings.

Exploring Further On-Surface Reactions The demonstration of aryl-halide coupling constitutes a first proof-of-principle for on-surface synthesis on the bulk insulator calcite. However, it is desirable to extent the toolbox of possible linking reaction. Moreover, using annealing to initiate the reaction can be difficult for molecules that anchor only weakly onto the surface. Furthermore, different kinds of molecular linking groups can be explored to either avoid a reaction upon annealing already in the crucible. Moreover, as many molecules are deposited by sublimation from a crucible, molecules that are prone to react upon annealing might undergo a linking reaction already in the crucible. Therefore, on-surface reactions stimulated in a different way, *i.e.* photochemically, shall be considered. Besides the way of initiation, also the reaction type should be considered in more detail. Especially in the light of molecular electronics, the size and type of side-products should be taken into account as well as the focus on the generation of π-conjugated systems which can act as conductive devices. Further, also the resulting dimension of the on-surface synthesized molecules should be considered, since for *e.g.* wires one dimensional/linear structures are mandatory. Therefore, all versions of condensation reactions are unfavorable, since the resulting product is no π-conjugated system and additionally, one part of product yield one part of side-product. Further, these by-products are polar molecules which would strongly interact with the calcite surface and are therefore difficult to completely remove from the substrate. In contrast other reaction types like cycloadditions *e.g.* [2+2] and [4+2] (Diels-Alder reaction), acetylene polymerization, diacetylene polymerization, Bergman cyclization and carbonyl analogue reactions provide the possibility of the formation of covalent coupled π-conjugated system excluding reaction based by-product. Furthermore, also reactions yielding only very small by-products, *e.g.* hydrogen molecules (H_2) can be interesting candidates, like homocoupling of terminal alkynes, Scholl reaction or N-heterocylcic dimerization, since H_2 should interact only very weakly with the calcite substrate and therefore an easy removal can be assumed. Additionally, also the effect of the calcite surface guiding or hindering a reaction because of the influence of the lattice structure on the self-assembly during the coupling process, should be taken into account. Hence, it may be beneficial if the self-assembly of the educt and the product would be similar, since no rearrangement during the reaction has to take place. Additionally, this would open up the possibility to already influence the final

structure by the designed self-assembly of the precursor. There is actually a way to realize that by using the strategies of the so called solid state reactions. The most famous one is the polymerization of diacetylenes, but also other reactions are known to occur in the bulk, like *e.g.* polymerization of acetylene, triacetylene or trienes, polycondensation and [2+2] cyclo reactions of olefins.[246–248] Besides their possible beneficial arrangement these types of reaction having the advantage to take place without any metal as catalyst and are often initiated photochemically. Therefore a successful transfer from the classical synthesis to an on-surface reaction is very likely.

Photochemical [2+2] Cycloaddition of C_{60} on Calcite (10.4) The first demonstration of a photochemically initiated reaction on a calcite (10.4) surface has been a [2+2] cycloaddition of C_{60}.[185] This reaction is known from bulk C_{60}[249] and has been shown on metal and semiconductor surfaces.[250–252] When deposited onto calcite (10.4), C_{60} forms ordered islands with a [2x15] superstructure,[234] (Fig. 4.6a,b). The lattice mismatch between the C_{60} islands and the calcite lattice gives rise to a moiré pattern, which is manifested by stripes running along the [010] direction. As a moiré pattern is very sensitive to slight changes in the lattice spacings, it serves as an indicator for changes in the C_{60}-C_{60} distance. Upon irradiation with a 405 nm laser

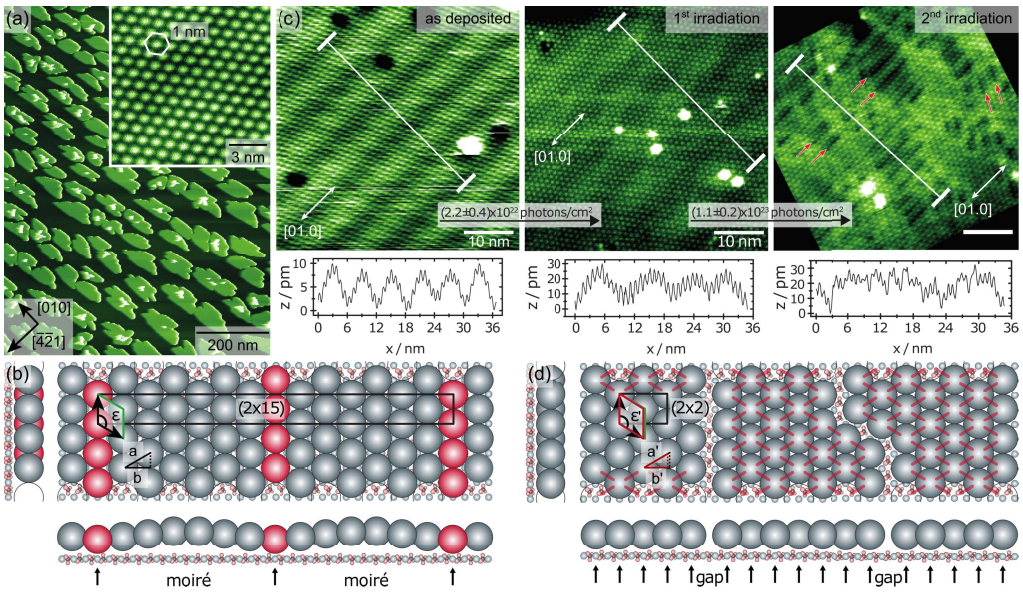

Fig. 4.6: (a) Image showing C_{60} islands on calcite (10.4). Image adapted from Ref.[234] (b) Proposed model explaining the superstructure and the origin for the observed moiré pattern. (c) Image series showing the changes induced upon irradiation of the film with a 405 nm laser diode. (d) Model explaining the preferential reaction direction by a reduction in the lattice mismatch. Images (b) to (d) adapted from Ref.[185]

diode, the moiré pattern becomes aperiodic and eventually vanishes as shown in the image series in Fig. 4.6c. Interestingly, dark rows appear in the layer (indicated by red arrows in the last image in Fig. 4.6c), which are predominantly aligned along

the [010] direction. These rows have been explained by the gaps that originate when two C_{60} molecules move closer to form a bond. As most gaps are aligned along the [010] direction, the majority of the C_{60}-C_{60} bonds formed are not oriented along [010], but form an angle of 60° to this direction. This preferential direction of the bond formation can be understood from the lattice mismatch with the underlying substrate. As illustrated in Fig. 4.6d, the lattice mismatch in $[42\bar{1}]$ direction can be reduced when forming a C_{60}-C_{60} bond along the direction marked with an a. Before reaction, this distance is about 1 nm, which means that the distance b is 0.93 nm. When forming a C_{60}-C_{60} bond, the distance a is reduced to a′, which is about 0.9 nm. This distance reduction implies that the distance b′ is now 0.8 nm, which results in a perfect match with the unit cell dimension along the $[42\bar{1}]$ direction. Therefore, this work has demonstrated that the choice of the underlying lattice in on-surface synthesis can be used to control the direction in which the reaction proceeds.

4.3 Conclusions and Outlook

In this chapter, overview is given about the current state-of-the-art on-surface synthesis on metals, semiconductors insulation films and the bulk insulator calcite. Compared to metal substrates, on-surface synthesis on bulk insulators is challenging due to the fact that molecule-surface binding is typically weak. This weak binding needs to be addressed by the specific design of the precursor molecules that often have to be equipped with anchor functionalities to prevent desorption upon reaction initiation by annealing. By now, it has proven possible to perform aryl-halide coupling on calcite (10.4). For one model molecule - iodobenzoic acid - detailed DFT insights exist that unraveled the detailed reaction pathway. These calculations have elucidated why the analogy of a classical Ullmann reaction can be induced even in the absence of catalyzing metal atoms. The key mechanism for this is closely related to the binding of the precursors towards the surface and their orientation with respect to each other. The latter can result in nontrivial cooperative mechanisms of double dehalogenation, strongly reducing the activation energy barrier. To extend the available toolbox of possible on-surface reactions, other classical synthesis routes have been explored, including light-induced [2+2] cycloaddition of C_{60} molecules. The latter reaction has been demonstrated to be governed by the underlying calcite lattice, demonstrating the potential to guide the reaction direction by a suitable choice of the surface lattice. From these examples it becomes evident that the concepts of on-surface synthesis can be extended to bulk insulator surfaces. Nevertheless, attention has to be paid to design suitable precursors that are tailored to meet the special requirements associated with the chosen bulk insulator substrate. Moreover, there is a lack of in-depth theoretical studies that address the special situation of on-surface synthesis in the case of non-conductive substrates.

5 Experimental Set-Up

5.1 UHV Chamber

All AFM measurement, presented in this thesis, are obtained with a commercial UHV system (Omicron Nanotechnology, Taunusstein, Germany) (Fig. 5.1) with a base pressure of $\leqslant 10^{-10}$ mbar. The system consists of three chambers, the preparation chamber (PREP) located to the left, the measurement chamber on the right (VT) and the load lock on the back-side, which is not visible in the image. The image Fig. 5.1b shows a zoom into the preparation chamber (PREP).

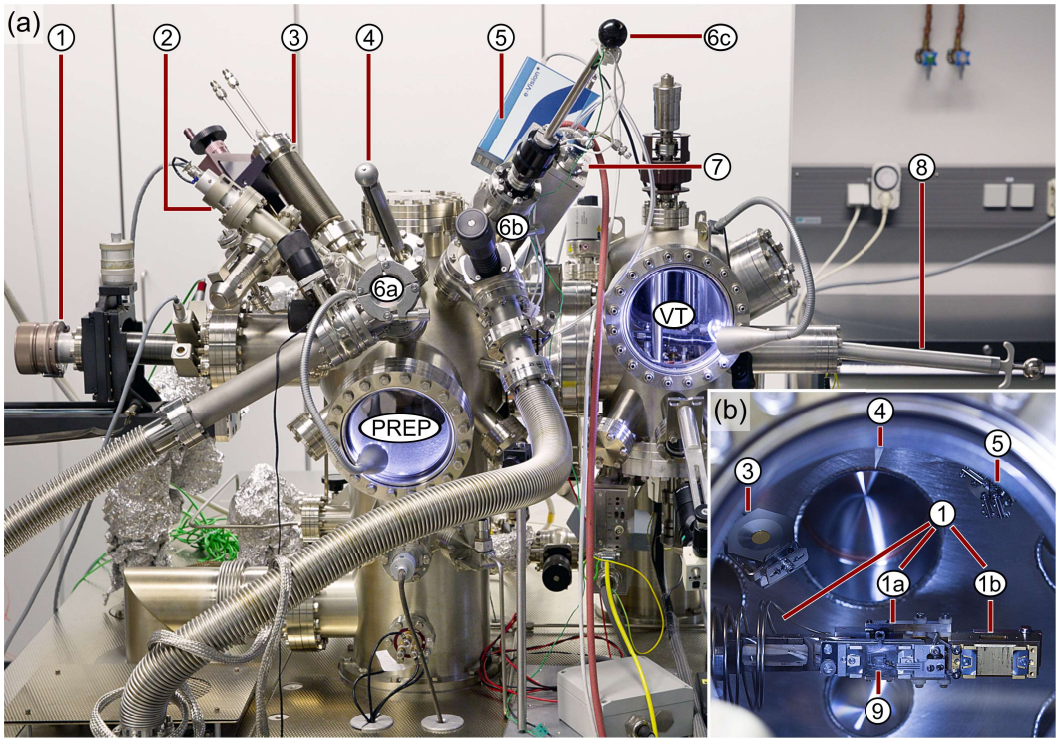

Fig. 5.1: (a) Frontal view of the UHV chamber composed of preparation chamber (PREP) and measurement chamber (VT). (b) Close up of the preparation chamber (PREP). The system is equipped with a manipulator (1) with heating (1a) and cooling (1b) stage, a sputter gun (2), a quartz crystal micro balance (3), a home-built crystal cleaver (4), a mass spectrometer (5), two sublimator positions (6a, 6b) and one molecule sublimator (6c), a UV-lamp (7) and a wobble stick (8). (Photographic images kindly provided by H. Adam)

Samples and cantilevers can be transferred *via* the load-lock from atmosphere to UHV and vice versa without breaking the vacuum. Starting from the load lock, the sample or cantilever is moved inside the preparation chamber (PREP) to the manipulator (1) (Vacuum Generators Ltd., Hastings, United Kingdom). This component allows for heating (1a), cooling (1b) and positioning in x, y and z direction, as well as the rotation of the sample (9) and cantilever. Additionally, the preparation chamber (PREP) is equipped with

- an ISE10 sputter gun (2) (Omicron Nanotechnology, Taunusstein, Germany) for tip preparation,
- a quartz crystal micro balance (3) (Inficon, Bad Ragaz, Switzerland),
- a home-built crystal cleaver for *in-situ* sample cleavage (4)[253, 254],
- a quadrupole mass spectrometer eVision+ (5) (MKS Instruments, Andover MA, USA) for the analysis of residual gases and sublimated molecules with a 0-200 mass-to-charge ratio,
- two sublimator positions (6a, 6b), in the image one home-built molecule sublimator is mounted (6c),
- a UV-lamp (7) (Peschl Ultraviolet GmbH, Mainz, Germany) for irradiation experiments,
- a wobble stick (Omicron Nanotechnology, Taunusstein, Germany),
- and a metal evaporator (Dr. Eberl MBE-Komponenten GmbH, Weil der Stadt, Germany) on the backside of the chamber (not visible in the image).

After preparation, the cantilever/sample is transferred to the measurement chamber (VT) *via* the manipulator and the wobble stick (8) into the AFM stage (2) which is visible in figure 5.2. All measurements were carried out with a commercial variable

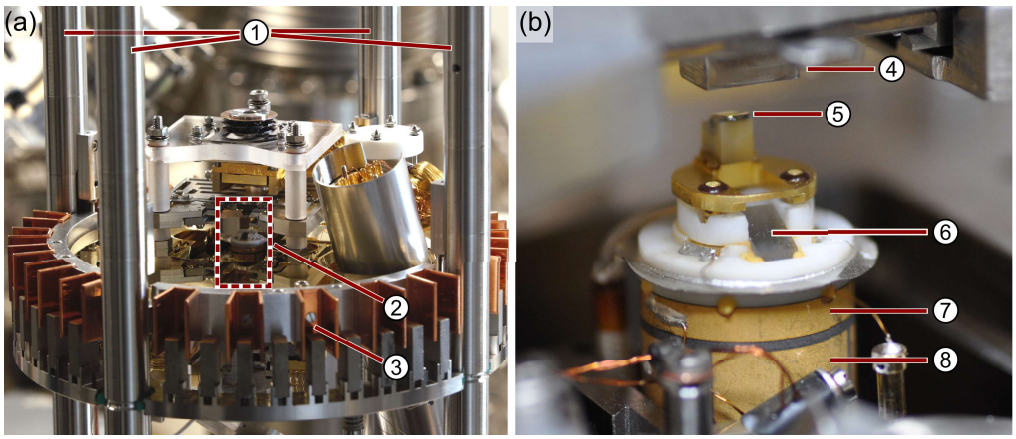

Fig. 5.2: (a) Image of the VT-AFM, suspended on springs (1), showing the AFM stage (2) and an eddy current damping system (3). (b) Close-up of the AFM stage, including a sample (4), the cantilever chip (5), the beam deflection mirror (6), the excitation piezo (7) and the piezo tube (8). (Photographic images kindly provided by H. Adam)

temperature AFM (VT-AFM) operated in the so-called *frequency modulation mode* (FM-AFM mode). Moreover, the AFM setup was optimized by R. Bechstein[255]

via introducing a new light source, a home-built preamplifier and a PLL (easyPLL, Nanosurf AG, Liestal, Switzerland).
Furthermore, to prevent mechanical noise in the measurements, the whole system is resting on active damping legs. Additionally the AFM stage (2) is suspended on springs (1) and equipped with an eddy current damping system (3) (Fig. 5.2a). A close-up of the AFM stage including the cantilever, the sample and the piezos is given in Fig. 5.2b.

5.2 Sample and Cantilever Preparation

5.2.1 Cantilever

The measurements are performed with n-doped silicon cantilevers of the type PPP-NCH (Nanosensors, Neuchâtel, Switzerland) with a typical eigenfrequency of 300 kHz, a force constant of 40 N/m and Q-factors of around 15000 in UHV. Before use, the cantilevers are sputtered with Argon (Ar^+) using the ISE10 sputter gun (Omicron Nanotechnology, Taunusstein, Germany) at 2 keV in two positions for 5 min each.

5.2.2 Substrate

The calcite (10.4) surface is used as substrate for all measurements. Optical quality calcite crystals are supplied from Korth Kristalle GmbH (Altenholz, Germany) and cut into 2x4x10 mm large samples by VARIO Kristallbearbeitung GmbH (Wildau, Germany). After determination of the absolute crystal orientation using the birefringence, the crystals are mounted into the sample holder as shown in the photographic image (Fig. 5.3a).[256] The sample holders were designed by L. Tröger and J. Schütte[253, 254] and fabricated by PLM GmbH (Neuhausen, Germany) out of stainless steel or tantalum.

After transfer into the UHV system, the calcite crystals were outgassed by annealing to 680 K for 3 h. Before molecule or iron deposition, the crystals were cleaved *in-situ* to prepare a clean (10.4) surface and subsequently heated for approximately 1 h to 625 K to remove surface charges. Next, the surface was investigated by AFM to assure a clean surface and to verify the crystal orientation.

5.2.3 Metal Evaporator

The metal deposition is performed with a metal evaporator of Dr. Eberl MBE-Komponenten GmbH (Weil der Stadt, Germany) of the type DCS 40-2x-1-14-2S

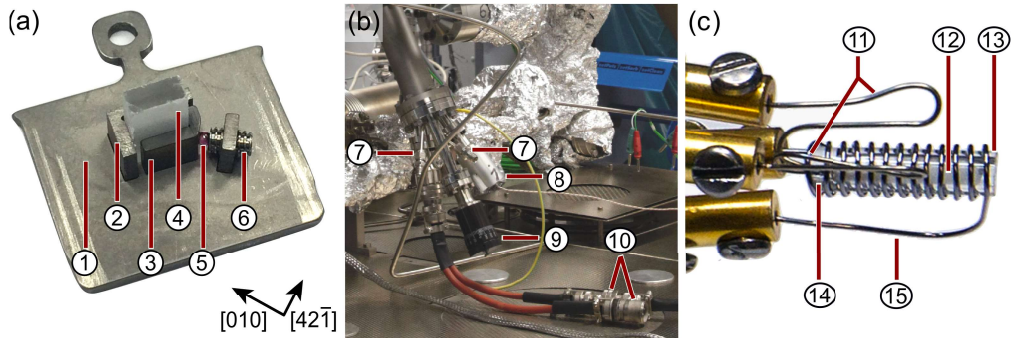

Fig. 5.3: (a) Home-built sample holder composed of the mounting plate (1) with a welded corner (2) and a mobile corner (3) for clamping the crystal (4). The mobile corner is pulled tight by a ruby sphere (5) and a grub screw (6). (b) Metal evaporator, including a pyrolytic boron nitride (PBN) crucible with Au and a Al_2O_3 crucible with Fe, the water cooling (7), a thermocouple (8), the shutter (9) and a high-voltage (HV) Y-piece (10) for separate direct heating of the crucibles. (c) Front part of a molecule sublimator with mounted crucible, containing a thermocouple wire (11), glass wool (12), the glass crucible (13), molecular material (14) and a Ta- wire (15). (Photographic images kindly provided by H. Adam)

with iron from Goodfellow (Huntingdon, Great Britain) having a purity of 99.99%. The metal evaporation chamber is situated on the backside of the system in between the load-lock and the preparation chamber. The lower part is shown in the photographical image (Fig. 5.3b). It includes a pyrolytic boron nitride (PBN) crucible with Au and a Al_2O_3 crucible with Fe. To guaranty a constant evaporation temperature, a cooling system (7) is embedded in the construction. The used evaporation temperatures and times are based on the evaporation curve recorded by S. Kuhn (see appendix Fig. 9.7) and the experiments done by L. Schüller.[256–259]

5.2.4 Molecule Sublimation

For the deposition of all precursor molecules a home-built molecule sublimator consisting of a self-made Knudsen cell (Fig. 5.3c) at a linear translator is used.[254] For the manufacturing of the Knudsen cell at first, a glass tube is closed *via* melting on one side to form a crucible (13). Second, a NiCr/Cr-thermocouple (11) is spot welded and then melted into the bottom of the glass crucible (13) for temperature read-out. Third, the crucible is filled with the molecular material (14) and subsequently capped with a piece of glass wool (12), which prevents the material from falling out. Fourth, a Ta-wire is wrapped around the crucible as filament (15).
For each type of molecule, a new crucible is fabricated and, before first filling, outgassed to 250°C in the molecular beam epitaxy (MBE) test chamber (Fig. 5.4a) to avoid contamination. Comparable to the UHV-chamber, also the MBE test chamber is equipped with

- a quartz crystal micro balance (1) (Inficon, Bad Ragaz, Switzerland),
- a sublimator position with a T-piece (2),

- and a quadrupole mass spectrometer eVision2 (3) (MKS Instruments, Andover MA, USA) for the analysis of residual gases and sublimated molecules with a 0-200 mass-to-charge ratio.

Moreover, all molecules are tested for suitable sublimation parameters in the MBE test chamber using the program "Justin" which was written by F. Kling.[260] A representative data set including the profile of the temperature (red), pressure (grey), thickness (black), voltage (blue) and applied current (pink) can be seen in Fig. 5.4b. A detailed description of this program can be found in the thesis of F. Kling.[260]

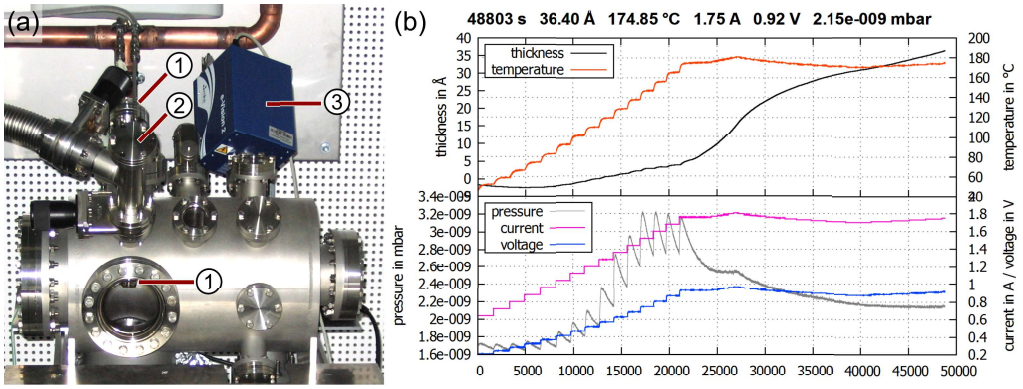

Fig. 5.4: (a) Molecular beam epitaxy (MBE) test chamber equipped with a quartz crystal micro balance (1), a sublimator position with a T-piece (2) and a quadrupole mass spectrometer eVision2 (3). (b) Representative data set of 3,3′-(1,3-butadiyne-1,4-diyl)bisbenzoic acid (3-BBA), including the profile of the temperature, pressure, thickness, voltage and applied current. (Photographic image (a) kindly provided by H. Adam)

Additionally, the mass spectrometer was running in most of the cases to gain further information about the sublimated molecule in the MBE test chamber and the preparation chamber. Spectra are attached in the appendix. When suitable parameters have been found at the MBE test chamber, the sublimator is mounted at one of the two T-pieces (6a, 6b) of the preparation chamber (PREP) (Fig. 5.1a), which allows for changing the molecular material without breaking the vacuum. After the translator with the crucible was moved into the chamber, the final sublimation position is about 90 mm apart from the sample. It must be pointed out that the gained sublimation data from the MBE test chamber cannot be taken one-to-one for the preparation chamber, since the used parameter are affected by the different volume of the chambers, the different distance of the sublimation positions and the inferior base pressure in the test chamber. Still the information gained at the MBE test chamber provides reliable starting parameter, which have to be only slightly modified for the UHV chamber.

The times and temperature to achieve a reproducible submonolayer coverage can be taken from the following table (Tab. 9.1).

Acronym	T_{Sub}/°C	r_{Sub}/ ML/min
3-EBA	30	- (mobile)
4-EBA	38	0.01
3-BBA	175	0.01
DETDCA	80/170	0.001/0.0015

Tab. 5.1: Overview about the times and temperature to achieve a reproducible submonolayer coverage with the used molecules. The acronyms can be found in subsection 5.4 "Molecules for on-Surface Synthesis on the Calcite (10.4) Surface" on page 38).

5.2.5 Annealing

The annealing experiments are performed with the implemented PBN heater attached below the heating stage of the manipulator. The temperatures given in this thesis are based on a calibration curve supplied by the manufacturer for this manipulator (see appendix Fig. 9.1). The used voltages and their conversion to temperatures are given in the following table (Tab. 5.2) and round to half decade. Nevertheless, this temperatures are only a rough estimate taken into account that the real temperature depends on the thickness of the crystal, the specific used sample holder, the thermal conductivity of calcite and the fact that the curve was originally recorded with a metal and not with a calcite sample.

Voltage/V	3	4	6	6.5	7	8	9	10	12
Temperature/°C	100	135	195	210	230	255	280	305	355
Temperature/K	375	410	470	485	505	530	555	580	625

Tab. 5.2: Temperatures (T) at the sample plate for specific voltages (V), according to calibration curve supplied by the manufacturer.

5.2.6 Irradiation

For all irradiation experiments, a UV-lamp (Peschl Ultraviolet GmbH, Mainz, Germany) with a spectrum shown in Fig. 9.3 was used.[261] The mercury-lamp (Hg-lamp) is mounted *ex-situ*, in front of a view port made of fused silica (VACOM Vakuum Komponenten & Messtechnik GmbH, Großlöbichau, Germany) with a lamp-sample distance of approximately 370 mm. The transmission as a function of wavelength and the power as a function of the distance are shown in the appendix (Fig. 9.2 and Fig. 9.4). In addition to the full Hg-spectra (Fig. 9.3), also a range can be employed by using appropriate filters of 256±10 nm and 302±23 nm (LOT-QuantumDesign GmbH, Darmstadt, Germany). The graphs concerning the transmission as a function of wavelength for both filters can be found in the appendix (Fig. 9.5 and Fig. 9.6).

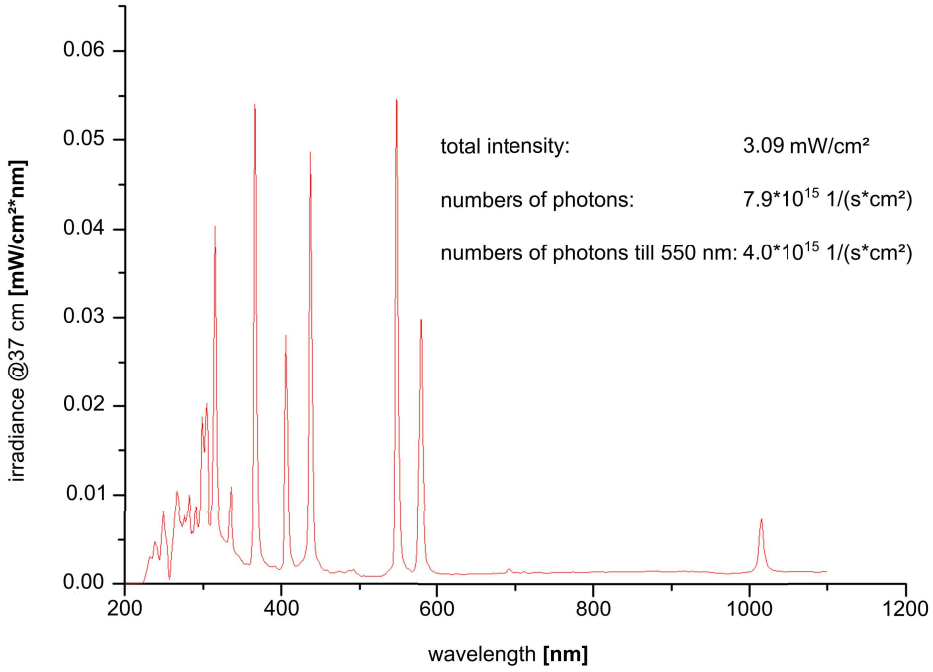

Fig. 5.5: Spectrum of the UV-Cube illustrated by the irradiance at a distance of 370 mm as a function of the wavelength, recorded according DIN 5031 part 10.[261]

5.3 Data Acquisition

The analyzes and processing of the images, shown in this thesis, is done with the open-source software Gwyddion (version: 2.46 and 2.48)[262] using the color package "reigreen". *Via* the program, the data was corrected for sample tilt[263] by using the plane-subtraction and, if necessary, a subtraction of a polynomial background or/and a three point-subtraction was done for large-scale images. If not stated otherwise, no further image treatment was applied. Depending on the visibility of the essential features either topography (z_p) images or detuning images (ν_{exc}) are shown. In all images a scale bar, the crystallographic directions and the slow (▲, ▼) and fast (▶, ◀) scan directions are shown. If necessary, the data was corrected for linear drift by using the self written programs "i12c" or "alphadrift" of F. Kling, which takes into account the lateral and vertical drift, as well as the calibration factors (f_x=0.83, f_y=0.91) for scaling in x and y.[260] In all topography images bright features correspond to high attractive interaction and dark features to low attractive or even repulsive tip sample interaction.[264] The used single and double color scale bars are shown in Fig. 5.6.

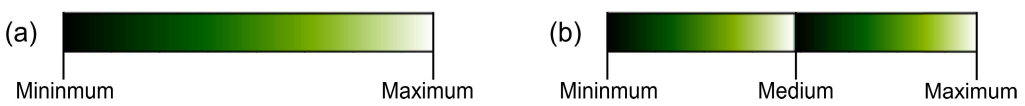

Fig. 5.6: Single (a) and double (b) color scales used for AFM images.

5.4 Molecules for On-Surface Synthesis on the Calcite (10.4) Surface

The molecules used in this thesis are synthesized by Chiara Venturini (CNRS, CEMES, Nanoscience Group) or Manuel Vilas-Varela (Centro de Investigación en Química Biolóxica e Materiais Moleculares (CIQUS) and Departamento de Química Orgánica, Universidade de Santiago de Compostela). In the following image, all tested molecules are presented and sorted according to the planned type of reaction.

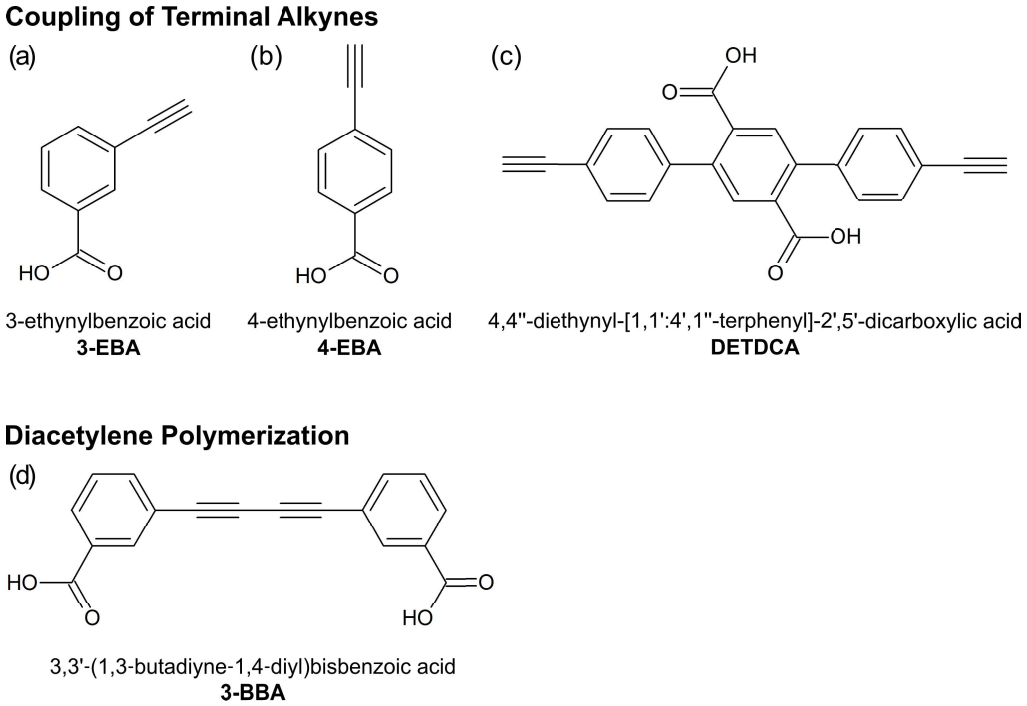

Fig. 5.7: Overview showing the tested molecules, sorted according to the planned reaction type.

6 Diacetylenes on Calcite (10.4)

This chapter is partly adapted from the article "Diacetylene polymerization on a bulk insulator surface" by A. Richter, V. Haapasilta, C. Venturini, R. Bechstein, A. Gourdon, A. Foster and A. Kühnle published in PCCP, 19, (2017), 15172-15176.[114] All AFM measurements and data analysis were performed by myself. The computational results were done and are kindly provided by V. Haapasilta of the group of A. Foster. Parts of the article are reproduced verbatim. The discussion has been extended when necessary.

6.1 Introduction

Initiating diacetylene polymerization of precursor molecules on surfaces has been recognized as a very promising concept for creating conductive polymer chains to connect functional molecular units.[116, 265] In the bulk, the solid state polymerization of diacetylene derivatives upon heating or light irradiation has been explained by a topochemical 1,4-polymerization.[266] For this reaction, the crystalline arrangement of the precursor monomers has been recognized as being of pivotal importance, as the acetylene units have to be within a distance of no more than 0.4 nm and the molecular backbones of two diacetylene monomers must form an angle close to 45° with respect to the crystal translational vector (Fig. 6.1a).[267] An elegant example of an on-surface polymerization initiated by a voltage pulse with the tip of a scanning tunnelling microscopy (STM) has been presented by M. Aono and co-worker (Fig. 6.1b-d).[91] In this seminal study, initiation and termination of the chain polymerization with remarkable nanoscale precision has been demonstrated using 10,12-nonacosadiynoic acid monomers on a graphite surface. The mechanism of the diacetylene polymerization is shown in Fig. 6.1. First an electronic excitation of single monomer occurs, *e.g.*, *via* a voltage pulse of a tip or irradiation with UV-light, within an array of diacetylene monomer molecules. This leads to the formation of a butatriene-type structure, containing a bi-radical with an unpaired electron at either end of the moiety and three double bonds in between (Fig. 6.1b). Second, caused by thermal movement, a neighboring molecule is approaching to the bi-radical, which initiates a subsequent addition reaction and results in a bi-radical dimer (Fig. 6.1c). Since the dimer has unpaired electrons at both ends, similar addition reactions can occur on either side, hence, maintaining in a chain polymerization (Fig. 6.1d).

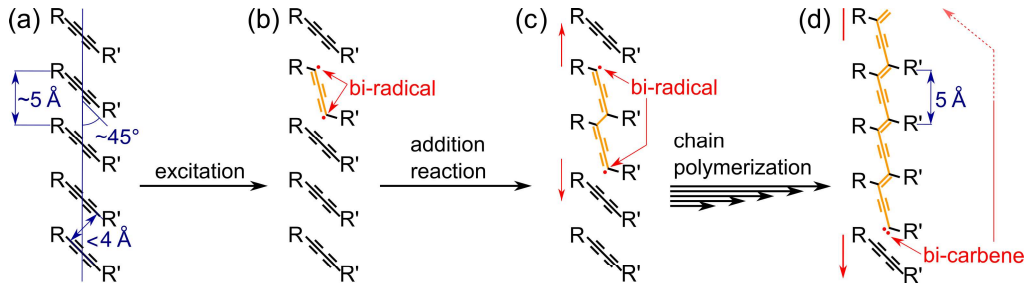

Fig. 6.1: (a) Topochemical requirements of the arrangement of the precursor units. (b) Formation of a bi-radical induced by, *e.g.*, electronic excitation or irradiation with UV-light. (c) Subsequent addition reaction under formation of a bi-radical dimer, so called butatriene-type structure. (d) Chain polymerization of the arranged precursor unit′s results in acetylene-type structure with a bi-carbene. Diacetylene reaction scheme inspired by Ref.[265]

With increasing chain length, a transition occurs from a butatriene-type structure with a bi-radical, containing two unpaired electrons (Fig. 6.1b,c) to the more stable acetylene-type structure with a bi-carbene, which exhibits four unpaired electrons on the ends (Fig. 6.1d).[268, 269] On the contrary to the addition reaction also a relaxation of the excited state monomer or dimer is possible, which would result in the ground state by dissipating the absorbed energy to the underlying substrate. This relaxation step can be suppressed by selection of a substrate with a high solid-state band gap, like calcite (band gap 5.9 eV), since the excitation energy of a diacetylene moiety is about 3.1 eV. Consequently, the suppression of the relaxation step results in an advanced lifetime of the excited states and therefore increases the probability of an addition reaction and hence of chain polymerization.[20]

By now, on-surface diacetylene polymerization has been reported for a large range of systems, including polymerization at the solid-liquid interface[270] as well as in air, [91, 271] and in ultra-high vacuum (UHV).[121, 123, 272] The majority of these studies have been carried out with a graphite support.[116, 270, 271, 273–276] Only a few other substrates have been studied for diacetylene polymerization, including, *e.g.*, Au(111),[121] MoS_2(0001)[116, 123] hexagonal boron nitride[20] and epitaxial graphene on SiC(0001).[21] Most importantly, no bulk insulator has been used so far. Besides, the above discussed expected advantages of bulk insulators concerning mechanistic aspect, they are also highly desired in the view of molecular electronics applications. Because bulk insulators offer the possibility of electronic decoupling of the functional molecular structures from the supporting substrate. Thus, when conductive polymer chains are intended to electrically connect functional units, bulk insulator substrates need to be explored.

6.2 3-BBA on Calcite

Here, we use 3,3′-(1,3-butadiyne-1,4- diyl)bisbenzoic acid (3-BBA) molecules (Fig. 6.2a) as precursors for on-surface diacetylene polymerization on the calcite (10.4) surface (Fig. 6.2b).

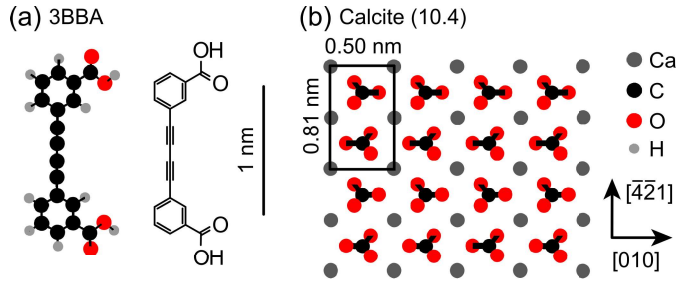

Fig. 6.2: The 3,3′-(1,3-butadiyne-1,4-diyl)bisbenzoic acid (3-BBA) precursor molecule (a) geometries after DFT optimization, yielding a planar structure (with skeletal formula) and the calcite (10.4) surface (b). The surface unit cell and the high symmetry surface directions are indicated. The scale bar applies to all subsets.

First, we investigated the structural arrangement of submonolayer coverage of 3-BBA deposited onto a freshly cleaved calcite (10.4) held at room temperature. The sublimation can be achieved using a self-made Knudsen cell with a cell temperature of around 450 K and a sublimation time of 25 min. As shown in Fig. 6.3a,b, the molecules self-assemble into molecular islands with an elongated shape. The island edges appear slightly fuzzy that is typically associated with attaching and detaching molecules and indicates a certain mobility of the precursor units. The long axis of the islands is oriented along the [010] calcite direction. A zoom into an island (Fig. 6.3c) shows a (1x3) superstructure forming bright rows along the [010] calcite direction. The apparent height of the islands is 0.6 nm, measured along

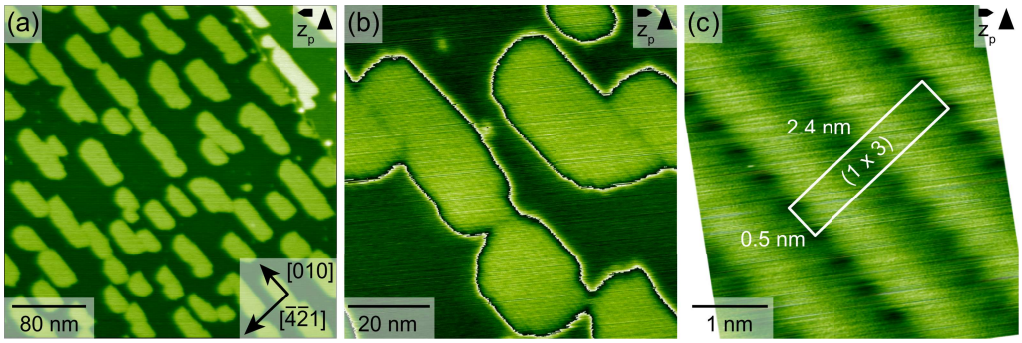

Fig. 6.3: Self-assembled molecular structures after sub-monolayer sublimation on a freshly cleaved calcite (10.4) surface held at room temperature in UHV. (a,b) Islands which exhibit an elongated shape appear to self-assemble on the surface (b) having a striped inner structure. (c) A zoom onto an island reveals a (1x3) inner structure with a unit cell marked with a white rectangular. The image is corrected for drift.

the white line in Fig. 6.4a, the corresponding height profile is shown in Fig. 6.4c. The islands consist of either an even or an odd number of rows as can be seen

in Fig. 6.4b. Furthermore, the neighboring rows are typically of different lengths, indicated by white arrows (Fig. 6.4a). Also a row termination within the island can be found, indicated by blue arrow in Fig. 6.4a. Together with the size of the precursor molecule, these AFM data suggests that there are two molecules within the (1x3) superstructure unit cell, that is, individual molecules cause the observed bright features. To obtain a more detailed molecular-level view of the formed structures,

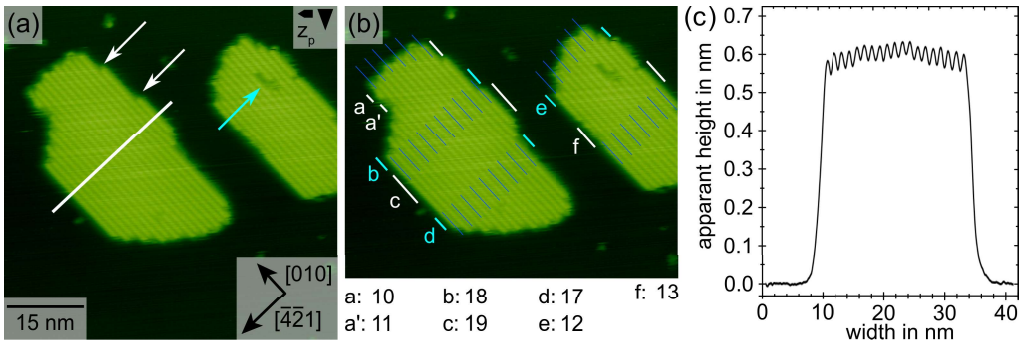

Fig. 6.4: (a,b) Molecular islands with striped inner structure. (a) Different lengths of neighboring rows, indicated by white arrows, and terminated rows in between the island indicated by blue arrow, are obtained. (b) Analysis reveals that the island patterns consist of either an even or odd number of rows as shown by the counted rows in between the areas a-g. (c) Height profile taken at the position, which is marked by the blue line (a). The scale bar, direction and scan directions applies to both subsets (a,b).

we performed DFT calculations and first-principles molecular dynamics (FPMD) simulations. A detailed description of the used computational methods and programs can be found elsewhere.[277] First, we investigated the adsorption of a single 3-BBA molecule onto the calcite (10.4) surface. The computations suggest that the preferred adsorption orientation is flat on the surface with both carboxyl (COOH) groups of the molecule forming hydrogen bonds with the calcite carbonate group oxygen atoms (Fig. 6.5a). According to the calculations, the adsorption energy is 2.4 eV, in line with room temperature adsorption and earlier calculations with similar molecules on calcite.[259] In a recent investigation, the biphenyl-4,4′-dicarboxylic acid (BPDCA) molecule, which also anchors to the surface *via* two COOH groups, was calculated to have several adsorption positions on calcite, all with similar energies.[259] Most probably, 3-BBA will also have several stable adsorption geometries with adsorption energies on the order of 2.4 eV. The lateral orientation shown in Fig. 6.5a is the one we consider most relevant towards the observed self-assembly pattern. However, the flat adsorption geometry adapted by the isolated 3-BBA molecule cannot be the orientation of the molecules in the self-assembled pattern: the flat orientation does not fit into the observed 0.5 nm repeat distance along the calcite [010] axis. This suggests that the individual molecules must be tilted upwards (see Fig. 9.11 and Fig. 9.12 in the appendix, subsection "Further Calculated Geometries" 9.5.1 on page 96). In the computations, a tilted molecular orientation emerges naturally when the molecules are brought close to each other. Fig. 6.5b shows such an optimized molecular geometry with the observed (1x3) superstructure periodicity, but with

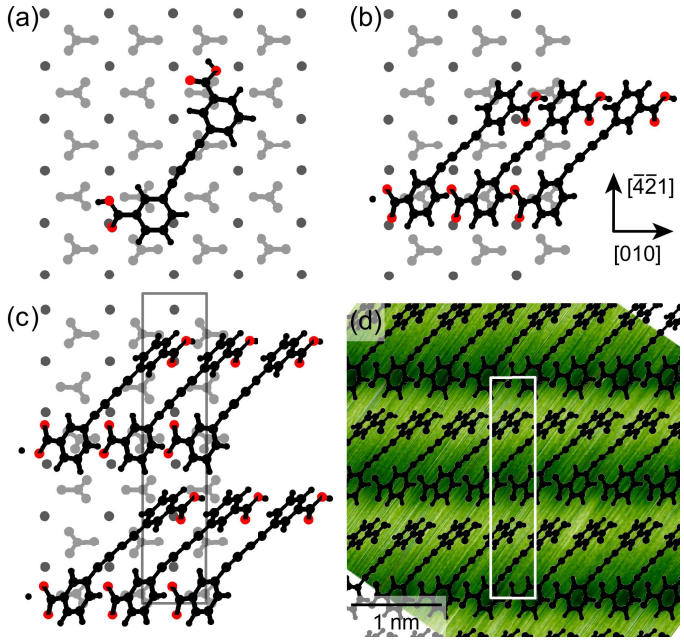

Fig. 6.5: Optimized isolated 3-BBA molecule (a), molecular row of 3-BBA molecules (b) and the molecular structure in the observed (1x3) arrangement (c) on the calcite (10.4) surface. In (c) and (d) the (1x3) supercell is indicated. For simplicity, carbonate groups are shown in light and calcium ions in dark grey, carbon atoms of the molecule are larger and hydrogen atoms smaller black spheres while oxygen atoms of the molecule are shown in red. In (d) the (1x3) arrangement is overlaid on top of an AFM image of the molecular island to illustrate the excellent match in size and pattern. Note that the absolute position of the overlay with respect to the image is unknown.

half the density, that is, one molecule in the (1x3) superstructure unit cell. Here, the adsorption (or the island formation) energy per molecule is 2.6 eV - there is a small favorable interaction between the molecules. In the optimized geometry, each 3-BBA molecule is still forming two hydrogen bonds with the surface. The two phenyl groups of a molecule form an angle of almost 90°. Finally, in Fig. 6.5c an optimized molecular structure corresponding to two molecules in the (1x3) superstructure unit cell is shown. In this case the adsorption/island formation energy per molecule is 2.7 eV. Here one of the two molecules in the (1x3) cell has the same bonding pattern as shown in Fig. 6.5b and the additional molecule is placed at a position 1.5 unit cell lengths along the [4̄2̄1] calcite direction. The additional molecule bonds *via* two hydrogen bonds and retains the rotated phenyl ring geometry. The calculated (1x3) superstructure is in excellent agreement with the experiments as is shown in the overlay in Fig. 6.5d.

Besides the above presented structure, also a second type of island can be found in some places on the surface (Fig. 6.6a). In the overview images it is not possible to distinguish between the two types of islands, because of their similar contrast and similar apparent height of approximately 0.6 nm (Fig. 6.4c and Fig. 6.6c). The long axis of the minority islands is oriented along the [4̄2̄1] calcite direction and

therefore, rotated by 90° compared to the main island structure as emphasized by the rectangular lines in Fig. 6.6a. A zoom onto an island (Fig. 6.6b) shows a (3x1) superstructure forming bright rows along the [4̄2̄1] calcite direction. Together with the size of the precursor molecule and the results of the DFT calculation of the main island type, these AFM data suggests that there is one molecule within the (3x1) superstructure. To illustrate a possible molecular arrangement an overlay on top of an AFM image is shown on the lower left part of Fig. 6.6b.

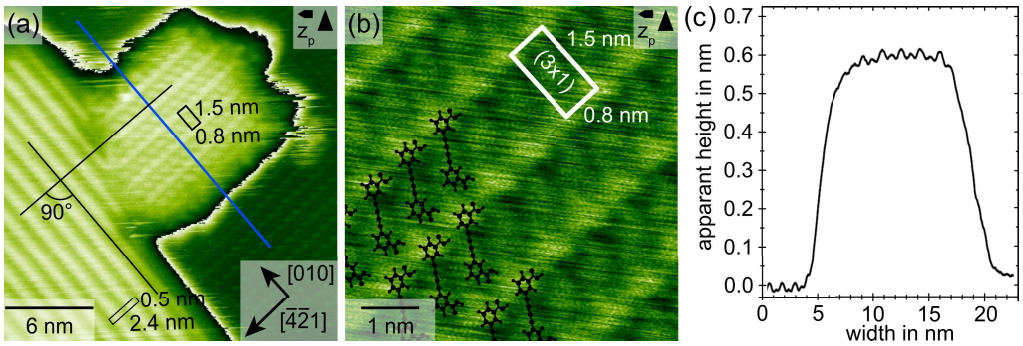

Fig. 6.6: (a) Main island structure (lower left corner) and minority island type (upper middle part) of 3-BBA. The inner stripe structure of both island types is perpendicular to each other, illustrated by the black lines. (b) A zoom onto an island reveals a (3x1) inner structure with a unit cell marked with a white rectangular. An overlay is shown on top of the AFM image to illustrate a possible orientation of the molecules. Both images (a,b) are corrected for drift. (c) Height profile taken at the position, which is marked by the blue line in (a).

For reducing the molecular mobility during the annealing experiments, also tests at high coverage have been performed. Increasing the coverage to nearly one monolayer can be achieved by a sublimation temperature of around 450 K and a sublimation time of approximately 5 h. In the obtained data, two additional characteristic observations can be made as is seen in Fig. 6.7a. First, very bright clusters can be

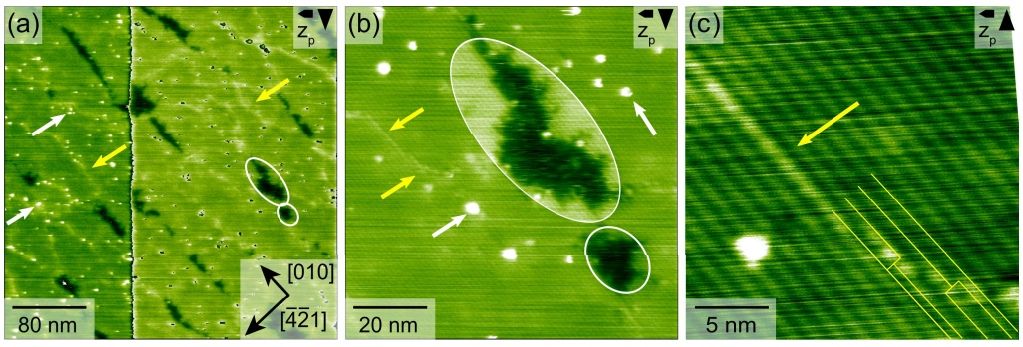

Fig. 6.7: Roughly one monolayer coverage of 3-BBA molecule self-assembled on the on the calcite (10.4) surface. Compared to low coverage three additional characteristic findings of the structure appear. (a,b) First streaky features marked with white ovals, indicative of diffusing molecular species. Second, bright clusters marked with white arrows which can be interpreted as contamination. Third, bright features marked with yellow arrow, indicative for island border. (c) Zoom in: Displacement of striped structure marked with yellow lines.

found on the surface, marked with white arrows in Fig. 6.7a-b. Since this inner

pattern could not be resolved, no further interpretation of the structure can be obtained. However, the long sublimation time of approximately 5 h requires to consider the possibility of contamination, coming from the preparation chamber or decomposition products during sublimation.
Second, bright one-dimensional features can be found on the surface, marked with yellow arrows in Fig. 6.7, which appear as stacking faults (displacement marked with yellow lines in Fig. 6.7c). Therefore, these features are interpreted as domain boundaries.
Additionally, "holes" with streaky features in between the striped structure are observed, indicative of diffusing molecular species marked with white ovals in Fig. 6.7a-b. Since the islands edges at low coverage appear slightly fuzzy, which is typically associated with attaching and detaching molecules, the mobility of the precursor molecules, which are not staying in the island structure, has most probably not changed, but is now more obvious detectable in the images.

6.3 Changes Induced by Annealing

Annealing the molecule-covered substrate at 485 K for 1 h results in three structural changes as can be seen in Fig. 6.8a. The number of islands has decreased and clusters have formed on the surface. Most importantly, single stripes oriented along the [010] direction have formed. These stripes can be up to 60 nm long. Most of them appear to be connected to an island, but also separated stripes can be found. Additionally,

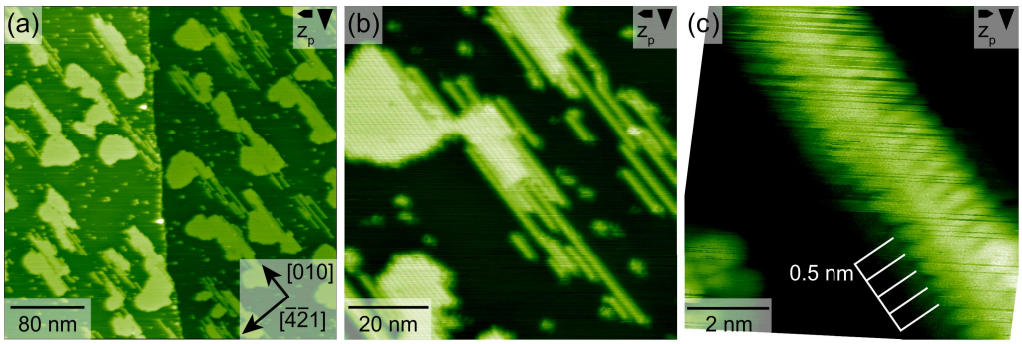

Fig. 6.8: Molecular structures after annealing. (a,b) Upon annealing at 485 K for 1 h, three distinct changes are observed: The number of islands has decreased. Clusters are formed. Most importantly, molecular rows exist on the surface. (c) Zoom onto a chain-like molecular row.

also changes in between the island structure can be found. The formerly uniform inner structure is now heterogeneous with darker rows (marked with blue arrows in Fig. 6.9) next to bright rows. The difference in apparent height between darker and bright rows appears somewhat smaller with approximately 0.02 nm. Hence, it

can be assumed, that the change of the inner-island rows is induced by the same molecular transformation as for the chain-like structures described before.

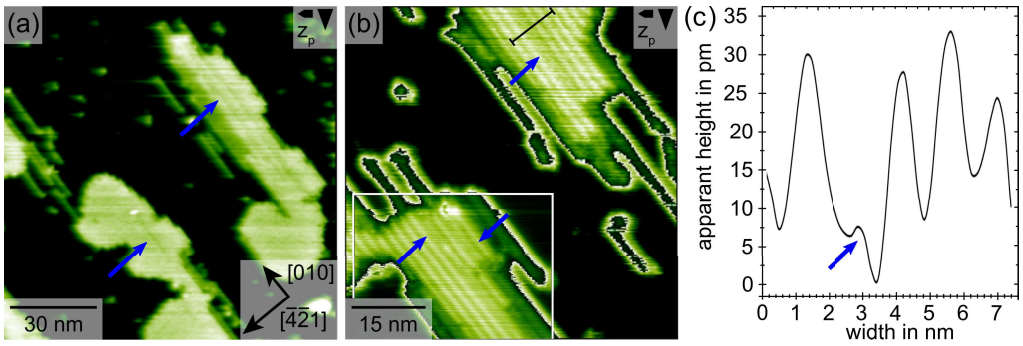

Fig. 6.9: (a,b) Molecular structure upon annealing at 485 K for 1 h. Breakup of the former homogeneous inner island structure by the appearance of rows with lower apparent height, marked with blue arrows. (c) Height profile taken at the position, which is marked by the black line in (b), averaged over 13 pixels.

When annealing instead at 520 K for 1 h the described structural changes advance further. Then, fewer islands are found while more clusters and even longer stripes have formed. After annealing at 555 K for 1 h, the islands have disappeared completely and only clusters and stripes are present on the surface as can be seen in Fig. 6.10. The fact that the stripes are more stable upon annealing than the

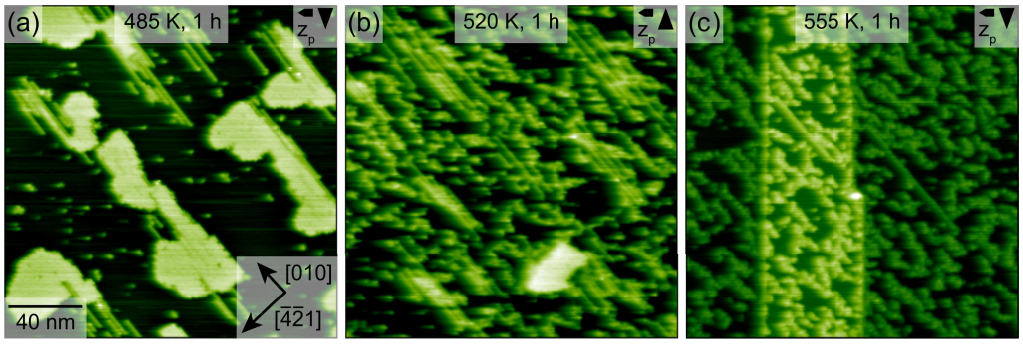

Fig. 6.10: Molecular structures after annealing. (a) Upon annealing at 485 K for 1 h, three distinct changes are observed: The number of islands has decreased. Clusters are formed. Most importantly, molecular rows exist on the surface. (b) Upon annealing at 520 K for 1 h the described changes in (a) advanced further (c) Upon annealing at 555 K for 1 h, the islands have disappeared completely and only clusters and stripes are present on the surface. The scale bar applies to all subsets.

islands indicates a stronger molecule-molecule interaction within the stripes as compared to within the island structure. These results suggest a covalent linkage of the precursors leading to a one-dimensional structure of superior thermal stability as compared to the self-assembled islands. From the high-resolution image of a single stripe (Fig. 6.8c), a periodic structure in the [010] direction with a repeat distance of 0.5 nm, in registry with the calcite surface, can be determined. This is strong indication for a successful diacetylene polymerization of the precursors on the (10.4) surface of calcite. To follow this hypothesis, we performed DFT

computations starting with the calculated island geometries. We identified several polymerized covalently bonded structures with 0.5 nm repeat distance along the [010] calcite direction. The most stable polymerized structure is shown in Fig. 6.11a. Further calculated geometries can be found in the appendix (subsection "Further Calculated Geometries" 9.5.1 on page 96). According to the optimization, the

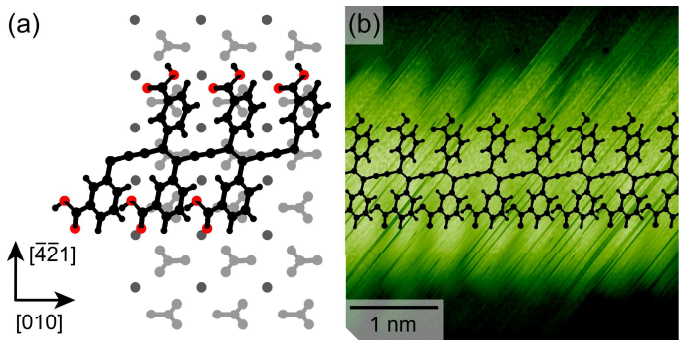

Fig. 6.11: Molecular structures after annealing. (a) Optimized polymerized molecular structure from DFT (colours as in Fig. 6.5). (b) Zoom onto a chain-like molecular row with superimposed diacetylene polymer structure from DFT.

polymerized configuration is 3.9 eV per molecule, *i.e.*, 1.2 eV more stable (per molecule) than the non-covalently bound (1x3) superstructure. In the experiments, the apparent height of the stripes is approximately 0.5 nm, *i.e.*, 0.1 nm lower than the islands. DFT optimization calculations report heights of 0.7 nm and 0.6 nm for the islands and polymer stripes, respectively, in qualitative agreement with the experiments. The striped structure of the polymer from DFT calculations is shown as an overlay in Fig. 6.8d. Again, the agreement between the experiments and theory is good. The favourable molecule-molecule distance for diacetylene polymerization has been identified to be in the range of 0.47 to 0.52 nm with an angle of 45° for the molecular axis with respect to the crystal translation,[267] which is perfectly matched in the main molecular islands formed prior to annealing: the molecule-molecule distance along the [010] direction is 0.5 nm as indicated in Fig. 6.3c. Based on DFT calculations the resulting distance between the diacetylene moieties in the majority islands is 0.36 nm. Therefore, it appears that the self-assembly of 3-BBA molecules on calcite (10.4) surface produces ideal conditions for polymer chain formation along the [010] surface direction. The reported islands, as well as the stripes, are stable on the surface at room temperature for several days when stored in the UHV chamber. This is further evidence that the observed structural changes were, indeed, induced by the annealing procedure. The observed clusters can be interpreted as by-products of the on-surface linking reaction. The molecules are obviously able to diffuse on the surface during the heating process and can, therefore, form a variety of reaction products. Moreover, the precursor arrangement favorable to initiate this topochemical reaction is obviously lost as soon as molecules start to diffuse. Consequently, a higher initial coverage - which reduces the molecules′ mobility - should lead to a suppression of byproduct formation and an increased yield for stripe

formation.

Therefore, in an attempt to increase the reaction yield, we also studied higher coverage upon annealing. Fig. 6.12c-f shows a calcite (10.4) surface that was covered with a full monolayer of the precursors after annealing the surface at 375 K for 12 h (c,d) and 520 K for 1 h (e,f). As expected, much fewer clusters are formed.

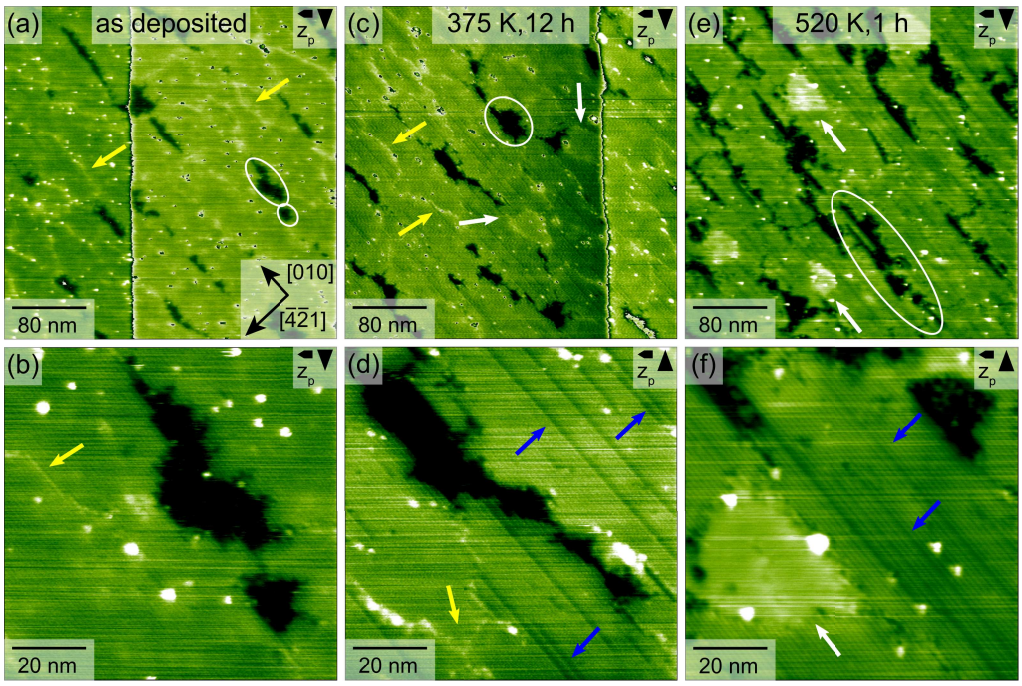

Fig. 6.12: (a,b) Molecular structures of roughly 1 ML coverage before annealing and after annealing the surface at 375 K for 12 h (c,d) and 520 K for 1 h (e,f).

Additionally, the same darker rows within the islands are obtained, marked with blue arrows in Fig. 6.12d,f. In contrast to the lower coverage, no separated stripes with an apparent height of 0.5 nm can be found. Due to the fact that nearly the whole surface is covered with the molecules, there is no space for their formation. Moreover, an annealing at 520 K again leads to a distinguishable change in coverage *via* desorption, comparable to Fig. 6.10b. Furthermore, the domain borders, which are still visible after annealing the sample to 375 K, have vanished completely upon annealing to 520 K. This can be caused either by the diffusion of the molecules transferring the domain borders to the island edges or by desorption of molecules leading to more space between the domains. Surprisingly, the formerly almost invisible minority island becomes more pronounced after each annealing step. In contrast to the main island type, no change in the inner structure can be found. This missing transformation in the minority island structure can be interpreted as no reaction has taken place. Therefore, the emerging difference in the apparent height of the two island types probable originates from a different interaction of the tip with the unreacted (minority islands) and the reacted molecules (main island

type). If the same transformation would have taken place in between both island types, no difference in the apparent height should be measured after annealing as it was the case for both as deposited (unreacted) island types before the annealing. A possible explanation why no reaction has taken place in the minority island structure could be, that the found periodicity of 0.8 nm in the $[42\bar{1}]$ direction does not fulfill the topochemical requirements Fig. 6.1. Hence, the observed distance between the molecular precursors would be too large. Furthermore, even the desired diacetylene structure with a resulting repeating distance of 0.5 nm, would lead to a significant mismatch with the underlying calcite substrate in the $[42\bar{1}]$ direction. Therefore, a failed initiation of the diacetylene polymerization is most probably caused by the underlying calcite lattice, which seem to hinder the on-surface reaction in the case of the minority island structure.

6.4 Changes Induced by Irradiation

The irradiation with the full Hg-lamp spectrum of a sample covered with a submonolayer of 3-BBA for approximately 12 hours results in the appearance of very irregular island edges while the overall island shape remains largely unchanged (Fig. 6.13a). When zooming onto an island, several structural changes can be seen in Figs. 6.13b,c.

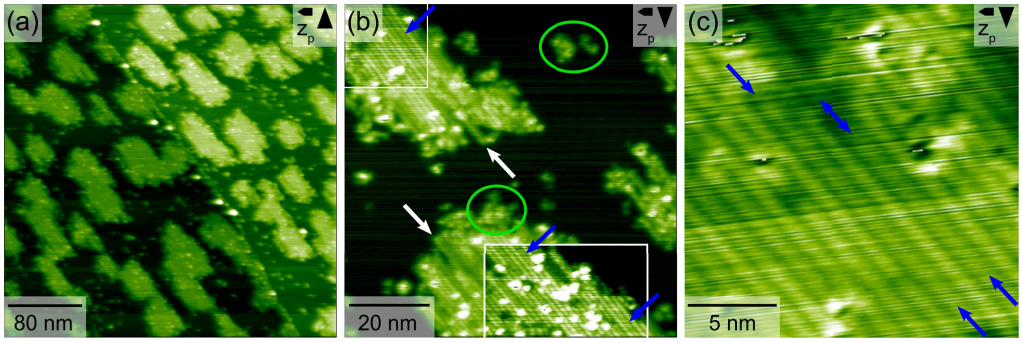

Fig. 6.13: Upon irradiation for approximately 12 hours with the full spectrum of the Hg-lamp, several changes are obtained. (a) The overall island shape remains largely unchanged, while the island edges appear very irregular. (b) A zoom onto an island reveals the formation of conglomerate structures (marked with green circulars). More importantly, single stripes with a lower apparent height, connected to islands or conglomerates (marked with white arrows), have formed. Finally, also darker appearing rows leading to an inhomogeneous inner island structure can be found, marked with blue arrows.

First of all, conglomerate structures (marked with green circulars) can be found, which appear connected to an island, but also exist separately on the surface.
Second, randomly distributed clusters are located on the islands.
Most importantly, again the formerly homogeneous inner island structure contains now darker appearing rows (marked with blue arrows in Figs. 6.13b,c) and single stripes with a difference in apparent height of approximately 0.1 nm compared to the inner island rows have been formed. These single stripes can be attached to

an island or a conglomerate structure (marked with white arrows in Figs. 6.13b). Since the same basic structural changes can be discovered upon annealing (Fig. 6.8 and Fig. 6.9) and irradiation (Figs. 6.13), it can be concluded that they presumably originated from the same molecular transformation. The additional clusters and conglomerates may result on the one hand, from using a broad range of wavelengths initiating not only the desired reaction but leading to further side-products.[278] On the other hand the mobility of monomer precursors may also lead to the formation of side-products, since the orientation of two monomer molecules next to each other, may also influence the reaction pathway. Therefore, it is expected that reducing the molecular mobility by increasing the coverage is beneficial for the diacetylene polymerization, as this forces the molecules to stay in the island structure. This fixed arrangement of the molecular precursors appears to be favourable for the topochemical reaction.

In order to prevent side-reactions, a range of wavelengths was tested, being within the absorption band of the triple-bond system and therefore enabling the polymerization in accordance to the literature.[21, 270] This reduced spectra, on the one hand side, decreases the thermal input by decreasing the transferred power to the surface. On the other hand, also degradation processes initiated by larger wavelengths can be avoided, which are known to happen in solution.[278] The preferred spectra was obtained by using a (302 $\pm$ 23) nm filter and a (256 $\pm$ 10) nm filter. Only little changes could be obtained by using a (256 $\pm$ 10) nm filter (see Fig. 9.9 in the appendix).

Irradiation of the molecular covered sample for approximately 15 hours using a (302 $\pm$ 23) nm filter leads to much less clusters and no conglomerates, while the change in the inner-island structure is again obtained (marked with blue arrows in Fig. 6.14. A zoom onto an island structure clearly shows that the periodicity in the [010] direction is still 0.5 nm (Fig. 6.14c). Additional, darker rows appear

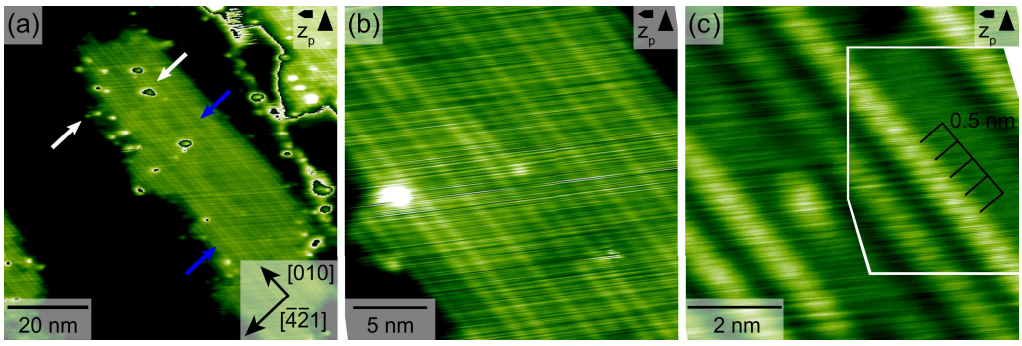

Fig. 6.14: Molecular structures after irradiation with a Hg-lamp using a (302 $\pm$ 23) nm filter for approximately 15 h. (a) The overall island shape remains unchanged, while a few clusters appear (marked with white arrows) and, importantly, darker rows within the formerly regular island are visible (marked with blue arrows). (b) Zoom onto the island showing the distribution between brighter and darker rows, appearing alternately but also paired or tripled. (c) A further zoom clearly reveals the unchanged periodicity in the [010] direction of 0.5 nm. The image is corrected for drift.

often alternately to bright rows, while the existence of two darker ones next to each other seems very rare. In contrast, the arrangement of several bright rows next to each other can be observed frequently. A possible explanation could have been that the reacted structures require a larger space per row in the $[\bar{4}\bar{2}1]$ direction. This, can be disproved by the comparison of the apparent height profiles before and after irradiation (Fig. 6.15, showing no significant difference in width). Furthermore, the irradiation time could have been too low, so that the reaction is still not completed. Unfortunately, no further long-term irradiation test was done to investigate this.

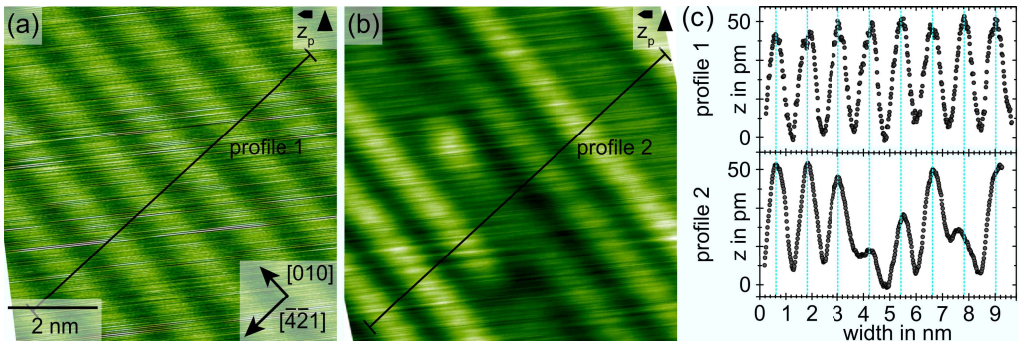

Fig. 6.15: (a) Self-assembly of the as-deposited molecular precursors, including the line profile 1, marked with a black line. (b) Molecular structures after irradiation with a Hg-lamp using a (302 ± 23) nm filter. The position of profile 2 is indicated. A change in brightness of individual molecular rows can be observed. (c) Comparison of the line profiles from (a) and (b), revealing no significant change in the intermolecular distances in the $[\bar{4}\bar{2}1]$ direction. Both AFM images are corrected for drift.

Even combined annealing and irradiation tests were done, which should lead to an entire change of the islands to striped structures. For these tests, a temperature of 375 K was chosen, which does not lead to a detectable desorption or formation of by-products, visible as conglomerations or clusters. Indeed, no significant change between the irradiation with the full Hg-spectra with and without heating the sample can be detected. Moreover, a distinct difference is obtained between the major islands and the minor self-assembled island structure, oriented in the $[\bar{4}\bar{2}1]$ direction (Fig. 6.16). The inner structure of the minor island type still appears homogeneous with a (3x1) superstructure (Fig. 6.16b,c) after combined annealing and irradiation, while darker rows can be observed in the inner structure of the major islands. Hence, no change of the inner structure of the minor islands was obtained. Additionally, much less clusters can be observed on the minor island type. Therefore, the experimental results give no indication that a reaction has taken place in the minor island structure. A possible reason why no diacetylene polymerization has taken place, is probably due to the following facts. Firstly, the arrangement of the monomer precursor has a periodicity of 0.8 nm in the $[\bar{4}\bar{2}1]$ direction, which does not fulfill the topochemical requirements. Hence, the distance of the monomer precursors in the island structure would be too large for the reaction. Secondly, the resulting diacetylene polymer structure, as was calculated by DFT (see Fig. 9.14

in the appendix) has a distance of the repeating units of 0.5 nm. Therefore, a mismatch between the polymer structure and the underlying calcite lattice in the $[\bar{4}\bar{2}1]$ direction is expected.

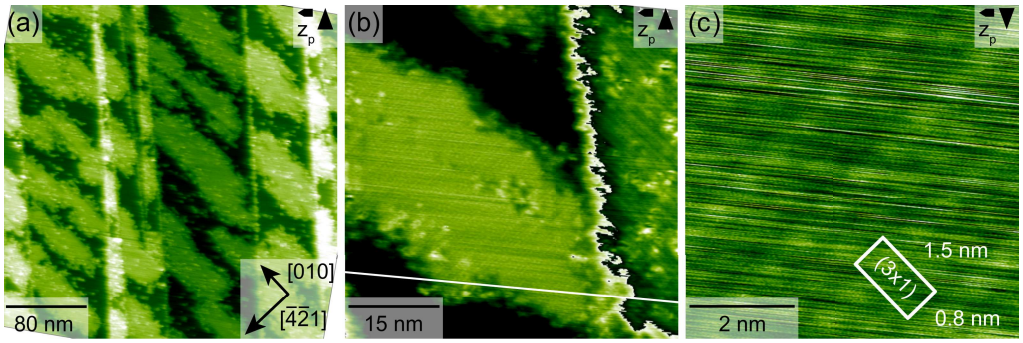

Fig. 6.16: Molecular structures after combined annealing and irradiation test for approximately 13 h. (a) Conglomerates and clusters appear, while the overall island shape remains largely unchanged except for the now irregular appearing island edges. (b) A zoom reveals the difference between the inner island change of the main type on the right side and the unchanged homogeneous inner island structure of the minority type on the left. (c) Zoom onto the minority type island reveals a (3x1) superstructure. The image is corrected for drift.

6.5 Conclusions

In conclusion, we present evidence for a diacetylene polymerization conducted on a bulk insulator surface. Using dynamic AFM operated in UHV, we show that 3,3′-(1,3- butadiyne-1,4-diyl)bisbenzoic acid precursor molecules deposited on calcite (10.4) form two types of ordered islands. The majority type reveals a (1x3) inner structure, while the minority island type exhibits a (3x1) superstructure. Additional, both island types are composed of rows running either in the [010] (majority type) or the $[42\bar{1}]$ (minority type) direction. Hence, the found arrangements are perpendicular to each other. Detailed density functional theory (DFT) calculations provide insights into the structure formation of the majority island type. The arrangement of the molecules within these islands is governed by a π-π interaction of the aromatic rings. Additional, the molecules adopt a relative orientation and spacing in this arrangement that is required for the topochemical diacetylene polymerization. To initiate the reaction, thermal, photochemical and combined stimulation experiments were performed. Irradiation of the surface with a mercury lamp or annealing the substrate to 485 K results in a distinct change in the self-assembled structures of the major islands. Besides the islands, newly formed clusters and row-like structures appear on the surface. These row-like-structures are observed separately on the surface or in between the former homogenous island structure. Furthermore, they exhibit the same inner pattern compared to the as deposited self-assembled molecules, but are imaged with a smaller apparent height. In case of the majority structure, DFT computations provides an energy gain of 1.2 eV per formed diacetylene monomer

unit. The obtained row-like structures excellently match the expected polymer chains in appearance and repeat distance. Further experiments demonstrate, that the reduction of the molecular mobility by increasing the coverage results in the decrease of the by-products, while the polymerization reaction still can be detected. Hence a high coverage is beneficial for the diacetylene polymerization, as this forces the molecules to stay in the island structure at elevated temperatures, which appears to be favorable for the topochemical reaction. In contrast, for the minority island type, no structural change upon annealing or irradiation is obtained, suggesting that no reaction has taken place. This difference in reactivity of the two arrangements can be explained by considering the dimensions of the underlying substrate. The specific substrate directions meet the required dimensions of the diacetylene polymerization and the final product for the majority island, while it does not for the minority island arrangement. Therefore the difference in reactivity provides evidence for a templating effect of the underlying calcite (10.4) surface. This work provides experimental and theoretical evidence for the concept of diacetylene polymerization on bulk insulator surfaces.

7 Terminal Alkynes on Calcite (10.4)

This chapter is partly adapted from the annual PAMS report 2017,[279] the article "Generic nature of long-range repulsion mechanism on a bulk insulator?" by J. L. Neff, A. Richter, H. Söngen, C. Venturini, A. Gourdon, R. Bechstein and A. Kühnle published in Faraday Discussion, 204, (2017), 419-428[79] and the article "Homocoupling of Terminal Alkynes on Calcite (10.4)" by A. Richter, M. Vilas-Varela, D. Peña, R. Bechstein and A. Kühnle published in Surface Science, (2017), 1-6.[132] All AFM measurements and data analysis were performed by myself. The computational results were obtained and are kindly provided by V. Haapasilta from the group of A. Foster. Parts of the articles and report are reproduced verbatim. The discussion has been extended when necessary.

7.1 Introduction

To enlarge the possible linking schemes for on-surface reactions, molecules with functional groups like terminal alkynes have been investigated. An overview of possible reaction pathways of this molecular moiety is shown in Fig. 7.1.

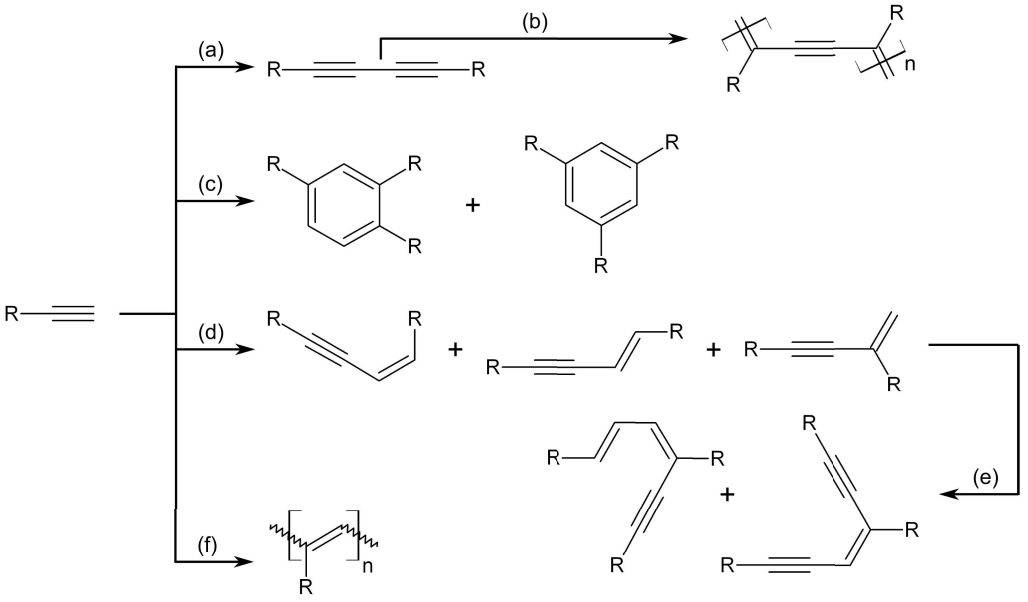

Fig. 7.1: Overview of reaction pathways based on terminal alkynes, namely (a) homocoupling of terminal alkynes with possible subsequent (b) diacetylene polymerization, (c) alkyne cyclotrimerization (d) alkyne dimerization, forming enynes with (e) further subsequent trimerization reaction and (f) acetylene polymerization.

One possible reaction of this class of molecules is the Glaser-inspired homocoupling[280] (Fig. 7.1a), which has been explored as a route to couple terminal alkynes and construct rigid linear linkers.[12, 281] This reaction leads to diacetylene moieties, which can subsequently undergo a diacetylene polymerization (Fig. 7.1b), as has been demonstrated in the previous chapter 6. The Glaser-inspired homocoupling has first been presented using 1,3,5-triethynyl-benzene (TEB) on a silver (111) surface,[127] and is now well studied on a wide range of conductive surfaces.[97–99, 282] Also, photochemical activation as an alternative route to annealing has been successfully presented.[99, 100] A detailed theoretical study has been devoted to unravel the molecular reaction mechanism of TEB linking on Ag(111) and to uncover the role of the surface, which is explained by constraining the molecular motion rather than contributing chemically in terms of electron transfer.[129] A comparison of the classical solvent-based and on-surface mediated reaction mechanisms is shown in the following figure (Fig. 7.2).

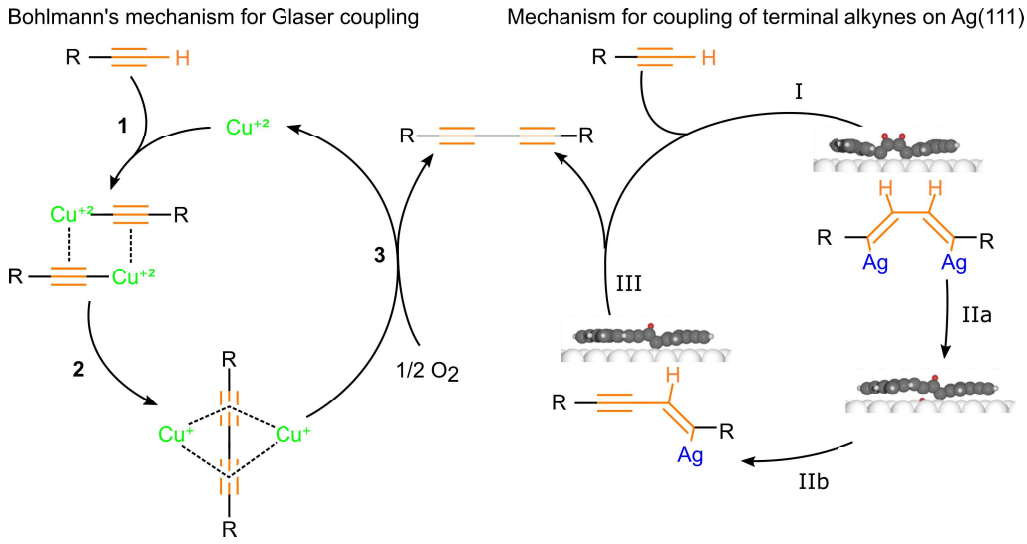

Fig. 7.2: The Mechanism proposed by Bohlmann *et al.*[283] for the classical Glaser coupling is shown on the left. The coupling mechanism of 1,3,5-triethynyl-benzene on Ag(111) proposed by Björk *et al.*[129] is illustrated on the right. Adapted from Ref.[12, 129]

The mechanism of the classical Glaser coupling is intricate and not fully understood, albeit it is known that the reaction depends strongly on experimental conditions.[12] The most accepted mechanism was proposed by Bohlmann *et al.* in 1963.[283]
In the first step (1), the reaction proceeds *via* a deprotonation of the terminal alkyne and a subsequent formation of a dinuclear Cu(II)alkynide complex. Afterwards (2,) an electron transfer from the alkynide anion to the Cu(II)-cation within the cupper-complex takes place, resulting in the reduction to Cu(I). In the last step (3), the complex is collapsing to the symmetric 1,3-diyne product, while the catalyst is regenerated by an oxidation of the Cu(I) *via* oxygen.[281]
In contrast to the classical mechanism in wet chemistry, the on-surface reaction starts not with a splitting off of hydrogen, but by the coupling of two TEB molecules.

This coupling leads to an intermediate state, a covalent nondehydrogenated dimer with a *cis* configuration (I). Then two dehydrogenation processes take place, which are assumed to be rate-limiting (II/III). To split off the first hydrogen, initially an intermediate state with a *trans* configuration (IIa) is obtained, followed by the formation of the first dehydrogenation transition state (IIb). Thereafter, the second dehydrogenation step (III) occurs, which is a single barrier process. Moreover, also the influence of the molecular mobility on the surface was investigated. It was found that the barrier for the diffusion is small compared to all other reaction steps. Hence, it is not the rate-determining step.

Besides the above described homocoupling, also (c) cyclotrimerization and (d) dimerization reactions, forming enynes, (Fig. 7.1c,d) as well as further trimerization reactions to the before generated dimers (Fig. 7.1e) are known to happen on the surface. However, these products are usually described as by-products.[97, 98]

Moreover, terminal alkynes are also known for acetylene polymerization (Fig. 7.1f). The first and probably most famous polymerization of acetylenes to a linear conjugated polymer was done by Natta *et al.* in 1958 using a $Ti(OBu)_4/AlEt_3$ catalyst.[284] With a modified synthesis route and an additional subsequent doping, this later on leads to the first conductive polymers.[62–64] Besides the nowadays immense number of applicable catalyst systems,[285–287] also reaction pathways in absence of metal catalysts have been explored.[288–290] Depending on the experimental conditions, there exist four stereoconformations in a polyacetylene chain, namely (a) *trans-transoidal*, (b) *trans-cisoidal*, (c) *cis-transoidal* and (d) *cis-cisoidal* diastereomers (Fig. 7.3)[291] as well as mixtures of them.

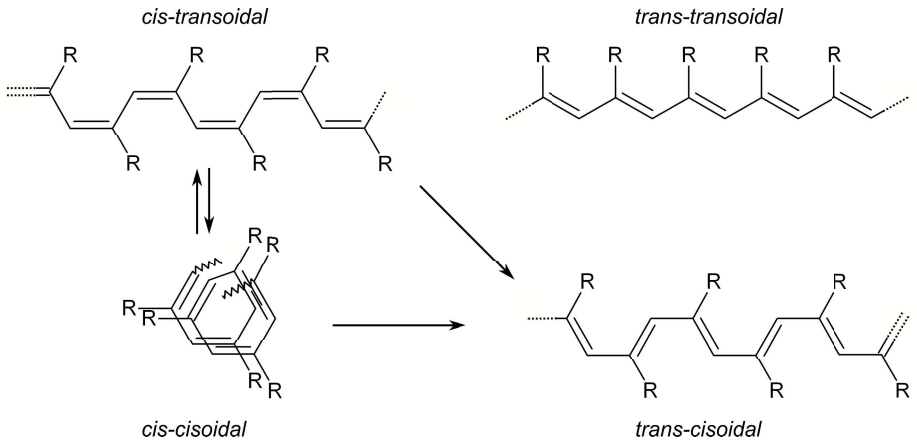

Fig. 7.3: Isomers obtained upon acetylene polymerization, namely (a) *trans-transoidal*, (b) *trans-cisoidal*, (c) *cis-transoidal* and (d) *cis-cisoidal* diastereomers. Adapted from Ref.[291]

Comparable to the diacetylene polymerization, also polyacetylenes can be obtained *via* a solid state reaction upon annealing or irradiation.[292–294] One might assume that the acetylene polymerization is as well based on a topochemical mechanism as is discussed for the polydiacetylene in the previous chapter. However, according to the literature this seems to be true only for the formation of dimers, trimers and

small oligomers, since the ongoing reaction leads to a phase separation. Hence, the mechanism is not only based on the orientation of the monomer in the crystal, but in an intense scope on the molecular mobility. Therefore, the entire polymerization is not a regular topochemical reaction, since the obtained phase separation suggests that the center of gravity of the molecules move from their proper lattice site, leading to an inhomogeneous reaction inside the parent crystal.[295] To overcome this geometrical difference in the crystal structures of the educt and product, several experimental conditions like varied molecular building blocks or high pressure at different temperatures have been investigated. Nevertheless, none of the so far used parameters could avoid the loss in crystallinity towards an amorphous system during the reaction.[288, 290, 293, 296, 297] To gain further inside into the mechanism, also the stability of the acetylene polymer has been investigated. The annealing of, *e.g.*, solid poly(4-carboxyphenyl) acetylene leads to a complete transformation to the cyclic trimer. This finding suggests that a head-to-tail reaction of the before generated polyacetylene has to take place, since only the symmetric cyclic trimer could be identified.[288] Furthermore, various *cis-trans* isomerization processes have been reported, activated, *e.g.*, by heating,[291] photonic[298] and ultrasonic irradiations.[299] These isomerization processes have been proposed to proceed through a radical mechanism. Accordingly, it can be concluded that also the reaction itself, initiated upon annealing or irradiation, is most probable proceeding *via* a radical mechanism. Nevertheless, a final mechanism of an acetylene polymerization in solid state is so far not available and needs further investigation. Besides, it seems that the mechanism is very much affected by the choice of the molecule and the used reaction parameters. The first and so far only on-surface synthesis of an oligo-acetylene was presented by Riss *et al.* on a Au(111) surface using an (E)-1,1′-bi(indenylidene) monomer (Fig. 7.4a).[136] In contrast to the solid-state reaction, no influence of the monomer

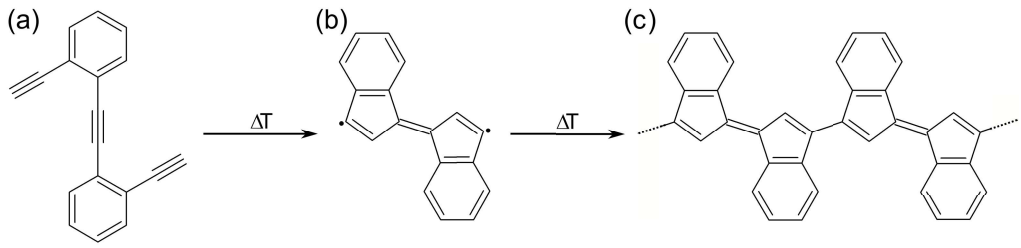

Fig. 7.4: Scheme of the thermally induced on-surface reaction of (E)-1,1′-bi(indenylidene) on Au(111). First the (a) monomer reacts to (b) a 3,3′-diradical intermediate *via* an intramolecular C1-C5 enediyne cyclization. Subsequent recombination with monomers lead to the formation of (c) an oligo acetylene. Adapted from Riss *et al.*[136]

orientation is proposed, since the first proposed reaction step is an intramolecular C1-C5 enediyne cyclization, leading to (b) a highly reactive 3,3′-diradical intermediate. Due to the diffusion of monomers and diradicals along the Au(111) surface, a subsequent recombination takes place which by a step-growth process leads to (c) an acetylene oligomer.

In the view of the growing body of research dedicated to reactions of terminal alkynes on metal substrates it is interesting to raise the question as to whether these reactions can also be achieved on a bulk insulator surface. For these purpose, we investigate 3-ethynylbenzoic acid (3-EBA), 4-ethynylbenzoic acid (4-EBA) and 4,4″-diethynyl-[1,1′:4′,1″-terphenyl]-2′,5′-dicarboxylic acid (DETDCA) (Fig. 7.5) on a well-known bulk insulating surface, calcite (10.4). For further analysis the homocoupled products

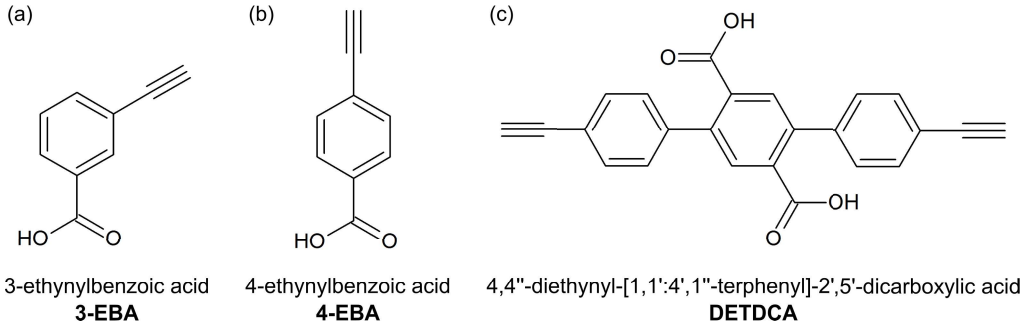

Fig. 7.5: All molecules tested for on-surface reactions of terminal alkynes.

of 3-EBA and 4-EBA, namely 3,3′-(1,3-butadiyne-1,4-diyl)bisbenzoic acid (3-BBA) and 4,4′-(1,3-butadiyne-1,4-diyl)bisbenzoic acid (4-BBA), have been synthesized by C. Venturini. Ideally, this allows for a comparison of the self-assembly of the dimers 3-BBA/4-BBA with the annealed/irradiated structures of 3-EBA/4-EBA on the surface. Unfortunately, it was not possible to deposit 4-BBA in a reproducible manner on the surface. Therefore, only a comparison between reacted 3-EBA structures and 3-BBA is possible.

7.2 3-Ethinylbenzoic Acid on Calcite (10.4)

3-Ethinylbenzoic acid (3-EBA) can be sublimated and deposited on calcite (10.4) in a reproducible manner. For additional analysis, mass spectra were recorded during the sublimation tests. One spectrum is exemplary attached in the appendix (Fig. 9.8). After sublimation at a crucible temperature of 305 K for 10 min, only fuzzy structures of mobile molecules are observed on the surface (Fig. 7.6). To reduce the molecular mobility, a usual procedure is increasing the coverage to approximately 1 ML. However, this seems not to be feasible for this molecule. Even though several sublimation conditions were tried, no pattern could be obtained. Nevertheless, by comparing with similar benzoic acid molecules an assumption of the interaction between 3-EBA and the calcite (10.4) surface can be made. For this purpose, an extensive AFM and computational study of 2,5-dihydroxybenzoic acid (DHBA) on calcite[236] will be discussed. Depending on the temperature hydrogen bonded dimers of DHBA coexist with monomers forming strong molecule-surface interactions on the (10.4 calcite surface. The existence of hydrogen bonded dimers is explained by their direct deposition from the bulk. The breaking of the intermolecular hydrogen

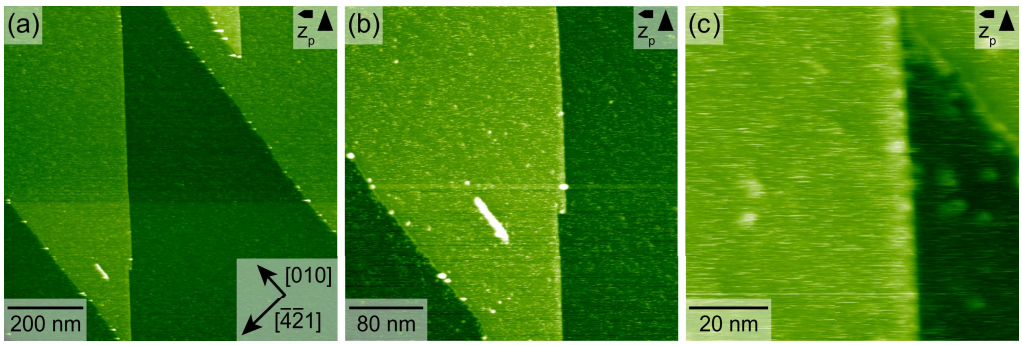

Fig. 7.6: Deposition of 3-EBA on a freshly cleaved calcite crystal reveals no ordered structure but mobile species on the calcite (10.4) surface.

bonds in favor of a molecule-surface binding is induced thermally and leads to the thermodynamical stable monomer interacting with the surface (Fig. 4.2).[236] Based on the DHBA results, also for 3-EBA the deposition of hydrogen bonded dimers is expected, since the crystal structure of 3-EBA comprises hydrogen bonded dimers, too (Fig. 7.7a).[300] Subsequently a breaking of the intermolecular hydrogen bonds might be possible. Unfortunately, no pattern, but fuzzy structures are obtained on the surface. Therefore, no proposal for the existence of monomers or dimers is possible on the basis of the self-assembled structure of 3-EBA. For this reason, a further comparison with the structural isomer 4-ethynylbenzoic acid (4-EBA) and its bulk and self-assembled structure seems useful. The crystal packing of 4-EBA

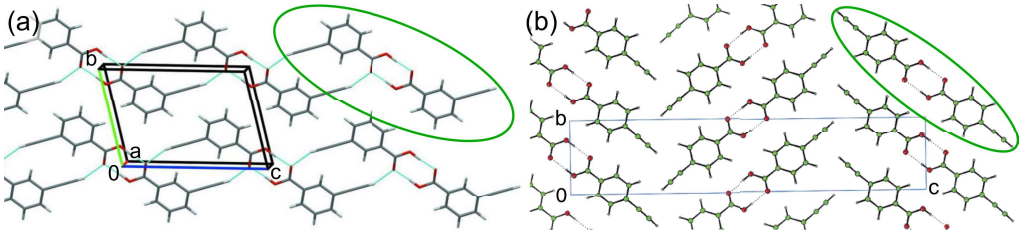

Fig. 7.7: Crystal packing of (a) 3-EBA and (b) 4-EBA viewed along the a/α axis. The hydrogen bonded dimer is marked with a green oval. Adopted from Venturini *et al.*[300] and Njus *et al.*[288]

contains hydrogen bonded dimers as well (Fig. 7.7b),[288] whereas the obtained self-assembled structure (see section 7.3) suggests the existence of monomers interacting with the surface, since no dimers are observed. Therefore, it is very probable that also the 3-EBA forms molecular monomers interacting with the calcite surface instead of the assembling of hydrogen bonded dimers. To obtain a more detailed insight of the molecule-surface interactions, DFT calculations were performed. Due to the before stated considerations, only monomers interacting with the surface were taken into account for the theoretical investigations. A description of the used computational methods and programs can be found elsewhere.[301] According to the calculations, the most stable configuration of 3-EBA is a flat-lying molecule with an adsorption energy of 1.5 eV, which is in line with room temperature adsorption (Fig. 7.8). The hydroxyl part of the carboxyl (COOH) group forms a hydrogen bond

with the calcite carbonate group oxygen atom, while the carbonyl oxygen interacts with the calcium ions *via* electrostatics. Based on the found mobility of 3-EBA at

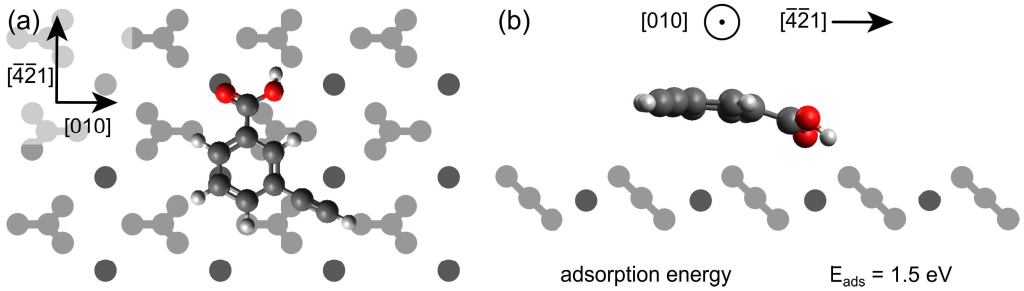

Fig. 7.8: Optimized isolated 3-EBA molecule on the calcite (10.4) surface (a) top view and (b) side view. Kindly provided by V. Haapasilta.

RT and recent DFT investigations for a comparable benzoic acid derivative,[259] it can be assumed that 3-EBA has several stable adsorption positions on calcite (10.4) with similar energies.

7.2.1 Changes Induced by Annealing

An extensive annealing series is shown in Fig. 7.9 with each step lasting for 1 hour. While annealing to (a) 405 K still shows only fuzzy structures, annealing the substrate to (b) 470 K results in two significant changes. Firstly, the amount of mobile species is reduced. Secondly and most importantly, stripes emerge that are oriented along the [42$\bar{1}$] substrate direction and are distributed on the surface. After further annealing (c-f) above 500 K, the mobile species vanish from the surface while the stripes are still visible even after annealing to 575 K. Moreover, an increase of the annealing temperature results in longer, but fewer stripes. A zoom onto the structures reveals the existence of two different kind of stripe features (Fig. 7.10). Bright stripes can be seen with a length of approximately 2 to 20 nm (some of them marked with white arrows) and an apparent height of approximately 0.4 nm. Besides, less bright and on average shorter stripes (exemplary marked with blue arrows) with an apparent height of approximately 0.3 nm are obtained. Furthermore, the less bright stripes can be found attached (1) in direct linear extension or (2) slightly displaced or (3) even isolated on the surface (Fig. 7.10b). *Via* a further zoom on the features, the inner structure of the stripes can be obtained (Fig. 7.11). An orientation of the structures in the [010] direction is observed for both stripes, highlighted via an overlay on top of the AFM image (a). An overlay on top of the AFM image (a) illustrates the observed inner structure along the [010] direction, which yields a side-by-side alignment for the bright stripe and a zigzag shape for the minor less bright stripe. Additionally, the bright stripes show a periodicity of 0.4 nm along the [42$\bar{1}$] direction (Fig. 7.11b), while the minority type of stripe has a periodicity of 0.8 nm (Fig. 7.11c). Hence, both features are commensurate

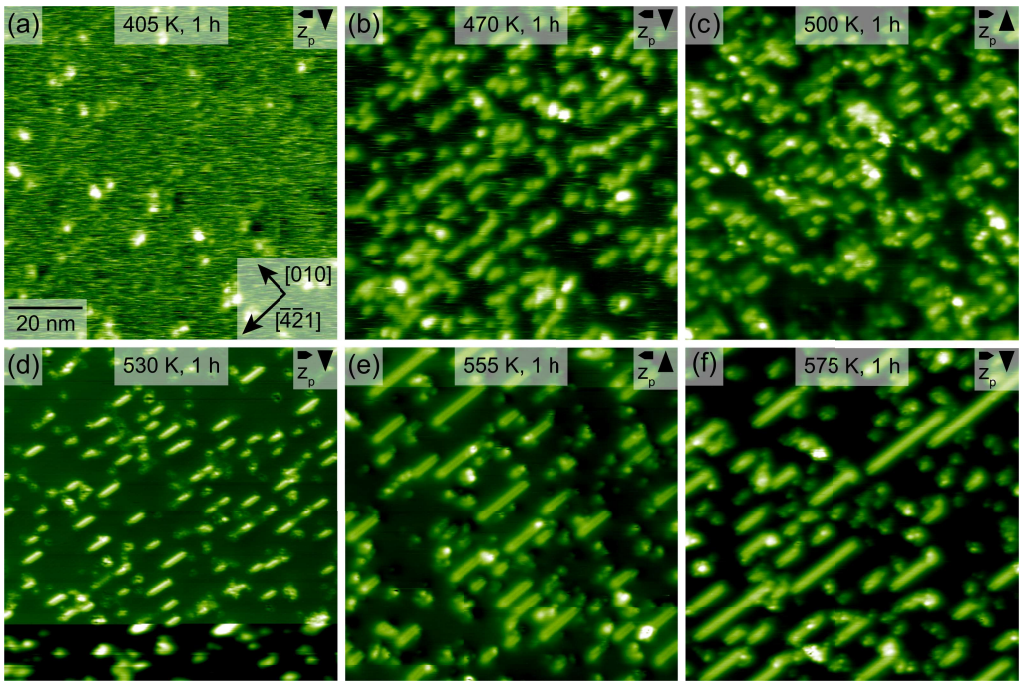

Fig. 7.9: Annealing series of 3-EBA, each step lasting for 1 hour. (a) Annealing to 405 K leads to no changes, while (b) annealing to 470 K results in a reduction of the mobile species and the appearance of stripe structures in the [42$\bar{1}$] direction. Further annealing to (c) 500 K yields in a disappearance of the fuzzy structures, while the stripes remain. Upon further increase the annealing temperature to (d) 530 K, (e) 555 K and (f) 575 K longer, but fewer stripes are observed.

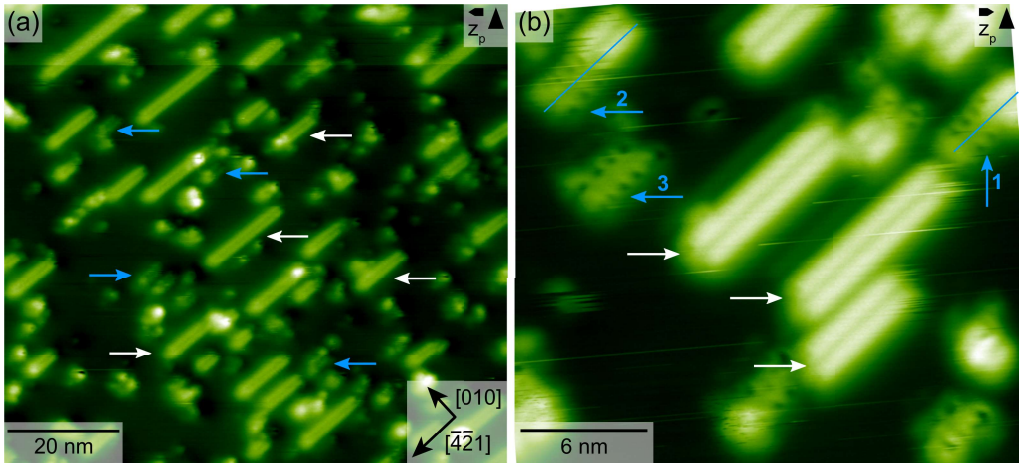

Fig. 7.10: Zoom onto the two different kind of stripe features formed upon annealing for 1 h to 555 K (a) and to 530 K (b). (b) Less bright stripes are either (1) linearly or (2) partly displaced to a bright stripe or found (3) separate on the surface.

to the underlying substrate. The reported mobile species, which can be observed directly after deposition, as well as the stripes, which appear upon annealing, are stable on the surface at room temperature for several days when stored in the UHV chamber. This is further evidence for the fact that the observed structural changes were, indeed, induced by the annealing procedure. Furthermore, both types of stripes remain unchanged even after annealing up to 575 K, while similar

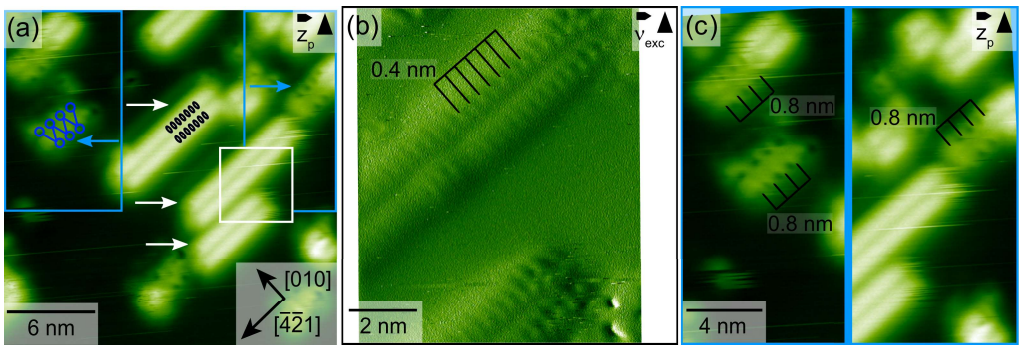

Fig. 7.11: Molecular structure obtained upon annealing for 1 h to 530 K (a,c) and 555 K (b). (a) White (side-by-side aligned) and blue (zigzag) arrows indicate two different kind of stripes along [42$\bar{1}$] direction. An overlay on top of the AFM image illustrates the observed inner structure along the [010] direction, which yields a side-by-side alignment for the bright stripe and a zigzag shape for the minor less bright stripe. High resolution image of (b) side-by-side aligned shaped stripes and (c) zigzag shaped stripes. Both structures are commensurate with the underlying substrate. All image are corrected for drift.

benzoic acid derivatives, like 3-hydroxybenzoic acid, 3,5-dihydroxybenzoic acid and 3-hydroxybenzoic acid ethylester do not undergo structural changes, but desorb at 550 K or lower temperatures.[240, 241] Hence, it can be assumed that the mobile species correspond to the as deposited monomers, which vanish at annealing the sample to 500 K in accordance with the above mentioned benzoic acid derivatives. Furthermore, the significant structural change, induced by annealing, suggests that the terminal alkynes underwent a linking reaction. A reacted structure hosts a higher number of anchoring groups per molecule, which consequently leads to a stronger molecule-surface interaction and a higher barrier for desorption. Both obtained stripe features are 1-dimensional along the [42$\bar{1}$] direction. Therefore, the creation of non-linear products is very improbable, like cyclic trimers (Fig. 7.1c) and addition products of the enyne structures (Fig. 7.1e). For this reason, only reactions yielding linear structures are considered in the following (Fig. 7.12). This further includes also the enynes, since they are planar and are, therefore, able to anchor in a similar way like the homocoupled 3-BBA molecule. To clarify whether the stripes are formed of the corresponding homocoupled dimer, the expected reaction product, 3-BBA, was deposited on the surface directly. The structures observed have been presented in the previous chapter. Also here, stripes are found. In contrast to the findings upon annealing the monomer, however, theses stripes arrange in islands and are oriented along the [010] direction. Interestingly, a second arrangement is observed upon deposition of compound 3-BBA, coexisting with the stripes oriented along the [010] direction. This minority structure (Fig. 7.13a) resembles the structure observed for the less bright stripes (Fig. 7.13b) as is illustrated in the overlay (Fig. 7.13c), showing the same periodicity in [42$\bar{1}$] direction and an analogue zigzag shaped pattern. Moreover, the dimensions of the resulting stripes indicate a side-by-side arrangement of the dimerized 3-EBA molecules, *i.e.*, compound 3-BBA. In fact, DFT calculations have indicated for a similar molecular system[259] that the energy

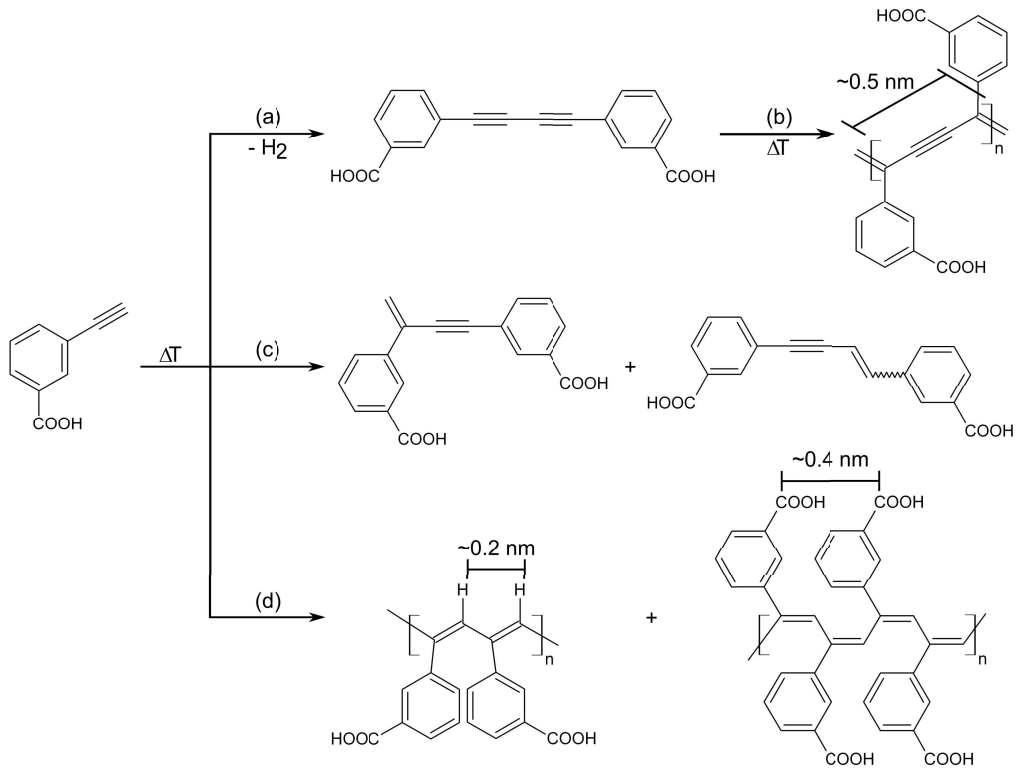

Fig. 7.12: Overview of probable reaction schemes which generate linear products. (a) On-surface homocoupling of 3-EBA to form 3-BBA, which can (b) further polymerize. (c) Dimerization forms planar enynes. (d) Acetylene polymerization leading to a *trans-transoidal* (left) or a *cis-transoidal* (right) product.

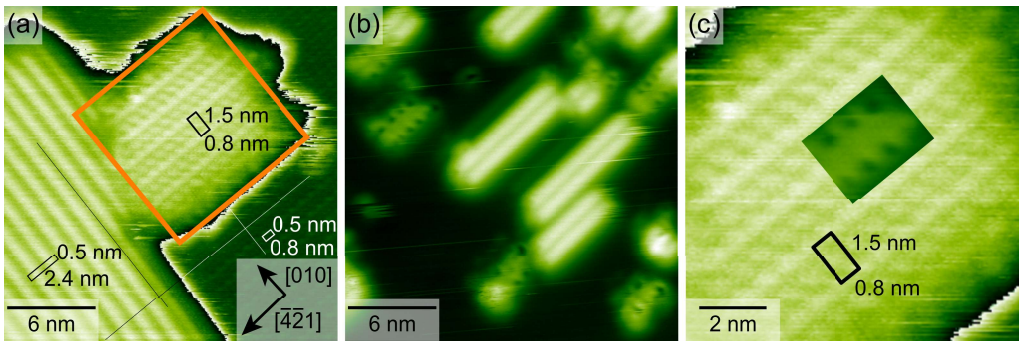

Fig. 7.13: Comparison of the minority structure obtained from 3-BBA (a), marked with an orange rectangle, with the zigzag-shaped stripes (b) formed upon annealing the sample with 3-EBA to 555 K for 1 hour. (c) Overlay image of the zigzag-shaped stripe on the minority island of 3-BBA.

difference between versatile arrangements on the surface is rather small. Considering this finding, it is well conceivable that the different reaction conditions result in a different arrangement of the dimers on the surface. The existence of two different arrangements is, therefore, not unexpected. A possible reason for single stripes instead of a striped island formation can be due to the low coverage.

Additionally, also a dimerization, forming enynes (Fig. 7.12c) is conceivable, leading to planar products, which should be able to self-assemble in a comparable way

like 3-BBA (Fig. 7.13b). The following overlays illustrate the possible arrangement of the proposed 3-BBA structure (a) and an exemplary chosen enyne structure (b) on top of an AFM image of a zigzag-shaped stripe and the model of a calcite (10.4) surface (Fig. 7.14). The used 3-BBA monomers correspond to the most stable DFT structures shown in Fig. 6.5 of chapter 6. The shown enyne molecular precursor illustrates the similarity between this planar enyne structure and the 3-BBA structure. The shown molecular enyne structures in Fig. 7.14b seem to overlap a bit, which is most probably not the case, since a tilting of the molecule in z-direction can be assumed, comparably to the 3-BBA (Fig. 9.12).

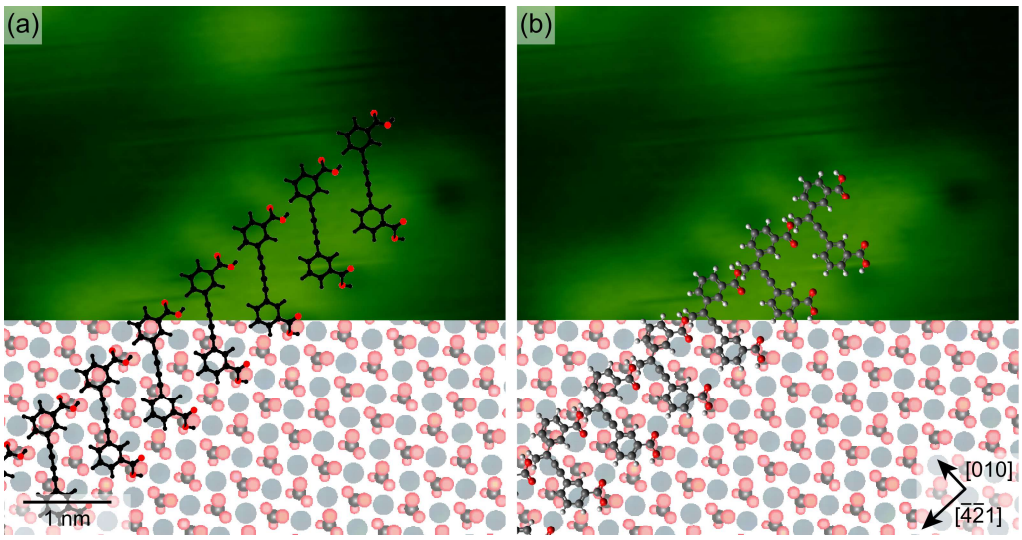

Fig. 7.14: After annealing of compound 3-EBA for 1 hour to 555 K (a) a minority structure composed of zigzag-shaped stripes along the [42$\bar{1}$] direction with a periodicity of 0.8 nm is obtained. (a) An overlay superimposed onto a model of the calcite (10.4) surface and the AFM image shows the suggested 3-BBA arrangement. (b) The model of enyne molecules overlaid on top of the AFM image to illustrate the similarity between this planar molecular structure and the 3-BBA. The AFM images are corrected for drift.

Another underlying reaction pathway can be a subsequent diacetylene polymerization (Fig. 7.12b) of the 3-BBA. The possibility of such a reaction type was demonstrated

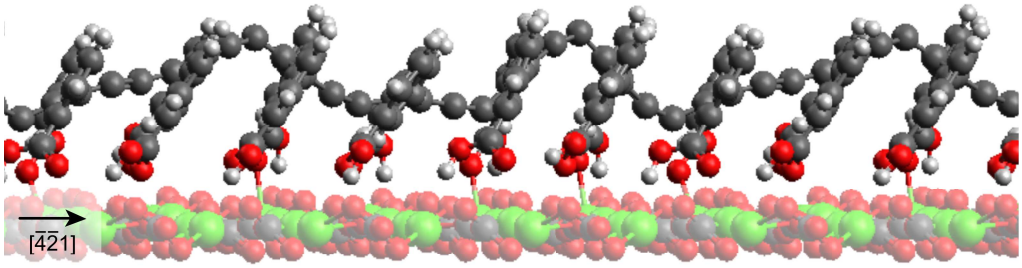

Fig. 7.15: DFT calculation of the rotated diacetylene polymer structure along the [42$\bar{1}$] direction, showing a strong deformation of the bonds. Results kindly provided by V. Haapasilta.

in the previous chapter. According to the literature the importance of the suitable

arrangement for a polymer formation has been highlighted. To gain further insight into a possible structure formation DFT calculations have were performed. Therefore, the resulting diacetylene polymer structure from chapter 6 has been taken and rotated by 90°. Because of this rotation, the available space per diacetylene moieties decreases from 0.5 nm along the [010] direction to 0.4 nm along the [42$\bar{1}$] direction. This has a tremendous influence on a possible structure formation as can be seen by the DFT calculated polymer structure in Fig. 7.15. The decreased space between the repeating units is too small for the diacetylene moieties and leads to a strong deformation of the bonds (Fig. 7.15). Hence, the formation of a diacetylene polymer can be excluded.

A fourth reaction possibility is the acetylene polymerization (Fig. 7.12d), subdivided into the formation of a *trans-transoidal* (left) or a *cis-transoidal* (right) product. A mixture of *cis* and *trans* moieties in between a stripe seems improbable, due to the fact that a formation of a nonuniform inner structure with an alternating periodicity is not observed. Furthermore, also the head-to-tail reaction towards the creation of a *trans-transoidal* product (left) seems unlikely, since an all-*trans* arrangement would lead to a 0.2 nm repeating distance of the benzenoic acid moieties. On the one hand, a *trans-transoidal* structure would imply that every second benzoic acid moiety would not have a suitable anchor position. On the other hand, this would lead to a very narrow stacking of the side groups and therefore to a strong sterical hindrance between the rings. Hence, no formation of a *trans-transoidal* product is expected. In contrast, the acetylene polymerization under creation of the *cis-transoidal* product would result in a repeating distance of approximately 0.4 nm, being commensurate to the underlying structure in the [42$\bar{1}$] direction. Furthermore, in agreement with the DFT results of 3-BBA (Fig. 9.12), also for the 3-EBA a higher coverage most probable leads to a tilting upwards of individual molecules. This tilting is further necessary to gain the 0.4 nm repeating distance of the acetylene polymer and to enable the overlap of the alkyne groups for the reaction. To get further molecular insight into the system, DFT calculations for polyacetylene were performed. Interestingly, already a geometry optimization of alternating arranged 3-EBA monomers results in the formation of a *cis-transoidal* acetylene polymer (Fig. 7.16a). This further suggests that the here considered reaction pathway has no or only a very small barrier. Moreover, the formation of the polymer is thermodynamically most favored, yielding 2.6 eV per molecule for the polymerized configuration, *i.e.* 1.1 eV more stable (per molecule) than the non-covalently 3-EBA structure, according to the optimization. One reason why the reaction can not be observed already at room temperature may be due to the fact, that the 3-EBA monomer precursors do not have a perfect aligned arrangement, which was supposed as starting point for the DFT calculation. Therefore, the probability for a successful reaction might be decreased at room temperature. In Fig. 7.16b, the optimized DFT structure of the acetylene polymer is shown as an overlay on top of the AFM image of a bright stripe and the calcite (10.4) surface. The calculated *cis-transoidal* polyacetylene structure

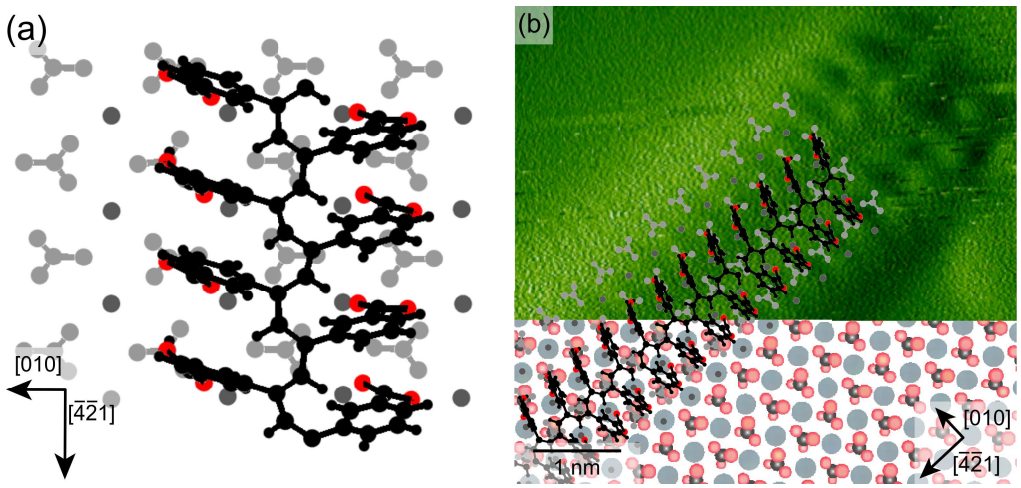

Fig. 7.16: Brighter linear molecular striped structure after annealing. (a) Optimized acetylene polymer structure on the calcite (10.4) surface upon a geometry optimization of alternating arranged 3-EBA monomers at 0 K (colours as in Fig. 6.5). (b) Zoom onto a bright stripe with superimposed acetylene polymer structure from DFT, further including the calcite (10.4) surface to illustrate the excellent match in size and pattern. Note that the absolute position of the overlay with respect to the image is unknown. DFT result kindly provided by V. Haapasilta. The image is corrected for drift.

is in excellent agreement with the experiments, as is illustrated by the match in size and pattern from the overlay.

In summary, the minor less bright striped structures are assumed to be dimer molecules, consisting of either homocoupled 3-BBA molecules or enyne structures, while the bright stripes are interpreted as polyacetylene structures.

Based on this successful reaction, the question arises how changed experimental parameter influence the formation of structures, their distribution and length. Therefore, different annealing conditions were explored.

Depending on the barrier and the energy of the reactions, it might be possible to change the ratio of the observed structures *via* changing the annealing temperature. Since a lower annealing temperature corresponds to a lower energy input into the system, first, the temperature between no observable change (405 K) and a beginning reaction (470 K) was examined in more detail. For this test 420 K and a longer annealing time of 12 h was used, since according to previous results, one hour seems to be too less to initiate any structural change. This results in the same changes observed for 470 K for 1 hour, namely mobile species and two kinds of short stripes (Fig. 7.17a,b). A zoom-in image further reveals again the same inner structure of the two different kinds of stripes (Fig. 7.17c). Additional, annealing of the sample to 420 K for 13 hours, in total 25 hours was done (Fig. 7.18a). This procedure leads to a complete desorption of the mobile species while the number of stripes has increased. Furthermore, the ratio of both striped features upon annealing at lower temperatures does not vary significantly from the shorter annealing tests with higher temperature (Tab. 7.1). From these experiments we deduce that no

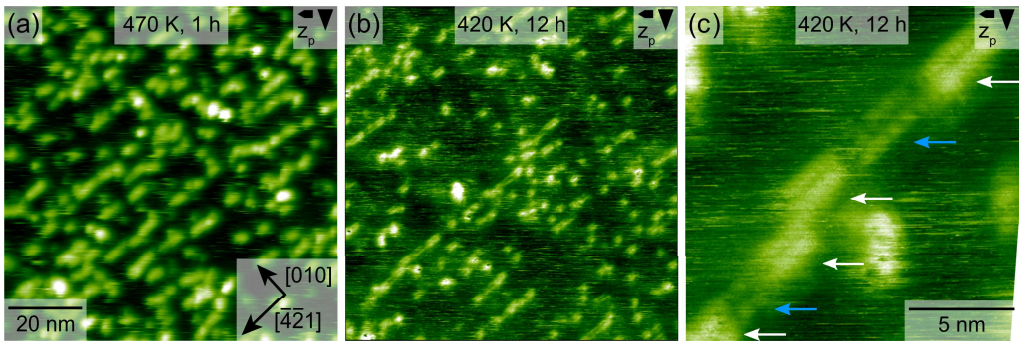

Fig. 7.17: Comparison of obtained molecular structures after annealing to (a) 470 K for 1 h with (b,c) 420 K for 12 h. In both cases, stripes along the $[42\bar{1}]$ direction and mobile species can be observed. (c) A zoom on the stripes yields the identical inner structure of the bright stripe, with aligned inner pattern (white arrows) and the darker zigzag shaped stripe (with blue arrows) as for higher annealing temperatures (Fig. 7.11). The image is corrected for drift.

large difference seems to exists between the barriers of both reaction pathways. In contrast to the ratio, the stripe length and length distribution is influenced by the heating temperatures as can be seen by comparing the samples upon annealing to 420 K, 530 K and 575 K (Fig. 7.18). Annealing at 420 K yields in the appearance of

Tab. 7.1: Number and ratio of the two different stripe features formed upon different annealing parameter per 100 nm^2.

Annealing parameter	number$_{aligned}$	number$_{zigzag}$	ratio$_{zigzag}$ in percent
470 K, 1 h	80	5	6
500 K, 1 h	75	12	14
530 K, 1 h	70	14	17
555 K, 1 h	49	9	16
575 K, 1 h	34	2	6
on 575 K hot crystal	39	8	17
420 K, 12 h	42	9	18
420 K, 13 h (total: 25 h)	137	6	4

short stripes with a homogeneous distribution of lengths and an average length of approximately 3 nm. In contrast, higher annealing temperatures like 575 K result in longer stripes with a length up to 20 nm, an inhomogeneous length distribution and a reduced number of stripes. Intermediate annealing temperatures like 530 K result in structures in between the described extreme situations. The increase in stripe length can be interpreted by two different kinds of processes, which are further related to low or high annealing temperatures. Lower annealing temperatures in the range of 470-500 K for 1 h or 420 K for 12 h still results in observable mobile species, assigned to monomers on the surface. Hence, an expansion of the stripe length can be interpreted as a reaction of monomers to existing stripes. This reaction further agrees with the observation of a very homogeneous length distribution, which can be explained by a uniform probability that randomly moving mobile molecules attach to a stripe end. If increasing the annealing temperatures to higher values like 500 K

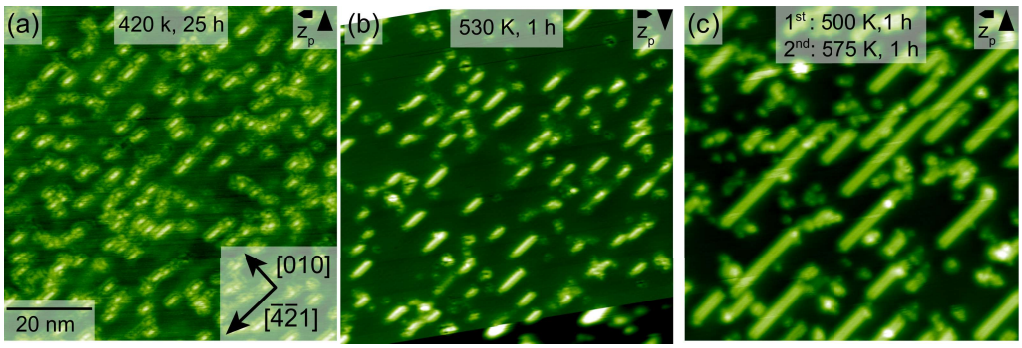

Fig. 7.18: Influence of annealing temperature on structure formation. (a) Annealing to 420 K reveals short stripes with approximately 3 nm and a homogeneous distribution of length. Higher annealing temperatures of (b) 530 and (c) 575 K yield a reduced number of stripes, a larger inhomogeneity of the distribution of length and an increase in length up to 20 nm.

for 1 h, the mobile species, that is the monomer, vanishes. As a result, no further monomers are available for subsequent annealing procedures. Hence, the elongation at higher annealing temperatures can be ascribed to a coalescence of shorter stripes. This coalescence is further consistent with the observed decrease of the stripe number and the increase of the inhomogeneity of the lengths distribution. Since the stripes consist of oligomers with a higher number of anchor groups, reducing their mobility on the surface, the probability of a coalescence is not uniform, but depends on the position of two stripes before merging.

In addition, also the influence of different pathways towards the same final temperature of 575 K was examined. As can be seen in Fig. 7.19, the final annealing temperature leads, independently of the before used parameters, to the same appearance of the sample. The results shown in Fig. 7.17, Fig. 7.18 and Fig. 7.19

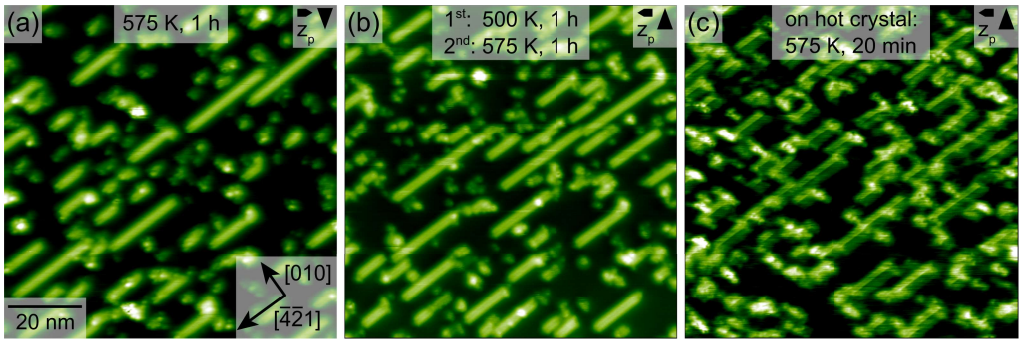

Fig. 7.19: Different pathways with the same final temperature of 575 K yields in no difference on the structure formation.

reveal that the same kind of structures are generated over a wide range of annealing temperatures and times. In contrast, the general appearance of the stripes can be influenced, that is the length and lengths distribution. Finally, the influence of the molecule coverage on the structure formation was investigated (Fig. 7.20). The higher coverage was achieved upon a double sublimation to a 575 K hot crystal for initially 20 min and subsequently 30 min and a crucible temperature of 310 K. As

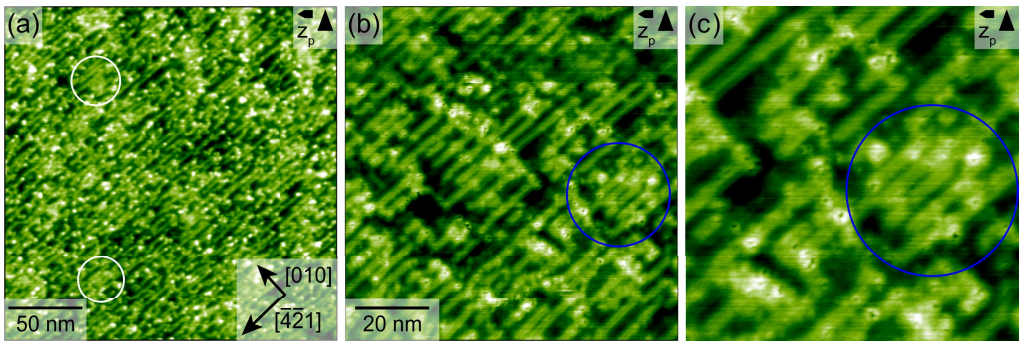

Fig. 7.20: Sample with high coverage of striped features obtained *via* two times sublimation on a 575 K hot crystal for first 20 min and then 30 min.

can be seen in Fig. 7.20, no enlarged islands are found, but randomly distributed stripes and a high number of clusters are obtained. Also, areas with higher stripe density are visible in the overview image (exemplary marked with white circles). A zoom-in image suggests only narrow aligned arrangement of the stripes but, no island formation (marked with blue circles in Fig. 7.20b,c). Hence, it can be speculated that no specific attraction between the already existing stripes and the nucleus of new forming stripes exist. Surprisingly, also no extended stripe length can be found on the surface. Possibly the relatively short stripe length can be due to the large number of clusters on the surface acting as a kind of termination agent, given that they can be found regularly at the end of a stripe.

7.2.2 Changes Induced by Irradiation

Photochemical induced reactions offer in many cases the possibility of fast and selective synthesis routes at low temperatures.[153] Since C-C-coupling reactions of terminal alkynes are known to be initiated with UV-light,[99, 100, 288] irradiation has further been investigated for the herein studied system. After irradiation of 3-EBA with the full mercury lamp spectrum for 14 h, immobile objects were observed and some remaining mobile species (Fig. 7.21). Hence, this significant change in

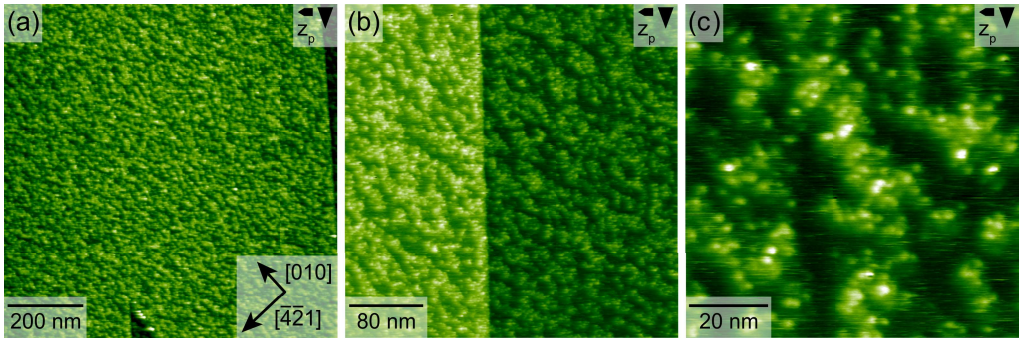

Fig. 7.21: Molecular structure formed at room temperature by 3-EBA on the (10.4) surface of calcite before (a, b) and after (c, d) irradiation for 14 h with a mercury lamp.

structure can be due to a reaction of the terminal alkyne moieties. The absence of any pattern can be caused by the initiation of side reactions, which may be as well initiated by the broad spectra of the mercury lamp. In order to prevent possible side-reactions, a suitable range of UV-light was tested, to meet the requirements reported in the respective literature,[100, 288] which was obtained by using a (256 ± 10) nm filter. Unfortunately, even an irradiation for 12 h with the filter does not

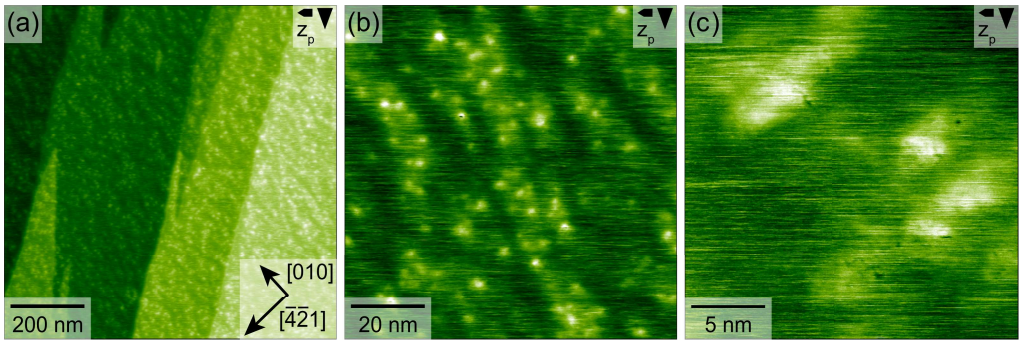

Fig. 7.22: Molecular structure formed at room temperature by 3-EBA on the (10.4) surface of calcite before after irradiation for 12 h with a mercury lamp containing a (256 ± 10) nm filter.

lead to a formation of any pattern, while still mobile species remained on the surface (Fig. 7.22). Hence, the missing formation of a nice pattern may be caused by the mobility of the molecular precursors. The mobility might decrease the probability of a suitable orientation of the alkyne groups to each other, necessary for a reaction.

7.2.3 Conclusion

In summary, we presented a detailed investigation of the structure formation and reaction of 3-ethynylbenzoic acid (3-EBA) molecules on a bulk insulator surface under UHV conditions. Upon deposition of 3-EBA on a calcite (10.4) surface fuzzy structures, assigned to mobile monomers, can be observed using FM-AFM. Annealing the substrate results in the formation of two different kinds of row-like structures. Both obtained striped structures are commensurate to the underlying surface. The majority striped structure exhibits an aligned inner pattern, perpendicular to the stripe axis, while the minority stripe is zigzag shaped. Detailed DFT calculations provide evidence that the majority stripes consist of a polyacetylene structure. Furthermore, the calculations suggest a very small barrier for this polymerization reaction. According to the calculations, the formation of the polymer is thermodynamically most favored, yielding 2.6 eV per molecule for the polymerized configuration, i.e. 1.1 eV more stable (per molecule) than the non-covalently 3-EBA structure. The obtained majority stripe excellently match the expected acetylene polymer chain in appearance and repeat distance. The minority stripe of 3-EBA reveals a similar zigzag shaped structure than the minority island arrangement of

the as deposited 3-BBA. Therefore, the minority stripe can be assigned to a dimer. Since the linear homocoupled dimer as well as the enyne molecular precursors are expected to be planar and similar in size, an assignment to either of the dimer structures is not possible. Furthermore, detailed experimental parameter variations were performed. The obtained results provide evidence that the structure formation of the polyacetylene can be influenced. Depending on the used annealing temperatures and times the length and the lengths distribution of the polyacetylene stripes can be selectively influenced. An irradiation with the full mercury lamp spectra leads to an interlinking reaction but only a mixture of products and in contrast to the literature no selective product formation is obtained. This work provides experimental and theoretical evidence that the concept of acetylene polymerization can be transferred to bulk insulator surfaces.

7.3 4-Ethinylbenzoic Acid on Calcite (10.4)

To gain information about the influence of the position of the functional terminal alkyne group on the self-assembly and reactivity, the structural isomer of 3-EBA was chosen, namely, 4-ethynylbenzoic acid (4-EBA) molecules (Fig. 7.23a). After

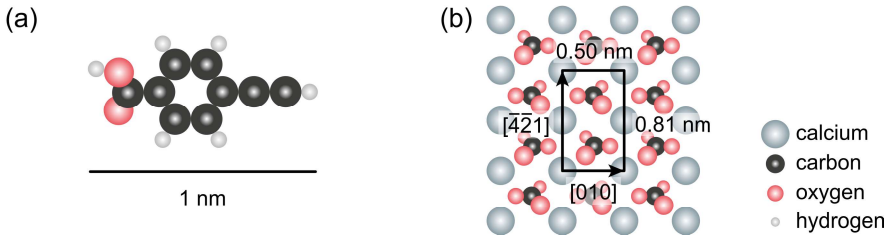

Fig. 7.23: (a) Model of 4-ethynylbenzoic acid (4-EBA) molecule studied here. (b) Model of the calcite (10.4) surface with the crystallographic axes. The surface unit cell is marked by the black rectangle. The scale bar applies to both subsets.

deposition at a crucible temperature of 310 K for 10 min, the molecules self-assemble into striped islands along the [42$\bar{1}$] direction onto a calcite (10.4) surface held at room temperature (Fig. 7.24a-b) with a (1x1) superstructure (Fig. 7.24c) and an apparent height of approximately 0.8 nm. The molecules are still mobile on the surface since island growth and dissolution can be observed in consecutive images. Furthermore, the stripes can be found directly next to each other even for the low coverage shown in Fig. 7.24a. Therefore, a short-range intermolecular attraction along the [010] direction (perpendicular to the long island axis) appears to favour broader islands composed of up to four stripes to be formed as compared to single stripes. On the other side, also a long-range repulsive force seems to exist, hindering the generation of an increased number of aligned stripes.
A more detailed analysis of the next-neighbour stripe distance distribution was done. For this purpose, the distances from stripe maximum to maximum was

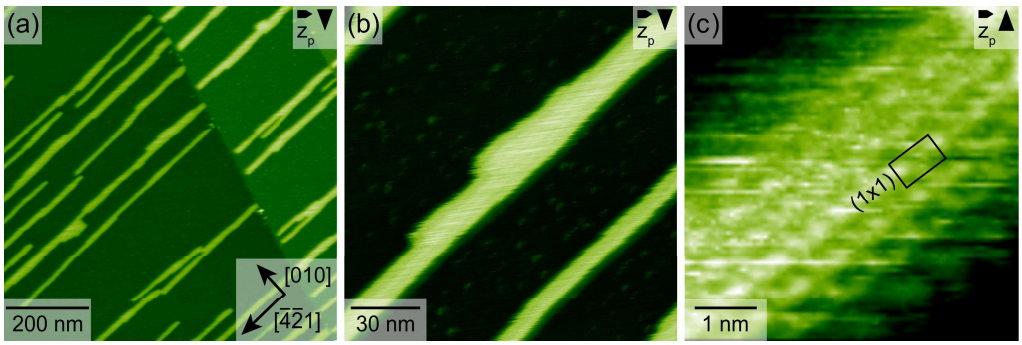

Fig. 7.24: Self-assembled molecular structures after sub-monolayer sublimation on a freshly cleaved calcite (10.4) surface held at room temperature in UHV. (a,b) Row like islands appear to self-assemble on the surface (b) having a striped inner structure. (c) A zoom onto an island reveals a (1x1) inner structure with a unit cell marked with a black rectangular. The image is corrected for drift.

evaluated, taken from drift corrected images, as exemplary shown in (Fig. 7.25a) with marked height profile, illustrated in (Fig. 7.25b). In the distance histogram (Fig. 7.25c), the obtained distance distribution (blue bars) is compared with the geometric distribution for the respective coverage (grey bars). First, a short-range

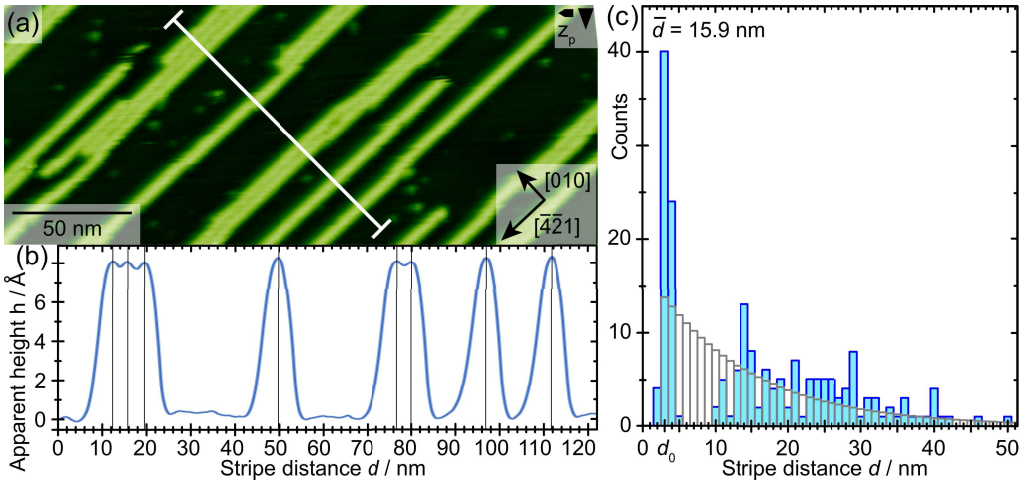

Fig. 7.25: (a) Drift-corrected AFM image of striped structures of 4-EBA with height profile position marked by a white line. (b) Representative height profile, which is averaged over points. (c) Corresponding next-neighbour stripe distance distributions (blue bars) and geometric distribution (grey bars) calculated for the same coverage is shown. Figure (c) adapted from Neff *et al.*[79]

attraction is evident in the displayed histogram from a clear additional peak at d_0, the nearest possible neighbour distance. Second, as can be seen from the clear deviation of the experimental results from the geometric distribution, the experimentally obtained distributions cannot be explained by randomly placed, non-interacting stripes. Thus, when excluding correlated growth kinetics, a long-range repulsion mechanism must be present. Therefore, a decisive interplay between short-range attraction and long-range repulsion is proposed. In analogy to the previous section, a model for the arrangement of 4-EBA on the surface can be proposed (Fig. 7.26) by

comparing the 4-EBA structure with the structure of similar benzoic acid derivatives. According to the detailed analysis of the self-assembly of DHBA[236] also in the case of 4-EBA an initial deposition of hydrogen bonded dimers on the surface is expected, since these dimers appear in the crystalline bulk structure (Fig. 7.7b).[288] The obtained unit cell is 0.5 nm in [010] direction and 0.8 nm in [42$\bar{1}$] direction. Since the dimensions of a single molecule are approximately 0.4 x 1.0 nm, the existence of a hydrogen bonded dimer does not seem to be reasonable, because this would implicate a doubled length of approximately 2 nm. Therefore, a split into molecular monomers interacting with the calcite surface is proposed, as is also suggested by AFM results and DFT calculations of the DHBA.[236] Furthermore, for several systems DFT calculations have suggested an interaction of the carbonyl groups with the calcium ions *via* electrostatics, while the hydroxyl groups form hydrogen bonds with the calcite carbonate group oxygen atoms,[114, 236, 259] which is used as a basic motif here. Since the molecule length is approximately 1.0 nm, while the available space per molecule according to the unit cell is less, a tilted upright position of 4-EBA is proposed (Fig. 7.26b). Hence, the required surface area per molecule would decrease, so that one molecule can fit into the observed unit cell. This is in agreement with the self-assembled motifs found by DFT calculations of similar structures like 3-BBA and DHBA.[114, 236] Moreover, this tilted upright standing position enables π-π-interactions between the aromatic rings and the terminal alkyne groups. The

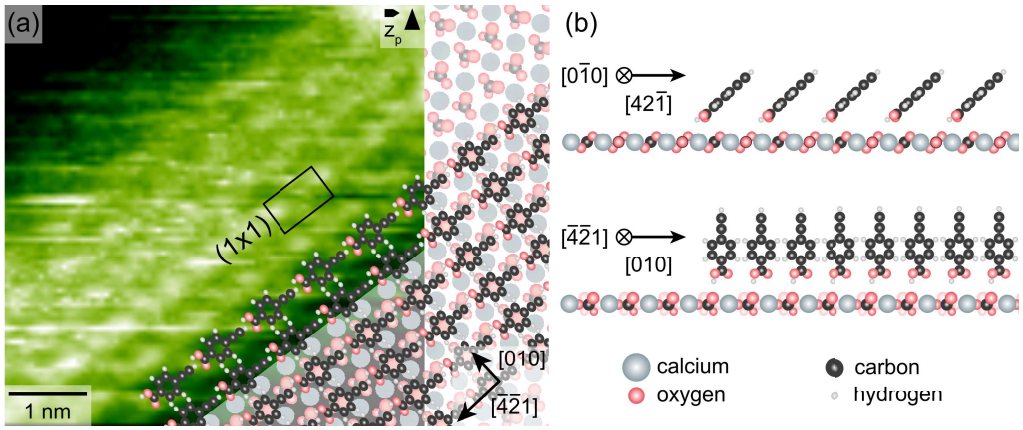

Fig. 7.26: (a) High-resolution AFM image of the (1x1) structure with a superimposed model of a possible 4-EBA monomer structure. The surface directions and the supercell are marked. The top-view structure of the 4-EBA molecules are shortened to illustrate the tilting along the [42$\bar{1}$] direction shown in (b). (b) Possible arrangement of the 4-EBA molecule (not shortened) in [42$\bar{1}$] and [010] direction. The scale bar applies to all images.

high-resolution AFM image shown in Fig. 7.26a includes a superimposed model of a possible 4-EBA monomer structure. In this illustration, the top view 4-EBA monomer is shortened in length (Fig. 7.26a) to illustrate the expected tilting along the [42$\bar{1}$] direction as can be seen in Fig. 7.26b. In the [010] direction no or only a slight rotation of the molecules along the z-axes is expected, in case of a small

overlap of the hydrogen atoms. The molecular models in Fig. 7.26b are not shortened in length.

7.3.1 Changes Induced by Annealing

Different annealing procedures were explored for on-surface reaction initiation on calcite (Fig. 7.27). An annealing at 440 K for 1 hour leads to no significant changes

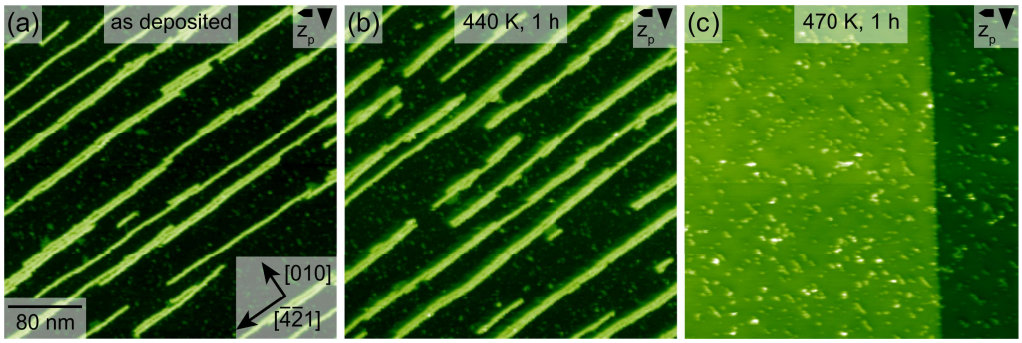

Fig. 7.27: Molecular structures formed at room temperature by 4-EBA on the (10.4) surface of calcite (a) before and upon annealing the sample to (b) 440 K (b) and (c) 470 K for 1 hour each.

while in contrast to the before shown results of 3-EBA, annealing of 4-EBA up to 470 K for 1 hour results in the desorption of the stripes. Therefore, a detailed analysis of annealing temperatures below the desorption temperature was done (Fig. 7.28). Unfortunately, no change of the self-assembled structure upon annealing

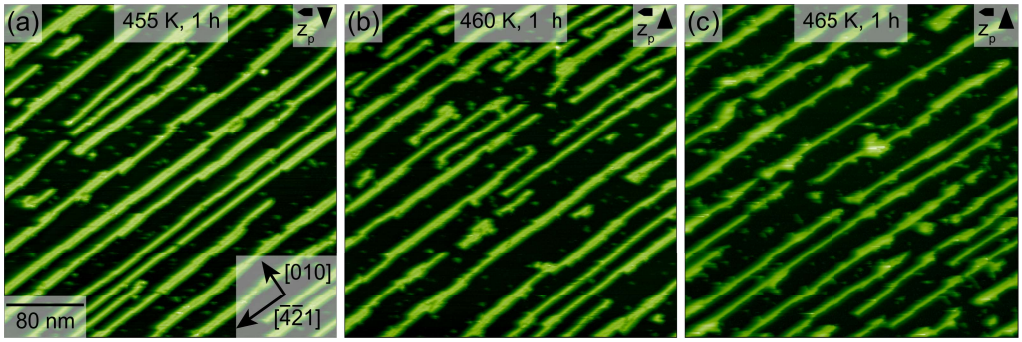

Fig. 7.28: Molecular structures formed upon annealing series to (a) 455 K, (b) 460 K and (c) 465 K for 1 hour each.

to 455 K, 460 K or 465 K for 1 h is obtained, but a partial desorption, starting upon annealing the sample to 460 K, is observed (Fig. 7.28b). To circumvent a desorption before a possible linking reaction can take place, also longer annealing times at lower temperatures was explored. First, a subsequent annealing step, after 465 K for 1 h (Fig. 7.29a), to 390 K for 19 h was performed (Fig. 7.29b,c). Besides the appearance of more clusters, still striped islands are visible on the surface. A zoom on such a stripe (Fig. 7.29c) yields the same inner pattern and the same apparent

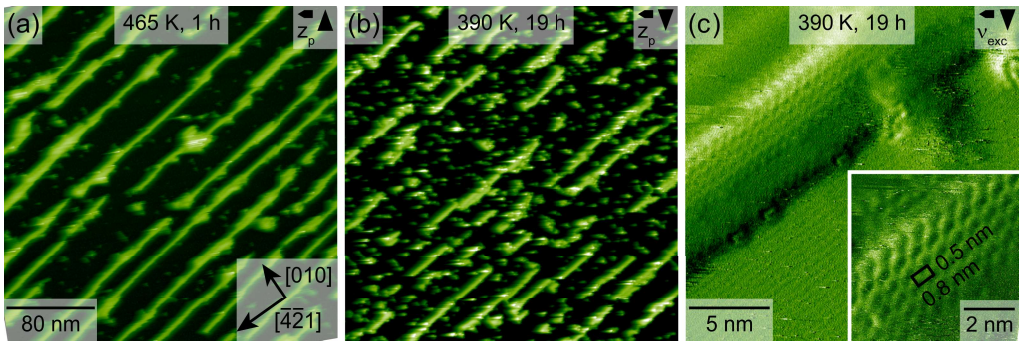

Fig. 7.29: (a) Structures obtained upon annealing the sample to 465 K for 1 h and after (b,c) upon annealing to 390 K for 19 h. (c) Zoom in on a striped island structure yields the same inner pattern as before any heating procedure.

height as the as deposited self-assembled structures (Fig. 7.24c). Therefore, it is concluded that no reaction in between the striped islands has taken place. The obtained clusters are assigned to a mixture of linked products or/and decomposition products. Unfortunately, no inner pattern of the clusters was obtained. Therefore, no further interpretation of the structure of the generated species can be made. The existence of a large number of unreacted stripes indicate that only few (if any) linking reactions were induced by the chosen parameters. Therefore, a higher temperature of 420 K was explored. Annealing at 420 K for 64 h does not result in the desorption

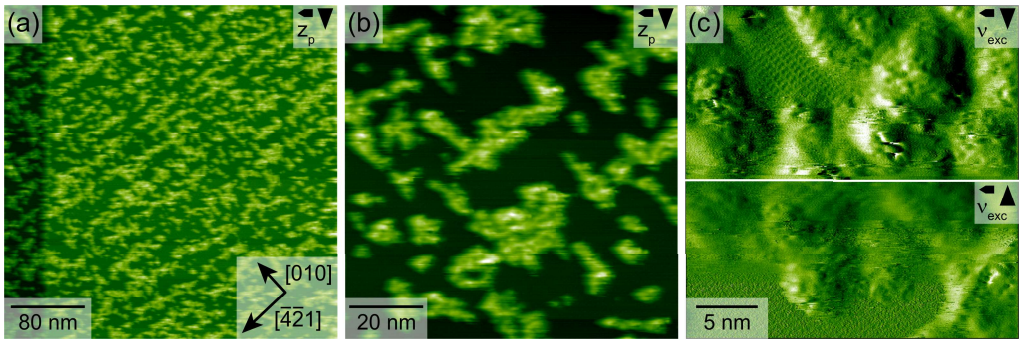

Fig. 7.30: Molecular structure upon annealing the sample with deposited 4-EBA to 420 K for 64 h. (c) Zoom on yield the calcite (10.4) surface structure while no inner pattern in the clusters can be obtained.

of the stripes, but in a significant change of the striped island structures. A zoom on the irregular structures reveals no inner pattern, while the calcite (10.4) surface structure can be identified. Hence, the missing of any resolvable structure is due to a real feature and not caused by poor imaging conditions. Nevertheless, the existence of a significantly transformed arrangement can be interpreted as a linking reaction. Due to the large number of possible products (Fig. 7.1), the finding of this kind of mixture is not very surprising. Hence, this result further indicates only a small difference between possible reaction pathways (Fig. 7.1), which makes it very complicated to find suitable parameters for the initiation of exclusively one reaction channel. Therefore, no further annealing experiments were done, since the

identification of the right annealing parameters seems very unlikely, if they exist at all.

One possible reason for the tendency for creation of mixtures could be found in the molecular assembly of the monomer. The proposed tilted upright position of the 4-EBA molecules in the striped islands does not lead to a convenient overlap of the terminal alkyne moiety. Since this overlap would be necessary for a new bond formation, it can be assumed that a reaction in between the stripes would be hindered. This suggestion agrees with the experimental finding that upon annealing only the decrease of the number of stripes and the formation of clusters is found, while the inner pattern of the remaining stripes stays unchanged.

7.3.2 Changes Induced by Irradiation

To avoid the initiation of by-products, also different irradiation procedures were explored for on-surface reaction initiation on calcite. The full spectrum of a mercury lamp was tested at room temperature and also only a part of the spectrum, which was obtained by using an appropriate filter (256 $\pm$ 10) nm. Upon irradiation of 4-EBA with the full mercury lamp spectrum for 15 h, a significant structural change of the molecular islands can be observed (Fig. 7.31). The overall shape of the

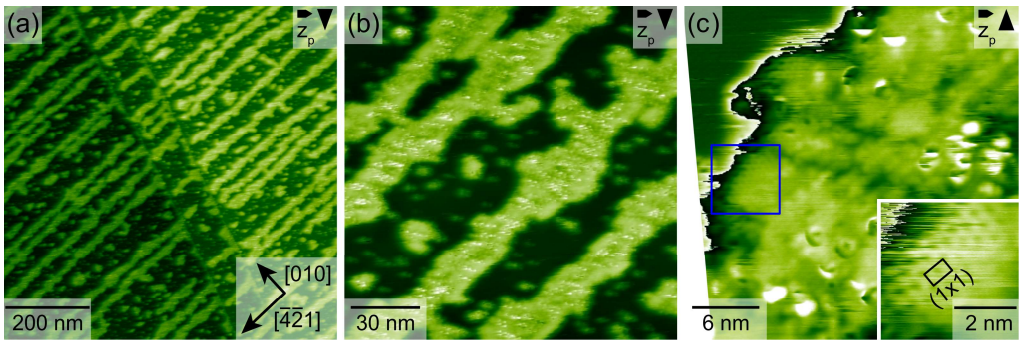

Fig. 7.31: Molecular structure formed after irradiation with the full spectra of a mercury lamp for 15 h. (a,b) Irregular shaped islands elongated in the [42$\bar{1}$] direction have formed. (c) A zoom on an island reveals a majoritarian loss of the inner pattern, except for some small regions, one marked with a blue rectangle, with a (1x1) superstructure as shown in the inset. Zoom images are corrected for drift.

molecular islands has changed. The straight island contour vanished and irregularly shaped island edges are observed instead (Fig. 7.31a,b). The island widths as well as the number of islands have increased, indicating that formerly mobile molecules were immobilized during irradiation. Furthermore, the regular inner structure of the islands is mostly lost (Fig. 7.31c). Only small areas of the unchanged (1x1) superstructure are still present, indicating remaining 4-EBA molecules and, hence, an incomplete reaction (Fig. 7.31c). Moreover, a subsequent annealing experiment of an irradiated sample to 505 K for 1 h was done (Fig. 7.32). To this end, a

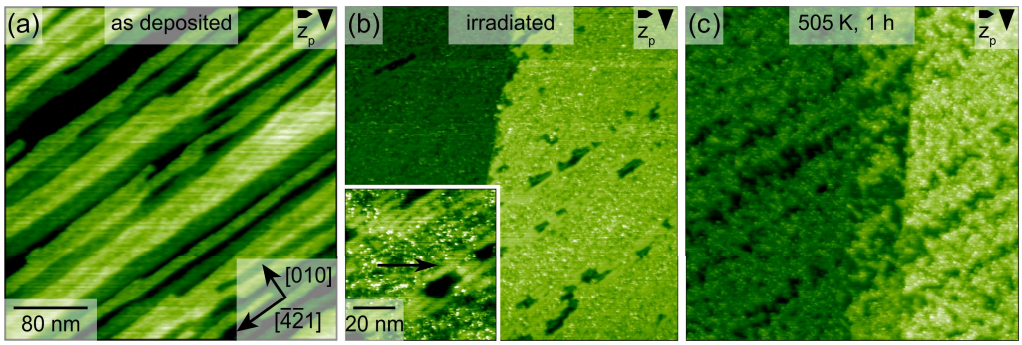

Fig. 7.32: Two step reaction series. (a) As deposited striped island structure of 4-EBA. Unfortunately, the sample was measured with a double tip, leading to an apparent higher coverage, caused by the doubling of the existing stripes. (b) Molecular structure formed after irradiation with the full spectra of a mercury lamp for 15 h, revealing changed irregular arrangements and remaining striped island structures, the latter is exemplary marked with a black arrow. (c) Irregular shaped structures upon annealing to 505 K, being 35 K higher as the desorption temperature of the as deposited structure.

higher coverage of the as deposited precursor molecule was chosen (Fig. 7.32a).[a] Again, a change of the inner island structure can be observed, next to areas of unchanged (1x1) superstructure, which can be interpreted as unreacted molecular precursors (Fig. 7.32b). In contrast to the annealing experiments of the as deposited structures, the irregular features remain on the surface, while most probably only the unreacted 4-EBA striped islands, which were still visible after irradiation (inset b), have desorbed. This gives further evidence that the obtained irregular structures upon irradiation are indeed linked reaction products, since a C-C coupling would lead to a higher number of anchoring groups per molecule and, therefore, to a stronger interaction and increased desorption barrier.

To circumvent side-products and instead favor the homocoupled reaction or acetylene polymerization[100, 288], an appropriate range of the lamp spectrum was used *via* a filter (256 ± 10) nm. The irradiation of 4-EBA with a (256 ± 10) nm filter for 14.5 h (Fig. 7.33) leads to no change of the striped island structure, as can be seen by a comparison of the as deposited structures (a-c) with the irradiated sample (d-f). Besides a significant change of the mobile species aside of the island stripes (marked with blue arrows) can be observed (d-f). Since streaky structures (blue circle in b) are always visible after deposition and is interpreted as mobile 4-EBA molecular precursors, the monitoring of very mobile striped structures with lower apparent height (marked with white arrows) are mainly not or only slightly observable. Hence, it cannot be excluded that these features are a contamination. Nevertheless, the periodicity of the formed small striped islands is clearly revealed, yielding 2.0 nm in the [010] direction and 0.8 nm in the [42$\bar{1}$] direction. The obtained (4x1) superstructure may fit to the size of the homocoupled 4-EBA molecule of

[a] The image Fig. 7.32 was measured with a double tip, leading to an apparently higher number of stripes, since the doubling occurs in the [010] direction.

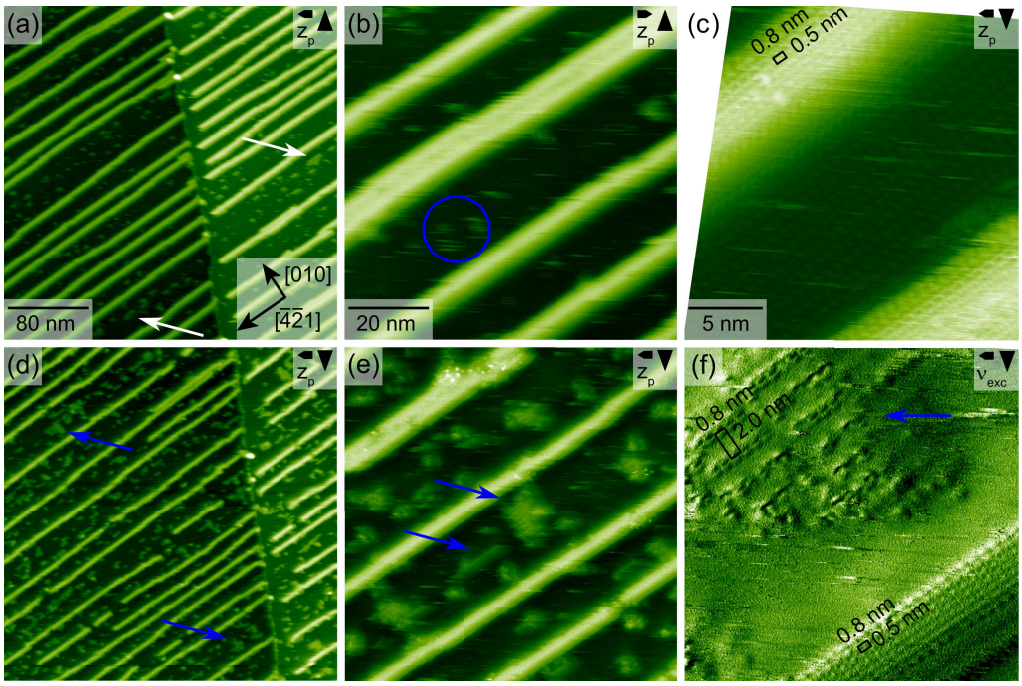

Fig. 7.33: Molecular structure formed at room temperature by compound 4-EBA on the (10.4) surface of calcite before (a-c) and after (d-f) irradiation for 14.5 h with a mercury lamp using a filter (256 $\pm$ 10) nm. After deposition, (a) small stripe like structures (exemplary marked with white arrows), (b) fuzzy features and usual striped islands (c) with (1x1) superstructure can be found. After irradiation, single stripes and side-by-side arranged stripes, forming small islands (marked with blue arrows) with a periodicity of 2.0 nm in [010] direction and 0.8 nm in [42$\bar{1}$] are observed, next to unchanged as deposited 4-EBA elongated islands. Images c and f are corrected for drift.

approximately 0.4 x 1.7 nm. These results suggest a successful dimerization reaction of the 4-EBA monomer.

7.3.3 Conclusion

In conclusion, an intensive study of the self-assembly and the induced structural changes upon annealing and irradiation of 4-EBA on the calcite (10.4) surface was presented. The molecular precursor forms elongated striped islands in the [42$\bar{1}$] direction with a (1x1) inner structure. The observation of up to four elongated islands next to each other, even for low coverages suggests a short-range attractive interaction. Furthermore, a detailed analysis of the next-neighbour stripe distance distributions reveals that the obtained arrangement clearly deviates from randomly placed, non-interacting stripes. When excluding correlated growth kinetics, this deviation provides evidence for a long-range repulsion being present during the assembly of the stripes. Additional, a significant difference is obtained between the self-assembly of the two structural isomers 3-EBA and 4-EBA, demonstrating the impact of the position of the terminal alkyne group. For the initiation of a reaction, thermal and photochemical stimulation experiments were performed. Shorter annealing times of

1 h below 470 K did not lead to changes of the inner structure of the striped islands. Further annealing to 460 K leads to a partial desorption and after annealing at 470 K no elongated islands of 4-EBA were observed. Therefore, similar desotption parameter are obtained for 4-EBA and 3-EBA, *i.e.* 470 K for 1 h and 500 K for 1 h. Hence, similar molecule-surface interactions of both molecular species can be assumed. Annealing the sample to 420 K for 64 h or irradiation with the full spectrum of a mercury lamp for 15 h results in a significant change. Now unordered structures are observed, which can be assigned to a successful linking reaction. A subsequent annealing experiment of an irradiated sample to 505 K, which is 35 K above the obtained desorption barrier, yields remaining unordered structures. This further indicates that, indeed, a linking reaction has taken place, leading to a higher number of anchor groups per molecule and, therefore, to an increased desorption barrier. Unfortunately, well-ordered assemblies of the reaction products could not be obtained in that case. Since terminal alkynes are known to undergo various different reaction pathways, the revealed unordered structures are interpreted as mixtures of reaction products. To circumvent the initiation of side-reaction, an appropriate range of wavelengths, according to the literature was used by inserting a filter (256 $\pm$ 10) nm. However, no change of the inner (1x1) striped island structure was revealed, but a significant change of the mobile species. Now, single stripes and striped islands with a (4x1) superstructure can be found, which can be tentatively ascribed to the structure of the homocoupled 4-EBA product.

7.4 4,4″-Diethynyl-[1,1′:4′,1″-terphenyl]-2′,5′-dicarboxylic Acid (DETDCA) on Calcite (10.4)

The 4,4″-diethynyl-[1,1′:4′,1″-terphenyl]-2′,5′-dicarboxylic acid (DETDCA) is investigated (Fig. 7.34a) on the (10.4) cleavage plane of calcite (Fig. 7.34b) using dynamic atomic force microscopy (AFM) operated in ultrahigh vacuum (UHV). The molecule

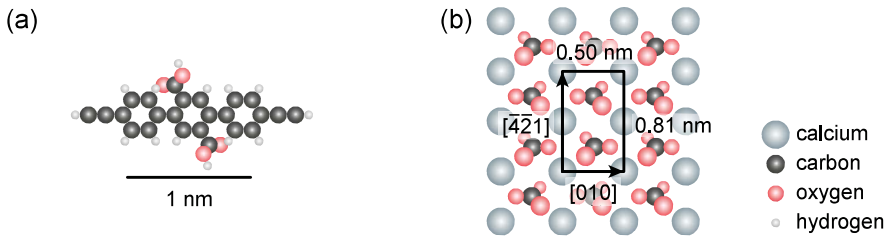

Fig. 7.34: (a) Model of 4,4″-diethynyl-[1,1′:4′,1″-terphenyl]-2′,5′-dicarboxylic acid (DETDCA) molecule studied here. (b) Model of the calcite (10.4) surface with the crystallographic axes. The surface unit cell is marked by the black rectangle. The scale bar applies to both subsets.

is equipped with two ethynyl groups, which are intended for on-surface homocoupling. Additionally, the molecule is also equipped with two carboxylic acid functionalities, which have previously proven to act as suitable anchors on the calcite (10.4) surface and prevent the desorption at elevated temperatures. Density-functional theory calculations have suggested an interaction of the carbonyl groups with the calcium ions *via* electrostatics, while the hydroxyl groups form hydrogen bonds with the calcite carbonate group oxygen atoms.[114, 236] Furthermore, a detailed investigation towards a possible deprotonation has been performed, suggesting a transition of the hydrogen from the hydroxyl group towards the oxygen of the carbonate group under formation of a hydrogen bond.[114, 236] Two anchor groups were chosen here for symmetry reasons and to also promote molecule-molecule interactions that can be beneficial for the formation of an ordered self-assembled structure as compared to mobile species. Our experimental results indicate that DETDCA dimerize in the crucible when choosing a high-temperature deposition route. When following a low-temperature deposition route, the monomers are deposited on the surface. Upon annealing the sample after monomer deposition results in AFM images that can be readily explained by the dimerization of the molecules on the calcite (10.4) surface. Thus, our work provides experimental indication for extending the concept of on-surface homocoupling of terminal alkynes to a bulk insulator surface.

7.4.1 Low-Temperature Deposition

After molecule deposition using the low-temperature deposition protocol (sublimation temperature of about 355 K for 12-15 hours), molecular islands are found on the surface as shown in Fig. 7.35a-c. In the low-coverage regime, these islands exhibit fuzzy edges, which are indicative of high molecule mobility, resulting in characteristic steaky features. A zoom onto an island in the low-coverage regime (Fig. 7.35c) does not reveal an inner structure. When increasing the coverage (Fig. 7.35d-f), the island structures become more stable, which is explained by a reduced molecule mobility. A zoom onto an island in the high-coverage regime unravels a highly ordered inner structure (Fig. 7.35f).

To further analyze this structure, we performed a high-resolution experiment as shown in Fig. 7.36. In this image, the (5x1) superstructure of the molecular island is indicated by a white rectangle. We superimpose a model of the molecules to the image to provide an impression of the molecular dimensions. This superimposed model suggests that the unit cell contains one DETDCA monomer. We also provide a model for the underlying calcite crystal to illustrate the arrangement of the monomers on the calcite surface. We stress, however, while the dimensions and orientation of the molecules are well defined from the experiment, the absolute position of the molecules on the surface is unknown. In the model, we assume that the molecule

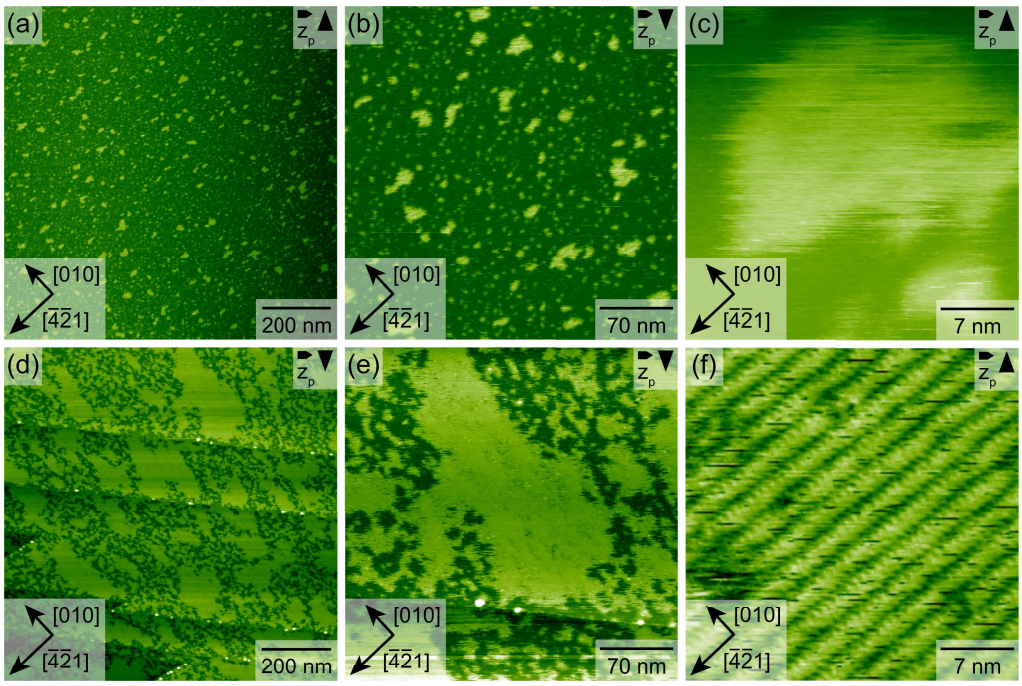

Fig. 7.35: AFM images acquired after low-temperature deposition before annealing the sample. Depending on the deposition protocol, low (a-c) and high (d-f) molecular coverages can be achieved.

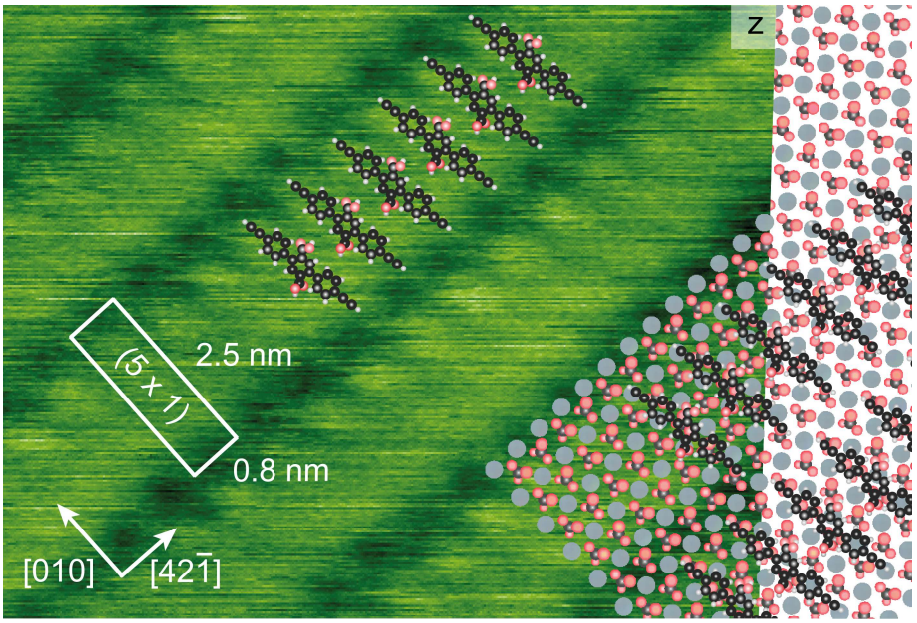

Fig. 7.36: High-resolution AFM image of the (5x1) structure with a superimposed model of a possible DETDCA monomer structure. The surface directions and the supercell are marked.

is not flat, given that the side groups in the 2-position, namely hydrogen and carboxylic acid group, would overlap. To circumvent this overlap, a rotation of the benzene rings transverse the molecular axes is expected. Hence, only one carboxylic acid group would anchor to the surface while the second one is pointing upwards

and perhaps forms a hydrogen bonds with the acid group of the neighboring molecule.

Next, we annealed the sample after low-coverage molecule deposition as shown in Fig. 7.35a-c to 555 K for about one hour. The result of such an annealing experiment is shown in Fig. 7.37. The overall appearance of the islands has remained unchanged upon annealing, as can be seen by comparing the two overview images shown in Fig. 7.35a and Fig. 7.37a, respectively. However, the inner structure of the islands has changed significantly as demonstrate in the zoom image given in Fig. 7.37c. After annealing, a stripe-like structure is observed, exhibiting somewhat irregular stripes with a width of about 4.5 nm. This width fits in length with dimerized DETDCA molecules that are linked *via* homocoupling of the terminal alkynes, as illustrated in the inset in Fig. 7.37c. Moreover, the island edges appear well-defined and do no longer present the fuzzy structure that was observed for the as-deposited molecular islands. Assuming that the dimers possess a reduced diffusivity on the surface as compared to the monomers, this observation is in line with the above made interpretation of DETDCA dimerization.

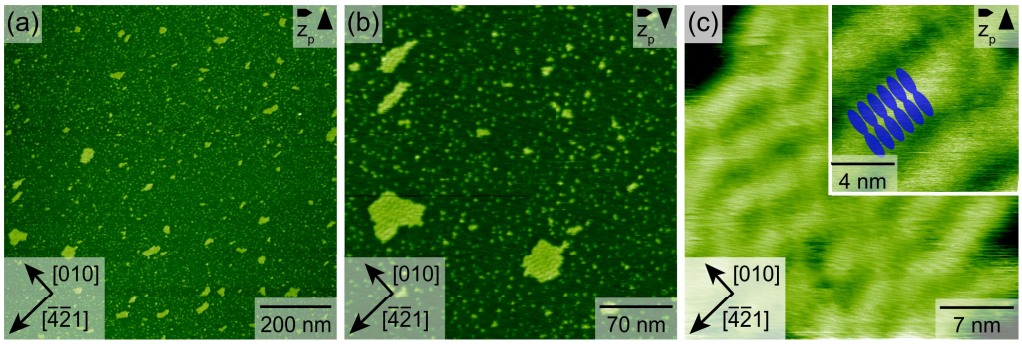

Fig. 7.37: AFM images acquired after low-temperature deposition and annealing the sample to 555 K for about one hour. A model illustrating the proposed alignment of the dimers within the stripes is given in the inset in (c).

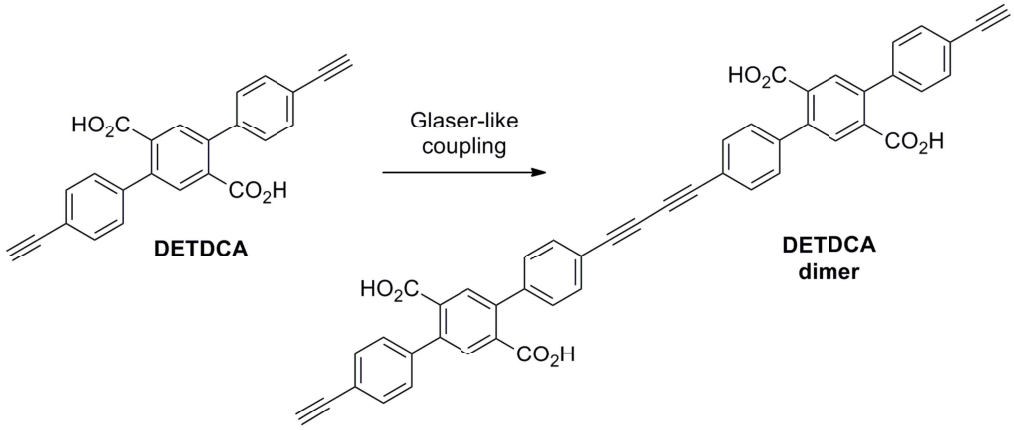

Fig. 7.38: Expected on-surface coupling of DETDCA.

7.4.2 High-Temperature Deposition

We also performed deposition experiments onto a sample held at room temperature with increased sublimation temperature (445 K) in an attempted to reduce the long sublimation times needed for the above-mentioned low-temperature deposition protocol. When sublimating with a sublimation temperature of 445 K for about 15 hours, molecular islands as shown in Fig. 7.39a-c are obtained. These islands exhibit the characteristic stripe-like inner structure that was reported above for the annealed sample obtained after the low-temperature deposition protocol. However, a clear difference can be recognized when comparing the island structures in Fig. 7.37 (low-temperature deposition after annealing) and Fig. 7.39a-c (high-temperature deposition without annealing). For the high-temperature deposition protocol without annealing, fuzzy edges and streaky features in between the molecular islands are observed, indicative of diffusing molecular species. These high-temperature deposition results can be explained by the direct sublimation of DETDCA dimers, i.e., we suggest that the high sublimation temperature induces dimerization directly in the crucible as has been reported before for 1,4-diethynylbenzene.[97] Besides the dimers, few monomers might be deposited simultaneously. These monomers might diffuse in between the island, resulting in the streaky structures observed in the images shown in Fig. 7.39a-c. Next, we examined the effect of annealing and

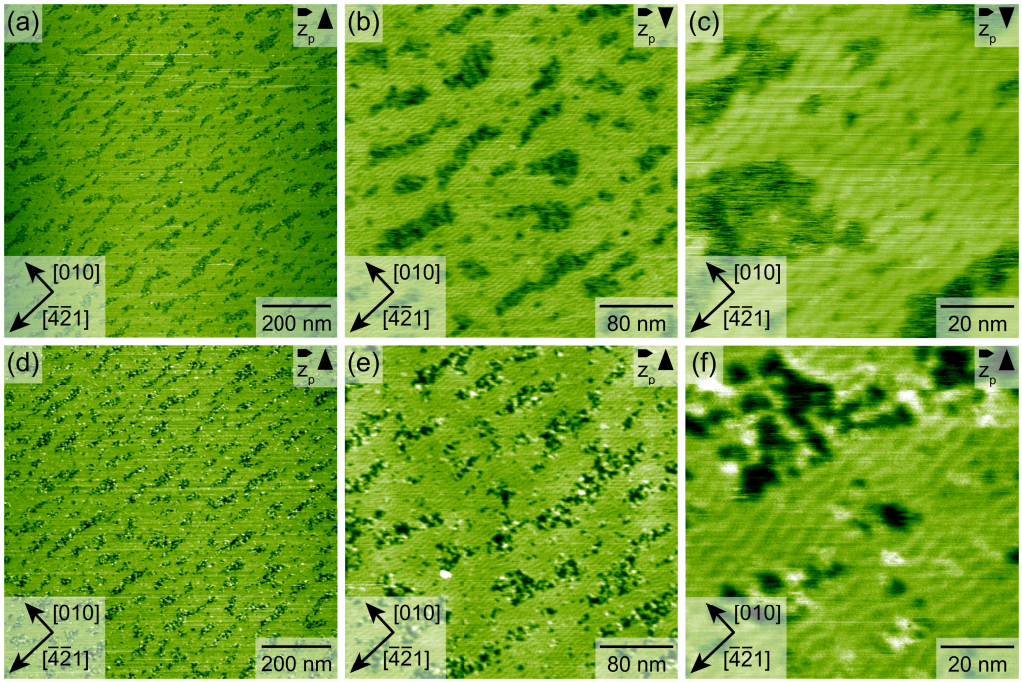

Fig. 7.39: AFM images acquired after high-temperature deposition before (a-c) and after (d-f) irradiating the sample.

irradiating the structures as obtained after high-temperature deposition. We found that both, annealing the sample to about 555 K and irradiating the sample with a mercury lamp (wavelength 220-590 nm), resulted in the same final conditions.

This observation agrees with previous results presented in the literature that have demonstrate that coupling of terminal alkynes can be induced by both, annealing or irradiation.[99] The changes induced are illustrated in Fig. 7.39d-f, which show a sample after irradiation for about 12 h. As can be seen, the inner structure is largely unchanged. However, the edges appear much more well defined and the streaky features in between the islands are vanished. This result indicates that remaining monomers react upon annealing or irradiation, thus, the diffusing species are removed.

To summarize, we suggest that both, annealing to 555 K and irradiating with mercury lamp (wavelength 220-590 nm) can induce homocoupling of the terminal alkynes. The fact that this is possible in the absence of a metal surface indicates that electron transfer from the support surface is not required to induce the reaction. This is in line with a recent theoretical study on coupling of terminal alkynes on Ag(111).[129] In the latter study, it was concluded that the surface plays a central role for the reaction in constraining the molecular movement as well as stabilizing reaction intermediates. It is, however, not chemically active in a sense that it, *e.g.*, donates electrons. For the present case, we speculate that the carboxylic acid groups at the molecule core are crucial for anchoring the molecule to the substrate and constrain the mobility on the surface. The limited mobility may furthermore explain why only dimers and no trimers or larger oligomers are formed. This interpretation is in agreement with previous observations in literature on Ag(111).[99]

7.4.3 Conclusion

In conclusion, we presented an experimental AFM study investigating the structure formation and reaction of DETDCA molecules on the (10.4) surface of the bulk insulator calcite. When depositing the molecules following a low-temperature deposition route, highly ordered islands are found on the surface that exhibit a (5x1) inner structure. This structure can be readily explained by an ordered arrangement of the DETDCA monomers. The characteristic streaky edges of these islands are explained by diffusing monomer species. Upon annealing, these islands drastically change their structure, as is expected when the monomers dimerize. Now, islands with a striped inner structure are found on the surface. Interestingly, the width of the stripes fits in size with the length of a dimer. Moreover, the fuzzy edges are vanished, giving further evidence for an on-surface dimerization. For the high-temperature deposition protocol, the striped islands are obtained directly, indicative of a direct deposition of the dimers. This result can be easily explained by a dimerization in the crucible, which has been observed before for another diyne molecule. Also here, fuzzy edges vanish after annealing or irradiation, indicative of few remaining monomers that are deposited during the high-temperature route. Thus, these experiments provide evidence for a homocoupling reaction on the bulk insulator calcite.

8 Summary

In conclusion, this thesis presents a detailed study of the self-assembly and on-surface reaction of four alkyne molecules on the bulk insulator calcite in ultra-high vacuum (UHV). Using frequency-modulated atomic force microscopy (FM-AFM), real space imaging of molecular arrangements with atomic precision is achieved on the calcite (10.4) surface. Molecules carrying terminal alkyne and diyne functionalities have been investigated, since these functional entities can form conjugated structures upon diacetylene polymerization, acetylene polymerization, linear homocoupling or dimerization reactions.

Evidence is presented for a diacetylene polymerization using 3,3′-(1,3-butadiyne-1,4-iyl)bisbenzoic acid (3-BBA) as the precursor molecule. A comprehensive study of the self-assembly reveals two types of molecular islands, which are both composed of rows running either in the [010] (majority type) or the [42$\bar{1}$] (minority type) direction. Hence, both arrangements are perpendicular to each other. For the majority island type, density functional theory (DFT) calculations provide insights into the molecular arrangement, which is governed by a molecule-molecule interaction *via* the aromatic rings. To initiate the reaction, thermal, photochemical and combined stimulation experiments are performed. The success of the reaction in case of the majority island type is directly evident from the appearance of new row-like structures, either visible separately on the surface or in between the former homogenous island structure. These row-like-structures exhibit the same inner pattern compared to the as deposited self-assembled molecules, but are imaged with a smaller apparent height. Detailed DFT computations show that the molecular arrangement in the majority self-assembled islands is suitable for polymerization with an energy gain of 1.2 eV per formed diacetylene monomer unit. The obtained row-like structures excellently match the expected polymer chains in appearance and repeat distance. Further experiments demonstrate that the mobility of the molecules can be reduced by increasing the coverage. When the mobility is reduced, fewer by-products are obtained, since the high coverage forces the molecules to stay in the island structure at elevated temperatures, which appears to be favorable for the topochemical reaction. In contrast, for the minority island type, no structural change upon annealing or irradiation is obtained, suggesting that no reaction has taken place. This difference in reactivity of the two arrangements can be explained by considering the dimensions of the underlying substrate. The specific substrate directions meet the required dimensions of the diacetylene polymerization and the final product for the majority island, while it does not for the minority island arrangement. Therefore,

the difference in reactivity provides evidence for a templating effect of the underlying calcite (10.4) surface. Finally, this study demonstrates that a rational building block design, indeed, enables the formation of conjugated molecular wire-like structures on an insulator surface.

Besides 3-BBA, the on-surface reaction of three terminal alkynes is studied, namely 3-ethynylbenzoic acid (3-EBA), 4-ethynylbenzoic acid (4-EBA) and 4,4″-diethynyl-[1,1′:4′,1″-terphenyl]-2′,5′-dicarboxylic acid (DETDCA). The terminal alkyne moiety is known for providing different conjugated reaction products, depending on the experimental conditions.
The molecular precursor 3-EBA has been chosen, since 3-BBA is its linear homocoupled dimer. This allows for a comparison between the 3-EBA structure after reaction initiation and the self-assembled 3-BBA precursor. The experimental study of 3-EBA presents the first example for an acetylene polymerization on a bulk insulator. 3-EBA has no tendency to form ordered self-assembled arrangements but diffuses on the surface. Upon thermal stimulation, the appearance of two types of linear stripe-like structures suggests the successful initiation of two types of on-surface reactions. The majority striped structure exhibits an aligned inner pattern, perpendicular to the stripe axis, while the minority stripe is zigzag shaped. DFT computations provides evidence that the majority stripes consist of a polyacetylene structure. Furthermore, the calculations suggest a very small barrier for this polymerization reaction and provide an energy gain of 1.1 eV per monomer unit. The minority striped structure can either be assigned to a linear homocoupled dimer or to an enyne dimer. This conclusion is based of a comparison with the as deposited 3-BBA structure. Unfortunately, linear homocoupled as well as enyne dimers are expected to be planar and similar in size. Therefore, no assignment to either of the dimer structures is possible. Additional, detailed experimental parameter variations provide evidence that the structure formation of the resulting acetylene polymers can be influenced. Depending on the parameters specific lengths distributions and stripe lengths can be obtained. This study clearly demonstrates the successful transfer of the acetylene polymerization reactions from a metal surface to the bulk insulator surface of calcite.

The structural isomer 4-EBA is investigated, having the terminal alkyne group in the para-position, as compared to the meta position of 3-EBA. 4-EBA forms highly ordered elongated island structures, oriented towards the $[42\bar{1}]$ substrate direction, coexisting with few diffusing monomers. The fact that up to four stripes can be found next to each other, even for low coverages, suggests a short-range intermolecular attraction perpendicular to the elongated island axis. Furthermore, a detailed analysis of the stripe-to-stripe distance distribution reveals, that the found arrangement clearly deviates from randomly placed, non-interacting stripes. Therefore, this deviation provides unambiguous evidence for a long-range repulsion being present during the assembly of the elongates striped-like islands. Thermal

stimulation to 470 K for 1 hour, leads to the desorption of the molecular precursors. Therefore, comparable desorption parameters are obtained for 4-EBA and 3-EBA monomer precursor. This can be assumed to similar molecule-surface interactions of both molecular species. Furthermore, an annealing with temperatures below the desorption temperature for 1 hour results in no visible changes of the inner structure of the elongated islands. In contrast, longer annealing below the desorption temperature and photochemical stimulation with a broad range of wavelengths leads to a significant change towards unordered structures, which is assigned to the formation of a mixture of reaction products. Furthermore, a successful dimerization reaction of the diffusing 4-EBA monomer precursors is observed upon irradiation with a mercury lamp using an appropriate filter, while the inner structure of the elongated islands remains unchanged. These experiments suggest that a reaction is possible between diffusing monomers, while the arrangement in islands hinders a reaction to take place. This study demonstrates the impact of the position of the terminal alkyne group on the self-assembly and the reaction ability, when comparing 3-EBA and 4-EBA.

Evidence is given for a successful linear homocoupling of the terminal alkyne molecule DETDCA on the calcite (10.4) surface. Two different deposition routes are investigated, referred to as low-temperature and high-temperature deposition. Upon the low-temperature deposition route, DETDCA is found to form highly ordered island arrangements. Characteristic streaky edges at the islands were obtained, which are explained by diffusing monomer species. When annealing the sample, a drastic change towards islands with a striped inner structure was observed, which matches the size of the expected dimer. Further, the fuzzy edges are vanished, giving additional evidence for a successful on-surface homocoupling reaction. Upon the high-temperature deposition protocol, the dimerization appears to happen already in the crucible and dimers are deposited directly on the surface. Also here, fuzzy edges vanish after annealing or irradiation, indicative of few remaining monomers that are deposited during the high-temperature route.

In summary, the results of this thesis demonstrate, for the first time, that the concept of on-surface reactions of terminal alkynes and dyines can be successfully extended to a bulk insulator surface. Furthermore, the achieved acetylene polymerization of 3-EBA and the diacetylene polymerization of 3-BBA lead to the formation of conjugated wire-like structures, which are interesting for future application in molecular electronics.

9 Appendix

9.1 Equipment

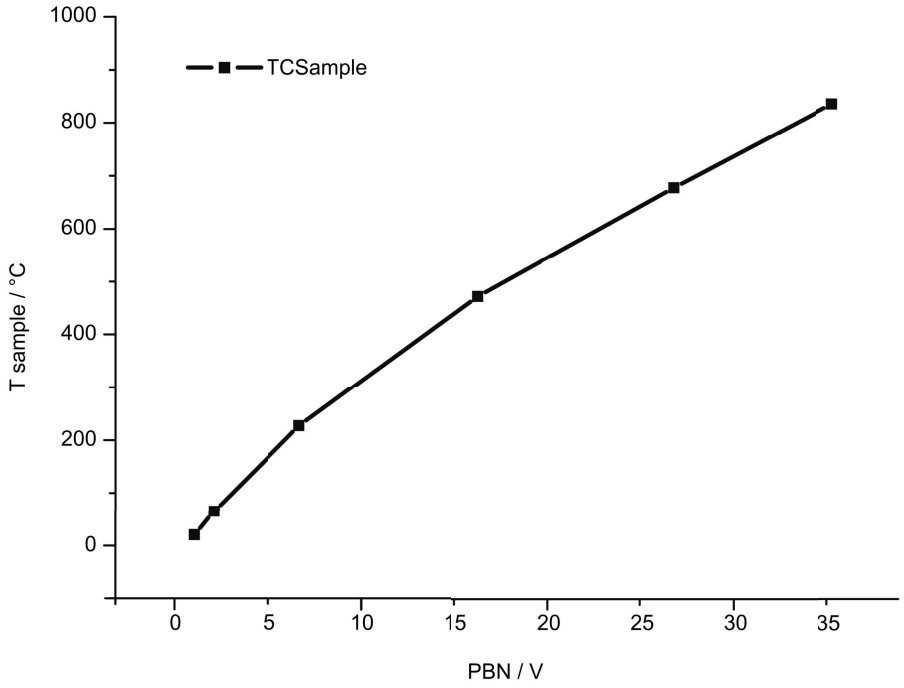

Fig. 9.1: Calibration curve supplied by Omicron Nanotechnology.

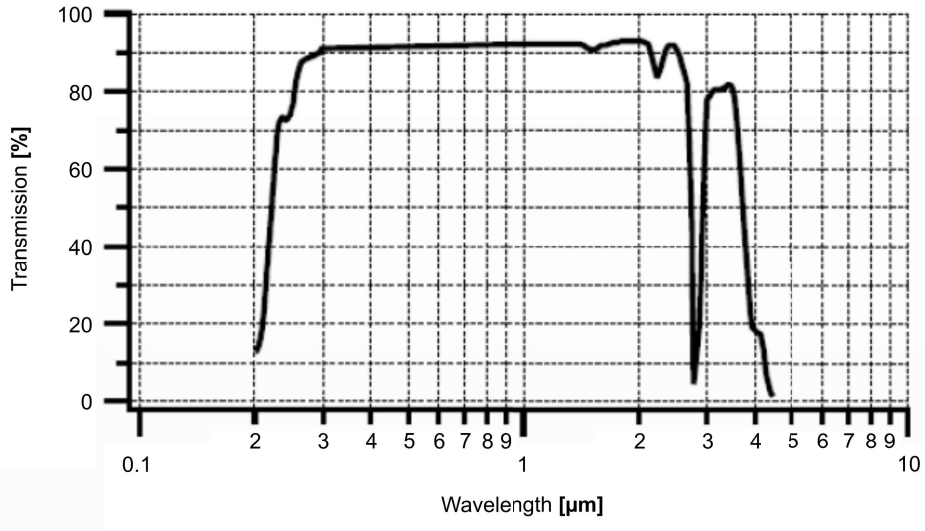

Fig. 9.2: Transmission of UHV window of fused silica.

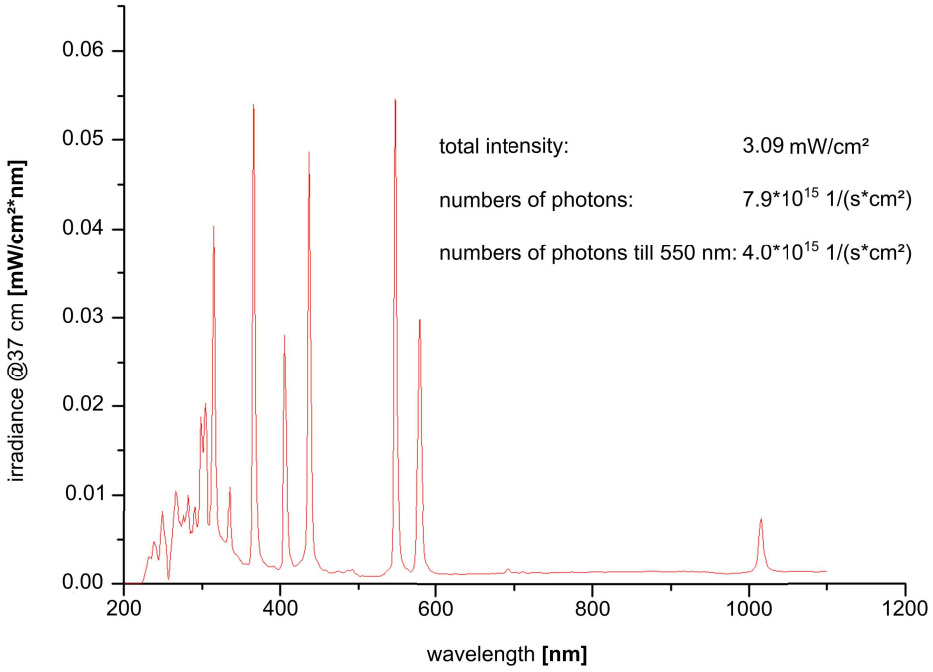

Fig. 9.3: Spectrum of the UV-Cube.

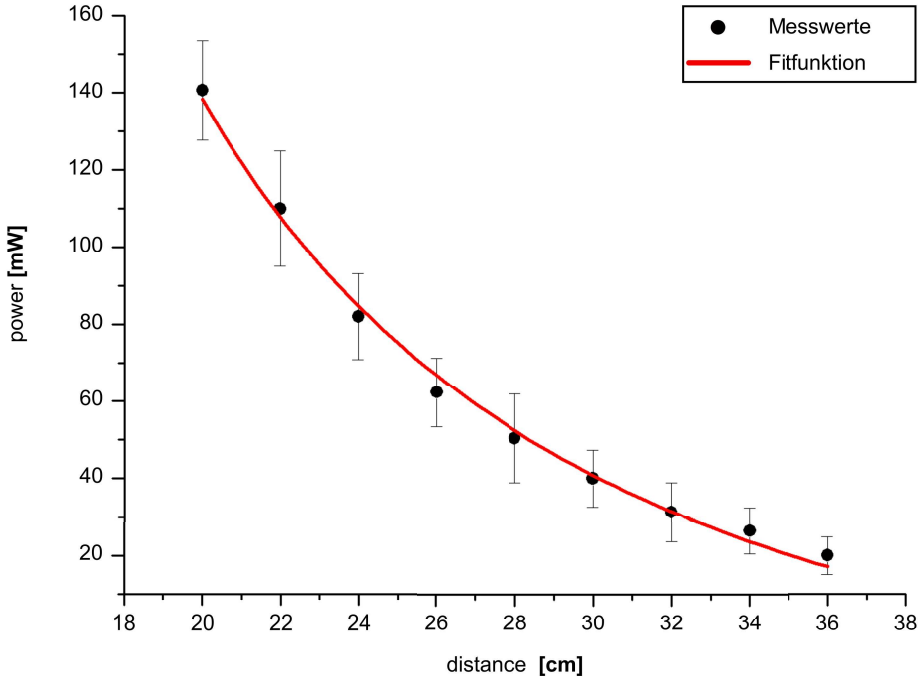

Fig. 9.4: Power distance fit of the UV-Cube.

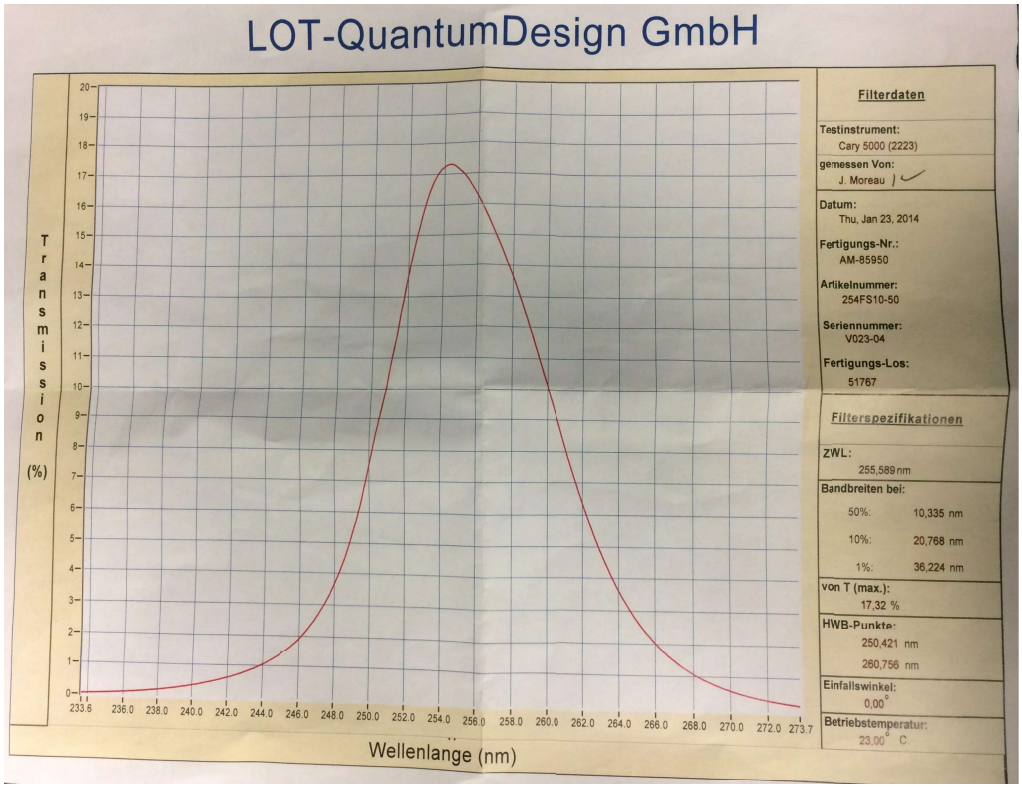

Fig. 9.5: Properties of (256 ± 10) nm filter.

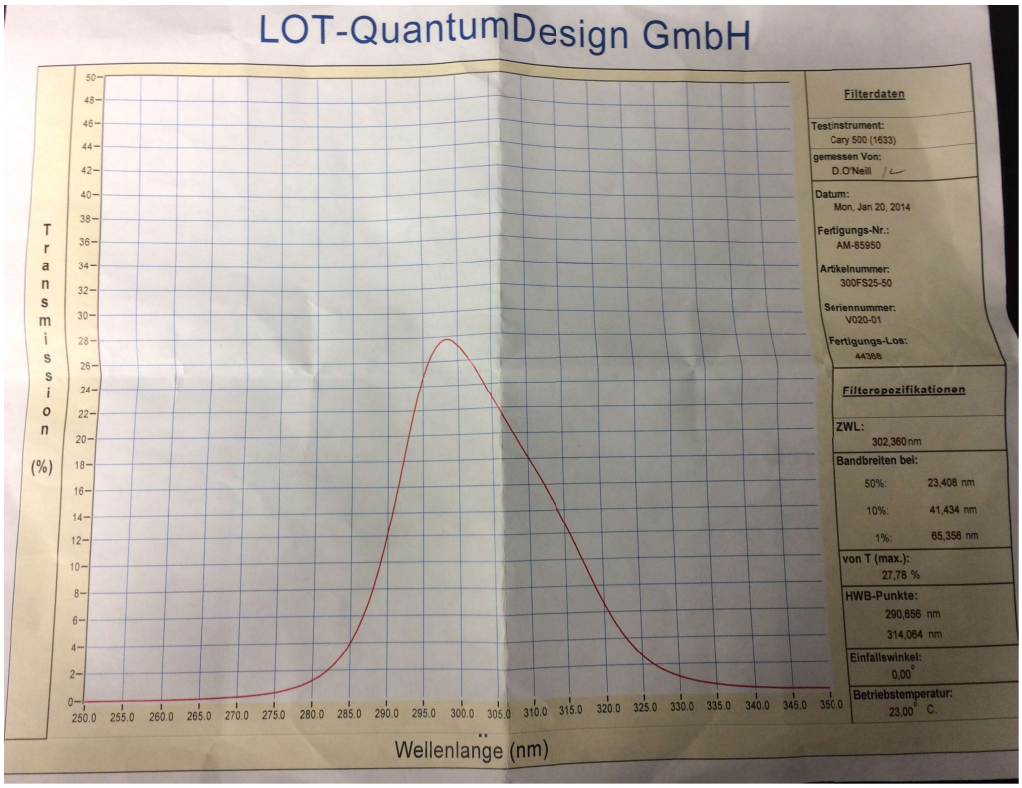

Fig. 9.6: Properties of (302 ± 23) nm filter.

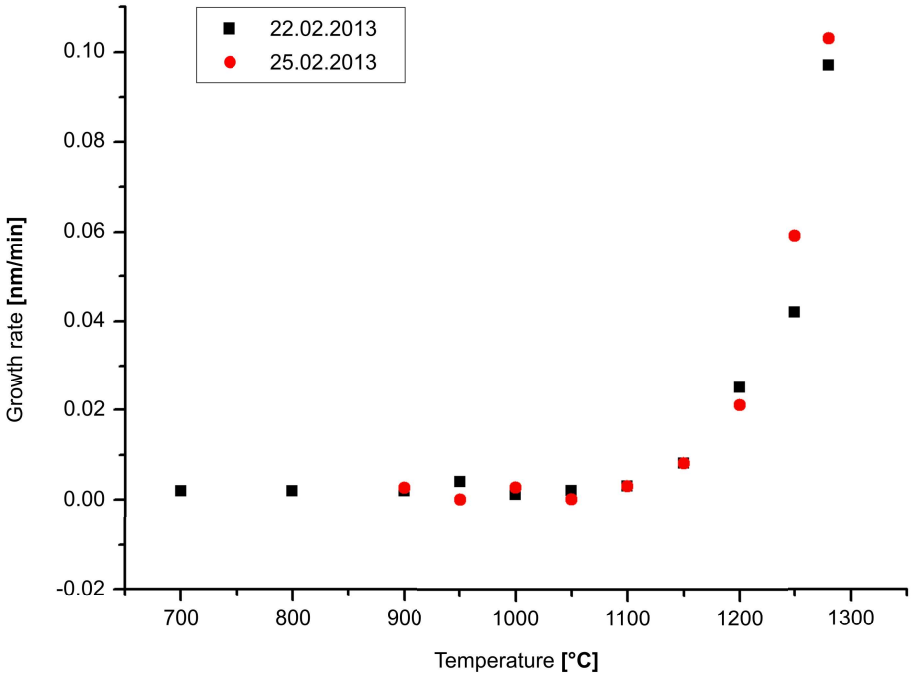

Fig. 9.7: Rate of iron evaporation against temperature. Adapted from Ref.[257]

9.2 Molecule Synthesis

The following description is adopted from the article "Diacetylene polymerization on a bulk insulator surface" by A. Richter, V. Haapasilta, C. Venturini, R. Bechstein, A. Gourdon, A. Foster and A. Kühnle and published in PCCP, 19, (2017), 15172-15176.[114]

3-BBA was prepared from commercial 3-iodobenzoic acid by analogy with literature procedures.[302–304] After methylation of the carboxylic group, Sonogashira coupling with trimethylsilylacetylene gave methyl 3-((trimethylsilyl)ethynyl)benzoate, followed by deprotection by tetra-n-butylammonium fluoride to yield methyl 3-ethynylbenzoate (64% for the two steps). Glaser coupling of the latter gave dimethyl 3,3′-(buta-1,3-diyne- 1,4-diyl)dibenzoate in 91% yield, which was then saponified by lithium hydroxide followed by acidification to yield 3-BBA (54%). Detailed procedures can be found elsethere.[277]

9.2.1 Molecule Analysis Data

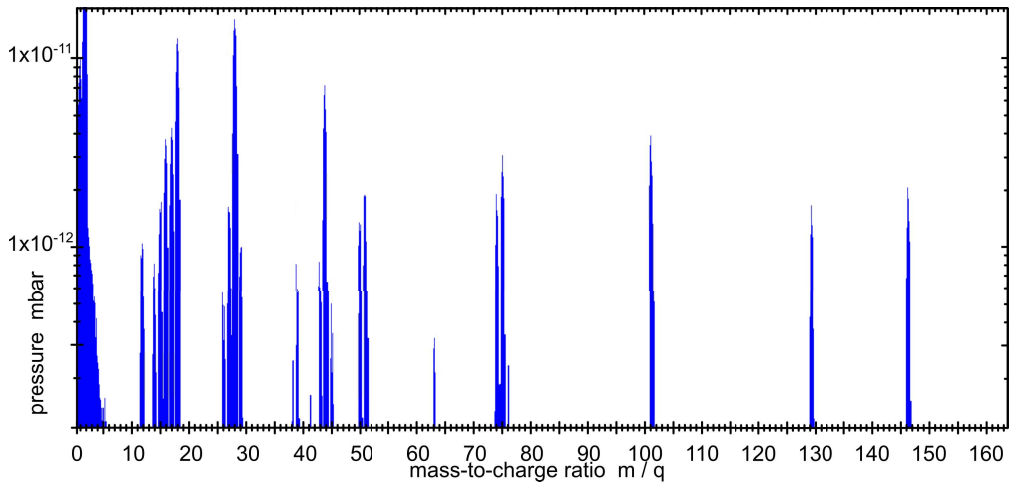

Fig. 9.8: Mass spectrum of 3-EBA

9.3 Irradiation of 3-BBA Sample with 256 ± 10 nm

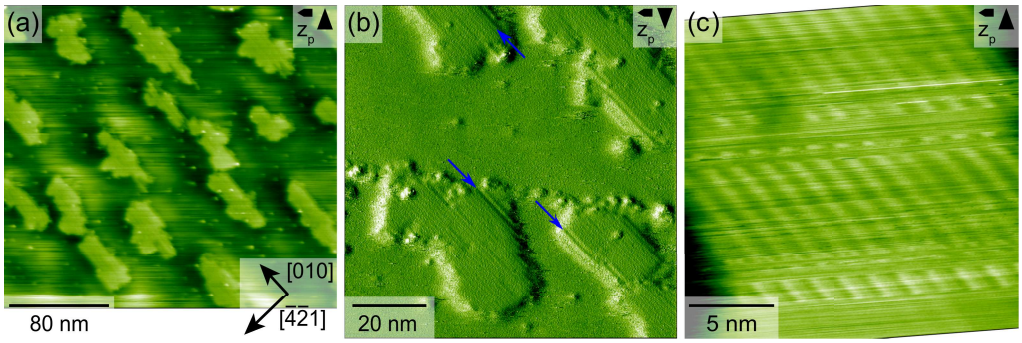

Fig. 9.9: Molecular structures after irradiation with a Hg-lamp using a (256 ± 10) nm filter for approximately 12 h. (a) The overall island shape remains unchanged. (b) Zoom on showing a few darker rows within the formerly regular island (marked with blue arrows). (c) A further zoom reveals the mainly unchanged inner island structure, assuming that (256 ± 10) nm seems not the optimum wavelength for initiating a diacetylene polymerization.

9.4 Further Investigated Molecules

The following molecules have been further investigated in this thesis, namely 3-hydroxybenzoic acid *iso*propyl ester (3-HBE*i*PE), 3-hydroxybenzoic acid ethyl ester (HBAEE), 2,5-diiodobenzoic acid (DIBA), 2,3,6,7-naphtalene tetra carbonitrile (NTCN) and 6,âĂŃ15-âĂŃdibromo-4-methyl-dibenzo[c,âĂŃg]âĂŃphenanthrene-âĂŃ3-carboxylic acid (Helicene). 3-HBAEE and 3-HBE*i*PE were investigated within the supervision of the bachelor thesis of J. Enns. DIBA was partially investigated within the supervision of the bachelor thesis of R. Scheid and partially within an own project.

Acronym	T_{Sub}/°C	r_{Sub}/ ML/min
3-HBAEE	30	0.09
3-HBE*i*PE	30	0.12
NTCN	70	0.005
Helicene	140	0.05
DIBA	35	0.0002

Tab. 9.1: Overview about the times and temperature to achieve a reproducible submonolayer coverage with the further investigated molecules.

9.5 Computations

The following description is adopted from the article "Diacetylene polymerization on a bulk insulator surface" by A. Richter, V. Haapasilta, C. Venturini, R. Bechstein, A. Gourdon, A. Foster and A. Kühnle and published in PCCP, 19, (2017), 15172-15176.[114] The computational results were done and are kindly provided by V. Haapasilta of the group of A. Foster.

We performed density functional theory (DFT) calculations (T = 0 K) and molecular dynamics (MD) simulations (T ≠ 0 K) using the CP2K program suite.[305] In all computations, the PBE functional[306] was used together with D3 dispersion correction scheme.[307] The Gaussian Plane Wave Method[308] was used to solve the electronic structure. Core electronic states were modelled with GTH pseudopotentials[309] and the valence electrons were described with molecularly optimized polarized double−ζ basis functions.[310] The electronic density was described with a plane wave basis with an energy cutoff of 500 Ry. More details can be found elsewhere.[277]

9.5.1 Further Calculated Geometries

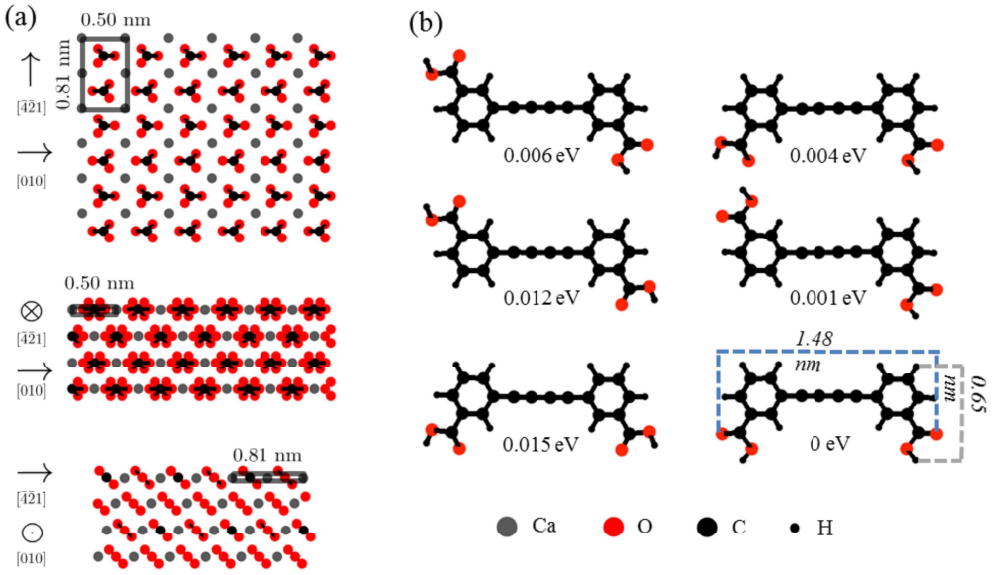

Fig. 9.10: Calcite slab of (6x3) surface unit cells with (10.4) surface is shown in (a) from three angles. In (b) six flat gas-phase configurations of the 3,3′-(1,3-butadiyne-1,4-diyl)bisbenzoic acid (3-BBA) are shown, with total energies with respect to the most stable one. The energetic differences are very small. All geometries are converged better than 0.003 $eV/$Å. Please note that here the surface and the molecules are not in scale. Image adopted from Ref.[277]

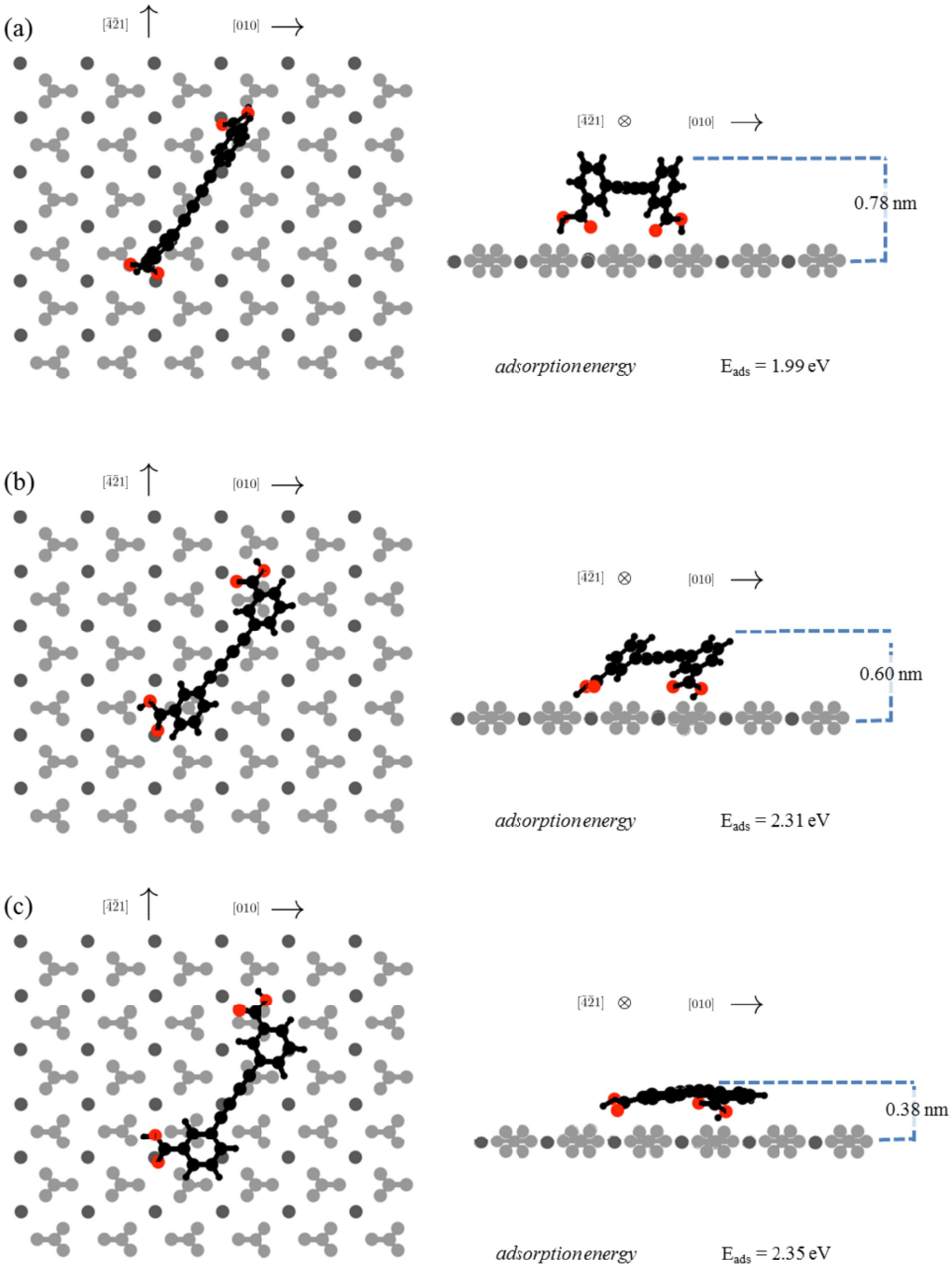

Fig. 9.11: An isolated 3-BBA molecule on calcite surface with different "tilt angles". The adsorption energies are reported, together with heights. The energetic difference between the flat and slightly tilted configurations is very small. Image adopted from Ref.[277]

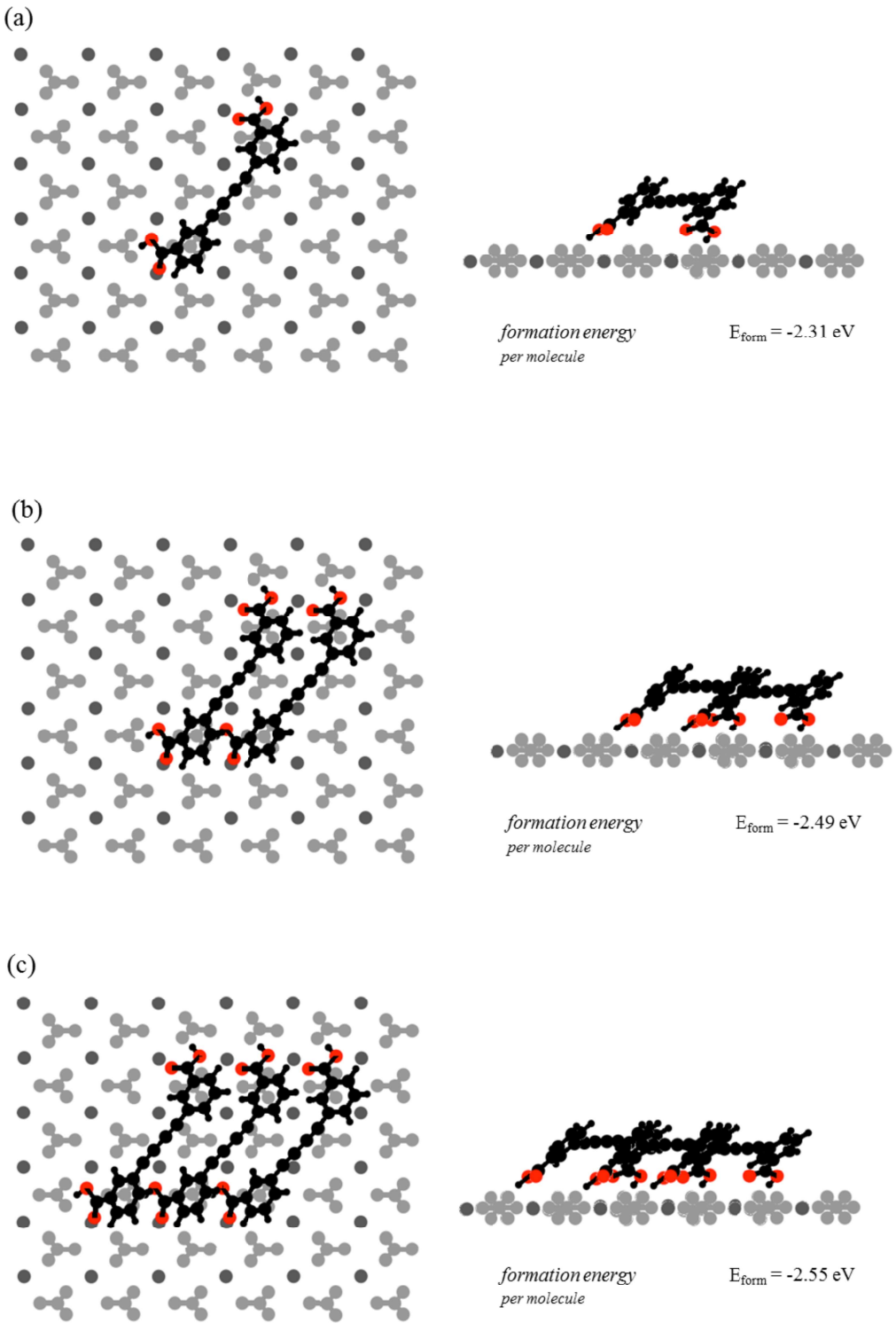

Fig. 9.12: 3-BBA monomer (a), dimer (b) and trimer (c) on calcite surface. The formation energies are shown, indicating small but attractive interaction between the molecules. Image adopted from Ref.[277]

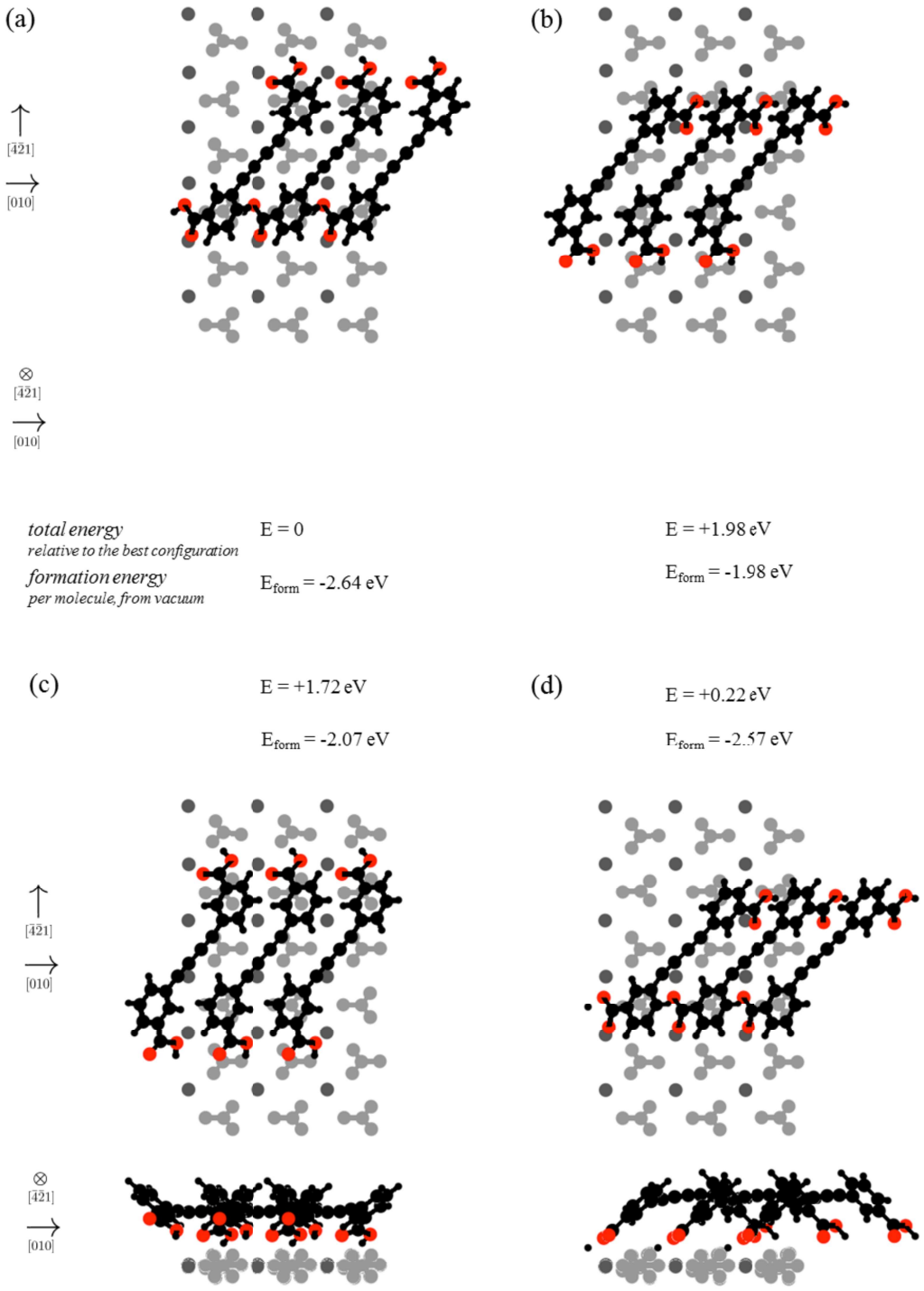

Fig. 9.13: Four optimized configurations for the (isolated) molecular rows. The total and formation energies are shown. Image adopted from Ref.[277]

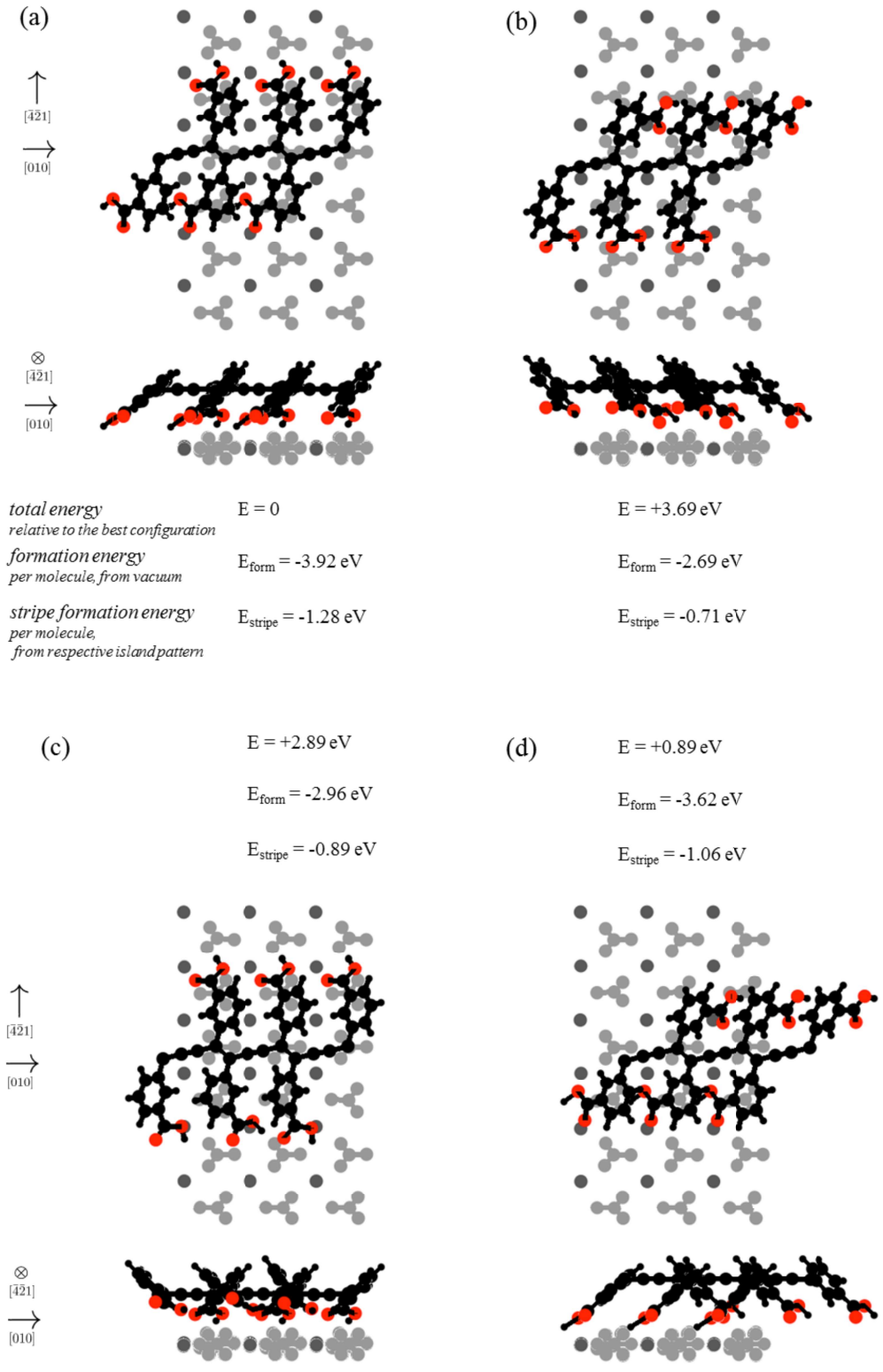

Fig. 9.14: Four optimized configurations for the polymerized stripes. The structures (a) to (d) are derived from the structures (a) to (d) shown in Fig. 9.13, respectively. The total and formation energies are shown. Image adopted from Ref.[277]

Bibliography

[1] M. Gille, L. Grill, S. Hecht, "Bottom-up zu molekularen Nanostrukturen", *Nachrichten aus der Chemie* **2012**, *60*, 986–990.

[2] R. L. Carroll, C. B. Gorman, "The Genesis of Molecular Electronics", *Angewandte Chemie - International Edition* **2002**, *41*, 4378–4400.

[3] K. Garg *et al.*, "A novel design for porphyrin based D-s-A systems as molecular rectifiers", *Chem. Sci.* **2016**, *7*, 1548–1557.

[4] J. Park *et al.*, "Coulombblockadeand theKondo effect in single-atom transistors", *Nature* **2002**, *417*, 722–725.

[5] P. Liljeroth, J. Repp, G. Meyer, "Current-Induced Hydrogen", *Science* **2007**, *317*, 1203–1206.

[6] C. Loppacher *et al.*, "Direct determination of the energy required to operate a single molecule switch.", *Physical Review Letters* **2003**, *90*, 066107.

[7] Z. J. Donhauser *et al.*, "Conductance switching in single molecules through conformational changes", *Science* **2001**, *292*, 2303–2307.

[8] T. Glatzel *et al.*, "Molecular assemblies grown between metallic contacts on insulating surfaces", *Applied Physics Letters* **2009**, *94*, 10–13.

[9] G. M. Whitesides, B. Grzybowski, "Self-assembly at all scales.", *Science (New York NY)* **2002**, *295*, 2418–2421.

[10] G. M. Whitesides, J. P. Mathias, C. T. Seto, "Molecular Self-Assembly and Nanochemistry: A Chemical Strategy for the Synthesis of Nanostructures", *Science* **1991**, *254*, 1312–1319.

[11] A. Gourdon, *On-Surface Synthesis Proceedings of the International Workshop On-Surface Synthesis, École des Houches, Les Houches 25-30 May 2014, Vol. 49*, (Eds.: A. Gourdon, S. E. Joachim, Christian), Springer, **2011**, p. 6221.

[12] F. Klappenberger *et al.*, "On-Surface Synthesis of Carbon-Based Scaffolds and Nanomaterials Using Terminal Alkynes.", *Accounts of Chemical Research* **2015**, *48*, 2140–50.

[13] R. Lindner, A. Kühnle, "On-surface reactions", *ChemPhysChem* **2015**, *16*, 1582–1592.

[14] G. Franc, A. Gourdon, "Covalent networks through on-surface chemistry in ultra-high vacuum: state-of-the-art and recent developments", *Phys Chem Chem Phys* **2011**, *13*, 14283.

[15] G. Binnig *et al.*, "Surface Studies by Scanning Tunneling Microscopy", *Physical Review Letters* **1982**, *49*, 57–61.

[16] G. Binnig, H. Rohrer, "Press Release: The 1986 Nobel Prize in Physics". Nobelprize.org. Nobel Media AB 2014. Web. 13 Mar 2018.

[17] G. Binnig, C. F. Quate, "Atomic Force Microscope", *Physical Review Letters* **1986**, *56*, 930–933.

[18] F. J. Giessibl, "Surface by Atomic Force Microscopy", *Science* **1995**, *267*, 68.

[19] T. R. Albrecht *et al.*, "Frequency modulation detection using high-Q cantilevers for enhanced force microscope sensitivity", *Journal of Applied Physics* **1991**, *69*, 668–673.

[20] M. V. Makarova *et al.*, "Self-assembled diacetylene molecular wire polymerization on an insulating hexagonal boron nitride (0001) surface", *Nanotechnology* **2016**, *27*, 1–8.

[21] A. Deshpande *et al.*, "Self-assembly and photopolymerization of sub-2 nm one-dimensional organic nanostructures on graphene", *Journal of the American Chemical Society* **2012**, *134*, 16759–16764.

[22] J. Krüger *et al.*, "Tetracene Formation by On-Surface Reduction", *ACS Nano* **2016**, *10*, 4538–4542.

[23] N. Pavliček *et al.*, "Synthesis and characterization of triangulene", *Nature Nanotechnology* **2017**, *12*, 308–311.

[24] N. Pavliček *et al.*, "On-surface generation and imaging of arynes by atomic force microscopy", *Nature Chemistry* **2015**, *7*, 623–628.

[25] M. Kittelmann *et al.*, "On-surface covalent linking of organic building blocks on a bulk insulator", *ACS Nano* **2011**, *5*, 8420–8425.

[26] A. Richter *et al.*, "On-surface synthesis on a bulk insulator surface", *Journal of Physics: Condensed Matter* **2018**, *30*, 133001.

[27] G. Meyer, N. M. Amer, "Erratum: Novel optical approach to atomic force microscopy", *Applied Physics Letters* **1988**, *53*, 2400–2402.

[28] H. Söngen, R. Bechstein, A. Kühnle, "Quantitative atomic force microscopy", *Journal of Physics: Condensed Matter* **2017**, *29*, 274001.

[29] F. J. Giessibl, "Advances in atomic force microscopy", *Reviews of Modern Physics* **2003**, *75*, 949–983.

[30] M. M. Nalbach, "In-situ Characterization of Surface Restructuring and Molecular Self-Assembly at the Calcite-Water Interface", PhD thesis, Johannes Gutenberg-Universität, **2017**.

[31] R. Lindner, "Stabilizing Molecular Self-Assemblies via On-Surface Reactions", PhD thesis, Johannes Gutenberg-Universität, **2015**.

[32] W. A. Deer, R. A. Howie, J. Zussman, *An introduction to the rock forming minerals*, Mineralogical Society of Great Britain and Ireland, **1992**.

[33] R. J. Reeder, *Carbonates: Mineralogy and Chemistry, Vol. 11*, Mineralogical Society of America, **1983**, p. 399.

[34] M. Ukita *et al.*, "Pressure-induced phase transition of calcite and aragonite: A first principles study", *Journal of Applied Physics* **2016**, *120*, 142118.

[35] W. Schumann, *Der grosse Steine- und Mineralienführer*, **1990**, p. 383.

[36] www.mainz.de/freizeit-und-sport/im-gruenen/geopfad tafeln.php, Geopfad Weisenau, (Ed.: Heike Tharun).

[37] J. Currey, "The design of mineralised hard tissues for their mechanical functions", *The Journal of Experimental Biology* **1999**, *202*, 3285–3294.

[38] H. Cölfen, S. Mann, "Higher-order organization by mesoscale self-assembly and transformation of hybrid nanostructures", *Angewandte Chemie International Edition* **2003**, *42*, 2350–2365.

[39] R. N. Smartt, W. H. Steel, "Birefringence of Quartz and Calcite", *Journal of the Optical Society of America* **1959**, *49*, 710.

[40] B. Zhang *et al.*, "Macroscopic invisibility cloak for visible light", *Physical Review Letters* **2011**, *106*, 1–4.

[41] S. Hirano, T. Yogo, K. Kikuta, "Synthetic calcite single crystals for optical device", *Progress in Crystal Growth and Characterization of Materials* **1991**, *23*, 341–367.

[42] J. W. Gifford, "The Refractive Indices of Fluorite, Quartz, and Calcit", *Proceedings of the Royal Society of London A: Mathematical Physical and Engineering Sciences* **1902**, *70*, 329–340.

[43] J. W. Anthony, R. A. Bideaux, K. W. Bladh, *Vol. 5*, Mineralogical Society of America, Chantilly VA US, **2003**, Chapter Calcite.

[44] D. W. Rankin, *CRC Handbook of Chemistry and Physics Internet (Internet Version 2009)*, *Vol. 89*, (Ed.: D. R. Lide), **2009**.

[45] D. R. Baer, D. L. Blanchard, "Studies of the calcite cleavage surface for comparison with calculation", *Applied Surface Science* **1993**, *72*, 295–300.

[46] V. E. Puchin *et al.*, "Theoretical modelling of steps on the CaF_2 (111) surface", *Journal of Physics: Condensed Matter* **2001**, *13*, 2081–2094.

[47] N. H. de Leeuw, T. G. Cooper, "A computational study of the surface structure and reactivity of calcium fluoride", *Journal of Materials Chemistry* **2003**, *13*, 93–101.

[48] W. C. Mackrodt, R. F. Stewart, "Defect properties of ionic solids: I. Point-defects at surfaces of face-centered cubic-crystals", *Journal of Physics C-Solid State Physics* **1977**, *10*, 1431–1446.

[49] G. C. Benson, T. A. Claxton, "Application of a shell model to calculation of surface distortion in alkali halide crystals", *Journal of Chemical Physics* **1968**, *48*, 1356–1360.

[50] J. J. Gilman, "Direct measurements of the surface energies of crystals", *Journal of Applied Physics* **1960**, *31*, 2208–2218.

[51] F. Van Zeggeren, G. C. Benson, "Calculation of the surface energies of alkali halide crystals", *The Journal of Chemical Physics* **1957**, *26*, 1077–1082.

[52] R. Shuttleworth, "The surface energies of inert-gas and ionic crystals", *Proceedings of the Physical Society. Section A* **1949**, *62*, 167–179.

[53] P. W. Tasker, "The surface energies, surface tensions and surface structure of the alkali halide crystals", *Philosophical Magazine A* **1979**, *39*, 119–136.

[54] T. Akiyama, K. Nakamura, T. Ito, "Atomic and electronic structures of $CaCO_3$ surfaces", *Physical Review B* **2011**, *84*, 085428.

[55] P. A. Rahe, "The Calcite(1014) Surface: A Versatile Substrate for Molecular Self-Assembly", PhD thesis, Johannes Gutenberg-Universität, **2011**.

[56] S. Kerisit, S. C. Parker, J. H. Harding, "Atomistic Simulation of the Dissociative Adsorption of Water on Calcite Surfaces", *The Journal of Physical Chemistry B* **2003**, *107*, 7676–7682.

[57] H. Effenberger, J. Zemann, K. Mereiter, "Crystal structure refinements of magnesite, calcite, rhodochrosite, siderite, smithonite, and dolomite, with discussion of some aspects of the stereochemistry of calcite type carbonates", *Zeitschrift für Kristallographie - New Crystal Structures* **1981**, *156*, 233–243.

[58] R. P. Feynman, "There's plenty of room at the bottom", *Engineering and Science* **1960**, *23*, 22–35.

[59] C. Brabec, N. Sariciftci, J. Hummelen, "Plastic solar cells", *Advanced functional materials* **2001**, *11*, 15–26.

[60] K. Müllen, U. Scherf, *Organic Light-Emitting Devices: Synthesis, Properties and Applications*, (Eds.: K. Müllen, U. Scherf), Wiley-VCH, Weinheim, **2006**, p. 426.

[61] J. Zaumseil, H. Sirringhaus, "Electron and ambipolar transport in organic field-effect transistors", *Chemical Reviews* **2007**, *107*, 1296–1323.

[62] H. Shirakawa *et al.*, "Synthesis of electrically conducting organic polymers: halogen derivatives of polyacetylene, $(CH)_x$", *Journal of the Chemical Society Chemical Communications* **1977**, 578–580.

[63] C. K. Chiang *et al.*, "Electrical conductivity in doped polyacetylene", *Physical Review Letters* **1977**, *39*, 1098–1101.

[64] C. K. Chiang *et al.*, "Synthesis of Highly Conducting Films of Derivatives of Polyacetylene, $(CH)_x$", *Journal of the American Chemical Society* **1978**, *100*, 1013–1015.

[65] H. Shirakawa, "Die Entdeckung der Polyacetylenfilme - der Beginn des Zeitalters leitfähiger Polymere", *Angewandte Chemie* **2001**, *113*, 2642–2648.

[66] A. J. Heeger, "Halbleitende und metallische Polymere : polymere Materialien der vierten Generation", *Angewandte Chemie* **2001**, *113*, 2660–26782.

[67] A. G. Macdiarmid, ""Synthetische Metalle": eine neue Rolle für organische Polymere", *Angewandte Chemie* **2001**, *113*, 2649.

[68] M. Rehahn, "Der Weg zu einer neuen Materialklasse Elektrisch leitfähige Kunststoffe", *Chemie unserer Zeit* **2003**, *4*, 18–30.

[69] G. G. Wallace *et al.*, *Conductive Electroactive Polymers*, *Vol. 3*, **2009**, p. 263.

[70] A. Aviram, M. A. Ratner, "Molecular rectifiers", *Chemical Physics Letters* **1974**, *29*, 277–283.

[71] M. Mayor, H. B. Weber, "Molekulare Elektronik", *Nachrichten aus der Chemie* **2002**, *50*, 1212–1217.

[72] K. M. Roth *et al.*, "Molecular approach toward information storage based on the redox properties of porphyrins in self-assembled monolayers ", *Journal of Vacuum Science and Technology B* **2000**, *18*, 2359.

[73] M. Stöhr *et al.*, "Controlling molecular assembly in two dimensions: The concentration dependence of thermally induced 2D aggregation of molecules on a metal surface", *Angewandte Chemie - International Edition* **2005**, *44*, 7394–7398.

[74] R. Van Hameren *et al.*, "Macroscopic hierarchical surface patterning of porphyrin trimers via self-assembly and dewetting", *Science* **2006**, *314*, 1433–1436.

[75] T. Yokoyama *et al.*, "Selective assembly on a surface of supramolecular aggregates with controlled size and shape", *Nature* **2001**, *413*, 619–621.

[76] J. P. Rabe, S Buchholz, "Commensurability and mobility in two-dimensional molecular patterns on graphite.", *Science (New York N.Y.)* **1991**, *253*, 424–427.

[77] N. Lin *et al.*, "Real-time single-molecule imaging of the formation and dynamics of coordination compounds", *Angewandte Chemie - International Edition* **2002**, *41*, 4779–4783.

[78] J. L. Neff *et al.*, "Decisive Influence of Substitution Positions in Molecular Self-Assembly", **2014**, *16*, 15437–15443.

[79] J. Neff *et al.*, "Generic Nature of Long-Range Repulsion Mechanism on a Bulk Insulator?", *Faraday Discussion* **2017**, *204*, 419–428.

[80] L. Grill *et al.*, "Nano-architectures by covalent assembly of molecular building blocks.", *Nature Nanotechnology* **2007**, *2*, 687–691.

[81] J. Sakamoto *et al.*, "Two-dimensional polymers: Just a dream of synthetic chemists?", *Angewandte Chemie - International Edition* **2009**, *48*, 1030–1069.

[82] A. Gourdon, "On-surface covalent coupling in ultrahigh vacuum", *Angewandte Chemie International Edition* **2008**, *47*, 6950–6953.

[83] Q. Fan, J. M. Gottfried, J. Zhu, "Surface-Catalyzed C-C Covalent Coupling Strategies toward the Synthesis of Low-Dimensional Carbon-Based Nanostructures", *Accounts of Chemical Research* **2015**, *48*, 2484–2494.

[84] A. P. Côté, "Porous, Crystalline, Covalent Organic Frameworks", *Science* **2005**, *310*, 1166–1170.

[85] A. Nitzan, "Electron Transport in Molecular Wire Junctions", *Science* **2003**, *300*, 1384–1389.

[86] M. Pivetta *et al.*, "Formation of Fe cluster superlattice in a metal-organic quantum-box network", *Physical Review Letters* **2013**, *110*, 1–5.

[87] Q. Shen, H. Y. Gao, H. Fuchs, "Frontiers of on-surface synthesis: From principles to applications", *Nano Today* **2017**, *13*, 77–96.

[88] S.-W. Hla *et al.*, "Inducing All Steps of a Chemical Reaction with the Scanning Tunneling Microscope Tip: Towards Single Molecule Engineering", *Physical Review Letters* **2000**, *85*, 2777–2780.

[89] F. Ullmann *et al.*, "Mittheilungen aus dem chemischen Laboratorium der Universitat Marburg", *Justus Liebigs Annalen der Chemie* **1905**, *343*, 75–99.

[90] Y. Okawa, M. Aono, "Linear chain polymerization initiated by a scanning tunneling microscope tip at designated positions", *The Journal of Chemical Physics* **2001**, *115*, 2317–2322.

[91] Y. Okawa, M. Aono, "Nanoscale control of chain polymerization.", *Nature* **2001**, *409*, 683–4.

[92] L. Lafferentz *et al.*, "Controlling on-surface polymerization by hierarchical and substrate-directed growth", *Nature Chemistry* **2012**, *4*, 215–220.

[93] R. Gutzler *et al.*, "Surface mediated synthesis of 2D covalent organic frameworks: 1,3,5-tris(4-bromophenyl)benzene on graphite(001), Cu(111), and Ag(110).", *Chemical Communications* **2009**, 4456–4458.

[94] J. Eichhorn *et al.*, "On-surface ullmann coupling: The influence of kinetic reaction parameters on the morphology and quality of covalent networks", *ACS Nano* **2014**, *8*, 7880–7889.

[95] J. Cai *et al.*, "Atomically precise bottom-up fabrication of graphene nanoribbons.", *Nature* **2010**, *466*, 470–473.

[96] M. Treier *et al.*, "Surface-assisted cyclodehydrogenation provides a synthetic route towards easily processable and chemically tailored nanographenes.", *Nature Chemistry* **2011**, *3*, 61–67.

[97] H. Y. Gao *et al.*, "Effect of metal surfaces in on-surface glaser coupling", *Journal of Physical Chemistry C* **2013**, *117*, 18595–18602.

[98] H.-Y. Gao *et al.*, "Glaser Coupling at Metal Surfaces.", *Angewandte Chemie International Edition* **2013**, *52*, 4024–4028.

[99] H. Y. Gao *et al.*, "Photochemical glaser coupling at metal surfaces", *Journal of Physical Chemistry C* **2014**, *118*, 6272–6277.

[100] L. Colazzo *et al.*, "Metal-Free on-Surface Photochemical Homocoupling of Terminal Alkynes", *Journal of American Chemical Society* **2016**, *138*, 10151–10156.

[101] N. A. A. Zwaneveld *et al.*, "Organized formation of 2D extended covalent organic frameworks at surfaces", *Journal of American Chemical Society* **2008**, *130*, 6678–6679.

[102] S. Schlögl *et al.*, "Synthesis of two-dimensional phenylene-boroxine networks through in vacuo condensation and on-surface radical addition", *Chemical Communications* **2011**, *47*, 12355–12357.

[103] T. Faury *et al.*, "Covalent interlinking of an aldehyde and an amine on a Au(111) surface in ultrahigh vacuum", *Journal of Physical Chemistry* **2012**, *116*, 4819–4823.

[104] S. Weigelt *et al.*, "Covalent interlinking of an aldehyde and an amine on a Au(111) surface in ultrahigh vacuum", *Angewandte Chemie - International Edition* **2007**, *46*, 9227–9230.

[105] M. Treier, N. V. Richardson, R. Fasel, "Fabrication of surface-supported low-dimensional polyimide networks", *Journal of the American Chemical Society* **2008**, *130*, 14054–14055.

[106] C. H. Schmitz, J. Ikonomov, M. Sokolowski, "Two-dimensional ordering of poly(p-phenylene-terephthalamide) on the Ag(111) surface investigated by scanning tunneling microscopy", *Journal of Physical Chemistry C* **2009**, *113*, 11984–11987.

[107] O. Diaz Arado *et al.*, "On-surface azide-alkyne cycloaddition on Au(111)", *ACS Nano* **2013**, *7*, 8509–8515.

[108] F. Bebensee *et al.*, "On-Surface Azide-Alkyne Cycloaddition on Cu(111): Does It "Click" in Ultrahigh Vacuum?", *Journal of American Chemical Society* **2013**, *135*, 2136–2139.

[109] J. Krüger *et al.*, "Decacene: On-Surface Generation", *Angewandte Chemie - International Edition* **2017**, *56*, 11945–11948.

[110] M. Matena *et al.*, "Transforming surface coordination polymers into covalent surface polymers: Linked polycondensed aromatics through oligomerization of N-heterocyclic carbene intermediates", *Angewandte Chemie - International Edition* **2008**, *47*, 2414–2417.

[111] M. Matena *et al.*, "Aggregation and contingent metal/surface reactivity of 1,3,8,10-tetraazaperopyrene (TAPP) on Cu(111)", *Chemistry - A European Journal* **2010**, *16*, 2079–2091.

[112] S. Blankenburg, E. Rauls, W. G. Schmidt, "Catalytic action of a Cu(111) surface on tetraazaperopyrene polymerization", *Journal of Physical Chemistry Letters* **2010**, *1*, 3266–3270.

[113] W. Schmidt *et al.*, "Copper Substrate Catalyzes Tetraazaperopyrene Polymerization", *High Performance Computing in Science and Engineering* **2012**, *11*, 47–56.

[114] A. Richter *et al.*, "Diacetylene polymerization on a bulk insulator surface", *Physical Chemistry Chemical Physics* **2017**, *19*, 15172–15176.

[115] H. Ozaki *et al.*, "Single Sheet of a Quasi-Planar Macromolecule Prepared by Photopolymerization at a Solid Surface", *Journal of the American Chemical Society* **1995**, *117*, 5596–5597.

[116] M. Nakaya *et al.*, "Nanojunction between fullerene and one-dimensional conductive polymer on solid surfaces", *ACS Nano* **2014**, *8*, 12259–12264.

[117] D. Takajo *et al.*, "Chain polymerization of diacetylene compound multilayer films on the topmost surface initiated by a scanning tunneling microscope tip", *Langmuir* **2007**, *23*, 5247–5250.

[118] R. Giridharagopal, K. F. Kelly, "Substrate-dependent properties of polydiacetylene nanowires on graphite and Mo S2", *ACS Nano* **2008**, *2*, 1571–1580.

[119] S. K. Mandal *et al.*, "Rate-determining factors in the chain polymerization of molecules initiated by local single-molecule excitation", *ACS Nano* **2011**, *5*, 2779–2786.

[120] P. C. M. Grim *et al.*, "Submolecularly Resolved Polymerization of Diacetylene Molecules on the Graphite Surface Observed with Scanning Tunneling Microscopy", *Angewandte Chemie International Edition in English* **1997**, *36*, 2601–2603.

[121] O. Endo *et al.*, "Structures of 17,19-hexatriacontadiyne monolayers on Au(111) studied by infrared reflection absorption spectroscopy and scanning tunneling microscopy", *Journal of Physical Chemistry B* **2006**, *110*, 13100–13106.

[122] D. N. Batchelder *et al.*, "Self-Assembled Monolayers containing Polydiacetylenes", *Journal of the American Chemical Society* **1994**, *116*, 1050–1053.

[123] O. Endo *et al.*, "Structures of a 17,19-Hexatriacontadiyne and Sashlike Polydiacetylene Monolayer on MoS_2(0001) Studied by UHV-STM", *Proceedings of the 17th International Vacuum Congress/13th International Conference on Surface Science/International Conference on Nanoscience and Technology*, 052058.

[124] P. A. Held *et al.*, "On-Surface Domino Reactions: Glaser Coupling and Dehydrogenative Coupling of a Biscarboxylic Acid To Form Polymeric Bisacylperoxides", *Angewandte Chemie International Edition* **2016**, *55*, 9777–9782.

[125] J. Eichhorn, W. M. Heckl, M. Lackinger, "On-surface polymerization of 1,4-diethynylbenzene on Cu(111)", *Chemical Communications* **2013**, *49*, 2900–2902.

[126] B. Cirera *et al.*, "2D Self-Assembly and Catalytic Homo-coupling of the Terminal Alkyne 1,4-Bis(3,5-diethynyl-phenyl)butadiyne-1,3 on Ag(111)", *ChemCatChem* **2013**, *5*, 3281–3288.

[127] Y.-Q. Zhang *et al.*, "Homo-coupling of terminal alkynes on a noble metal surface.", *Nature Communications* **2012**, *3*, 1286.

[128] B. Cirera *et al.*, "Synthesis of extended graphdiyne wires by vicinal surface templating", *Nano Letters* **2014**, *14*, 1891–1897.

[129] J. Björk *et al.*, "Unraveling the mechanism of the covalent coupling between terminal alkynes on a noble metal", *Journal of Physical Chemistry C* **2014**, *118*, 3181–3187.

[130] J. Liu *et al.*, "Lattice-Directed Formation of Covalent and Organometallic Molecular Wires by Terminal Alkynes on Ag Surfaces", *ACS Nano* **2015**, *9*, 6305–6314.

[131] X. Zhang *et al.*, "Polymerization or Cyclic Dimerization: Solvent Dependent Homo-Coupling of Terminal Alkynes at HOPG Surface", *Scientific Reports* **2014**, *4*, 1–5.

[132] A. Richter *et al.*, "Homocoupling of terminal alkynes on calcite (10.4)", *Surface Science* **2018**, *000*, 1–6.

[133] T. Wang *et al.*, "Highly Selective Synthesis of *cis*-Enediynes on a Ag(111) Surface", *Angewandte Chemie International Edition* **2017**, *56*, 4762–4766.

[134] J. Liu *et al.*, "Cyclotrimerization of arylalkynes on Au(111).", *Chemical communications (Cambridge England)* **2014**, *50*, 11200–11203.

[135] H. Zhou *et al.*, "Direct visualization of surface-assisted two-dimensional diyne polycyclotrimerization", *Journal of the American Chemical Society* **2014**, *136*, 5567–5570.

[136] A. Riss *et al.*, "Local electronic and chemical structure of oligo-acetylene derivatives formed through radical cyclizations at a surface", *Nano Letters* **2014**, *14*, 2251–2255.

[137] C. Sánchez-Sánchez *et al.*, "The flexible surface revisited: Adsorbate-induced reconstruction, homocoupling, and sonogashira cross-coupling on the Au(100) surface", *Journal of Physical Chemistry C* **2014**, *118*, 11677–11684.

[138] V. K. Kanuru *et al.*, "Sonogashira coupling on an extended gold surface in vacuo: Reaction of phenylacetylene with iodobenzene on Au(111)", *Journal of the American Chemical Society* **2010**, *132*, 8081–8086.

[139] C. Sánchez-Sánchez *et al.*, "Sonogashira cross-coupling and homocoupling on a silver surface: Chlorobenzene and phenylacetylene on Ag(100)", *Journal of the American Chemical Society* **2015**, *137*, 940–947.

[140] D. G. De Oteyza *et al.*, "Noncovalent Dimerization after Enediyne Cyclization on Au(111)", *Journal of the American Chemical Society* **2016**, *138*, 10963–10967.

[141] Q. Sun *et al.*, "On-surface formation of one-dimensional polyphenylene through Bergman cyclization", *Journal of the American Chemical Society* **2013**, *135*, 8448–8451.

[142] A. Riss *et al.*, "Imaging Single-Molecule Reaction Intermediates Stabilized by Surface Dissipation and Entropy", *Nature Chemistry* **2016**, *8*, 678–683.

[143] D. G. de Oteyza *et al.*, "Direct Imaging of Covalent Bond Structure in Single-Molecule Chemical Reactions", *Science* **2013**, *340*, 1434–1437.

[144] Q. Sun *et al.*, "Dehalogenative Homocoupling of Terminal Alkynyl Bromides on Au(111): Incorporation of Acetylenic Scaffolding into Surface Nanostructures", *ACS Nano* **2016**, *10*, 7023–7030.

[145] Q. Sun *et al.*, "The stereoselective synthesis of dienes through dehalogenative homocoupling of terminal alkenyl bromides on Cu(110)", *Chemical Communications* **2016**, *52*, 6009–6012.

[146] Q. Sun *et al.*, "Dehydrogenative Homocoupling of Terminal Alkenes on Copper Surfaces: A Route to Dienes", *Angewandte Chemie - International Edition* **2015**, *54*, 4549–4552.

[147] A. C. Aragonès *et al.*, "Electrostatic catalysis of a Diels-Alder reaction", *Nature* **2016**, *531*, 88–91.

[148] B. Cirera *et al.*, "Thermal selectivity of intermolecular versus intramolecular reactions on surfaces", *Nature Communications* **2016**, *7*, 11002.

[149] M. M. Abdel-Mottaleb *et al.*, "Photodimerization of Cinnamate Derivatives Studied by STM", *Nano Letters* **2001**, *1*, 353–359.

[150] Q. Sun *et al.*, "On-Surface Formation of Cumulene by Dehalogenative Homocoupling of Alkenyl gem-Dibromides", *Angewandte Chemie - International Edition* **2017**, *56*, 12165–12169.

[151] J. Björk, F. Hanke, S. Stafström, "Mechanisms of halogen-based covalent self-assembly on metal surfaces", *Journal of the American Chemical Society* **2013**, *135*, 5768–5775.

[152] M. Bieri *et al.*, "Two-dimensional polymer formation on surfaces: Insight into the roles of precursor mobility and reactivity", *Journal of the American Chemical Society* **2010**, *132*, 16669–16676.

[153] A. Basagni *et al.*, "On-surface photo-dissociation of C-Br bonds: towards room temperature Ullmann coupling", *Chem. Commun.* **2015**, *51*, 12593–12596.

[154] S. Zint *et al.*, "Imaging Successive Intermediate States of the On-Surface Ullmann Reaction on Cu(111): Role of the Metal Coordination", *ACS Nano* **2017**, *11*, 4183–4190.

[155] M.-T. Nguyen, C. A. Pignedoli, D. Passerone, "An ab initio insight into the Cu(111)-mediated Ullmann reaction.", *Physical Chemistry Chemical Physics* **2011**, *13*, 154–160.

[156] R. Gutzler *et al.*, "Ullmann-type coupling of brominated tetrathienoanthracene on copper and silver.", *Nanoscale* **2014**, *6*, 2660–8.

[157] M. Di Giovannantonio *et al.*, "Mechanistic Picture and Kinetic Analysis of Surface-Confined Ullmann Polymerization", *Journal of the American Chemical Society* **2016**, *138*, 16696–16702.

[158] J. A. Lipton-Duffin *et al.*, "Synthesis of polyphenylene molecular wires by surface-confined polymerization", *Small* **2009**, *5*, 592–597.

[159] Q. Fan *et al.*, "On-Surface Pseudo-High-Dilution Synthesis of Macrocycles: Principle and Mechanism", *ACS Nano* **2017**, *11*, 5070–5079.

[160] M. Bieri *et al.*, "Porous graphenes: two-dimensional polymer synthesis with atomic precision.", *Chemical communications (Cambridge England)* **2009**, 6919–6921.

[161] C Morchutt *et al.*, "Covalent coupling via dehalogenation on Ni(111) supported boron nitride and graphene", *Chemical Communications* **2015**, *51*, 2440–2443.

[162] W. Zhao *et al.*, "Cu- and Pd-Catalyzed Ullmann Reaction on a Hexagonal Boron Nitride Layer", *Chem. Commun.* **2016**, *52*, 13225–13228.

[163] D Sloan *et al.*, "Photochemistry of Iodobenzene Adsorbed on Sapphire(0001)", *The Journal of Physical Chemistry B* **1998**, *102*, 6825–6830.

[164] P. Olszowski *et al.*, "Aryl Halide C-C Coupling on Ge(001):H Surfaces", *Journal of Physical Chemistry C* **2015**, *119*, 27478–27482.

[165] J. Adisoejoso *et al.*, "A single-molecule-level mechanistic study of pd-catalyzed and cu-catalyzed homocoupling of aryl bromide on an au(111) surface", *Chemistry - A European Journal* **2014**, *20*, 4111–4116.

[166] L. Dong *et al.*, "Transition Metals Trigger On-Surface Ullmann Coupling Reaction: Intermediate, Catalyst and Template" in *On-Surface Synthesis, Advances in Atom and Single Molecule Machines*, (Ed.: A. Gourdon), **2016**, pp. 269–287.

[167] C. A. Palma *et al.*, "Photoinduced C-C reactions on insulators toward photolithography of graphene nanoarchitectures", *Journal of the American Chemical Society* **2014**, *136*, 4651–4658.

[168] C. Bombis *et al.*, "Single molecular wires connecting metallic and insulating surface areas", *Angewandte Chemie - International Edition* **2009**, *48*, 9966–9970.

[169] M. Kittelmann *et al.*, "Sequential and site-specific on-surface synthesis on a bulk insulator", *ACS Nano* **2013**, *7*, 5614–5620.

[170] C. Guo *et al.*, "Mechanisms of Covalent Dimerization on a Bulk Insulating Surface", *Journal of Physical Chemistry C* **2017**, *121*, 10053–10062.

[171] M. Kittelmann *et al.*, "Controlled activation of substrate templating in molecular self-assembly by deprotonation", *Journal of Physical Chemistry C* **2013**, *117*, 23868–23874.

[172] J. R. Sanchez-Valencia *et al.*, "Controlled synthesis of single-chirality carbon nanotubes", *Nature* **2014**, *512*, 61–64.

[173] O. Snezhkova *et al.*, "Iron phthalocyanine on Cu(111): Coverage-dependent assembly and symmetry breaking, temperature-induced homocoupling, and modification of the adsorbate-surface interaction by annealing", *Journal of Chemical Physics* **2016**, *144*.

[174] Q. Sun *et al.*, "On-surface aryl-aryl coupling via selective C-H activation", *Chem. Commun.* **2014**, *50*, 11825–11828.

[175] C. Zhang *et al.*, "Formation of polyphenyl chains through hierarchical reactions: Ullmann coupling followed by cross-dehydrogenative coupling", *Chem. Commun.* **2015**, *51*, 495–498.

[176] Q. Li *et al.*, "Surface-Controlled Mono/Diselective ortho C-H Bond Activation", *Journal of the American Chemical Society* **2016**, *138*, 2809–2814.

[177] S. Blankenburg *et al.*, "Intraribbon heterojunction formation in ultranarrow graphene nanoribbons", *ACS Nano* **2012**, *6*, 2020–2025.

[178] N. Kocić *et al.*, "Control of reactivity and regioselectivity for on-surface dehydrogenative aryl-aryl bond formation", *Journal of the American Chemical Society* **2016**, *138*, 5585–5593.

[179] X. Y. Wang *et al.*, "Heteroatom-Doped Perihexacene from a Double Helicene Precursor: On-Surface Synthesis and Properties", *Journal of the American Chemical Society* **2017**, *139*, 4671–4674.

[180] Q. Chen *et al.*, "Steering On-Surface Reactions by a Self-Assembly Approach", *Angewandte Chemie - International Edition* **2017**, *56*, 5026–5030.

[181] A. Wiengarten *et al.*, "Surface-assisted dehydrogenative homocoupling of porphine molecules", *Journal of the American Chemical Society* **2014**, *136*, 9346–9354.

[182] Q. Sun *et al.*, "On-surface formation of two-dimensional polymer via direct C-H activation of metal phthalocyanine", *Chemical Communications* **2015**, *51*, 2836–2839.

[183] B. V. Tran *et al.*, "Surface-confined [2 + 2] cycloaddition towards one-dimensional polymers featuring cyclobutadiene units", *Nanoscale* **2017**, *9*, 18305–18310.

[184] P. Fesser *et al.*, "Visualizing the product of a formal cycloaddition of 7,7,8,8-tetracyano-p- quinodimethane (TCNQ) to an acetylene-appended porphyrin by scanning tunneling microscopy on Au(111)", *Chemistry - A European Journal* **2011**, *17*, 5246–5250.

[185] R. Lindner *et al.*, "Substrate templating guides the photoinduced reaction of C60 on calcite", *Angewandte Chemie - International Edition* **2014**, *53*, 7952–7955.

[186] B. Yang *et al.*, "Synthesis of surface covalent organic frameworks via dimerization and cyclotrimerization of acetyls", *Journal of the American Chemical Society* **2015**, *137*, 4904–4907.

[187] H. Y. Gao *et al.*, "Decarboxylative polymerization of 2,6-naphthalenedicarboxylic acid at surfaces", *Journal of the American Chemical Society* **2014**, *136*, 9658–9663.

[188] K. Sun *et al.*, "A new on-surface synthesis pathway to 5-armchair graphene nanoribbons on Cu(111) surfaces", *Farraday Discussion* **2017**, 1–9.

[189] F. Albrecht *et al.*, "Characterization of a Surface Reaction by Means of Atomic Force Microscopy", *Journal of the American Chemical Society* **2015**, *137*, 7424–7428.

[190] L. E. Dinca *et al.*, "Unprecedented transformation of tetrathienoanthracene into pentacene on Ni(111)", *ACS Nano* **2013**, *7*, 1652–1657.

[191] L. E. Dinca *et al.*, "Tailoring the Reaction Path in the On-Surface Chemistry of Thienoacenes", *Journal of Physical Chemistry C* **2015**, *119*, 22432–22438.

[192] O. Díaz Arado *et al.*, "On-Surface Reductive Coupling of Aldehydes on Au(111)", *Chem. Commun.* **2015**, 1–4.

[193] Q. Sun *et al.*, "Single-molecule insight into Wurtz reactions on metal surfaces", *Physical Chemistry Chemical Physics* **2016**, *18*, 2730–2735.

[194] Z. Cai *et al.*, "Linear Alkane C-C Bond Chemistry Mediated by Metal Surfaces", *ChemPhysChem* **2015**, *16*, 1356–1360.

[195] D. Zhong *et al.*, "Linear alkane polymerization on a gold surface", *Science* **2011**, *334*, 213–216.

[196] M. I. Veld *et al.*, "Unique intermolecular reaction of simple porphyrins at a metal surface gives covalent nanostructures", *Chemical Communications* **2008**, 1536–1538.

[197] J. Zhang *et al.*, "Step-Edge Assisted Direct Linear Alkane Coupling", *Chemistry - A European Journal* **2017**, *23*, 6185–6189.

[198] R. Zuzak *et al.*, "Nonacene Generated by On-Surface Dehydrogenation", *ACS Nano* **2017**, *11*, 9321–9329.

[199] J. Björk, "Thermodynamics of an Electrocyclic Ring-Closure Reaction on Au(111)", *Journal of Physical Chemistry C* **2016**, *120*, 21716–21721.

[200] X. Leng *et al.*, "Surface-assisted dehydrogenative homocoupling and cyclodehydrogenation of mesityl groups on a copper surface", *Chem. Commun.* **2017**, *53*, 9151–9154.

[201] M. Abel *et al.*, "Sheet on Metal and Thin Insulating Film", *Journal of the American Chemical Society* **2011**, 1203–1205.

[202] E. Nardi *et al.*, "On-Surface Reaction between Tetracarbonitrile-Functionalized Molecules and Copper Atoms", *The Journal of Physical Chemistry C* **2014**, *118*, 6–10.

[203] O. Ourdjini *et al.*, "Substrate-mediated ordering and defect analysis of a surface covalent organic framework", *Physical Review B* **2011**, *84*, 1–9.

[204] T Faury *et al.*, "Sequential Linking To Control Growth of a Surface Covalent Organic Framework", *The Journal of Physical Chemistry C* **2012**, *116*, 4819–4823.

[205] J. F. Dienstmaier *et al.*, "Synthesis of well-ordered COF monolayers: Surface growth of nanocrystalline precursors versus direct on-surface polycondensation", *ACS Nano* **2011**, *5*, 9737–9745.

[206] S. Clair *et al.*, "Tip- or electron beam-induced surface polymerization.", *Chemical communications (Cambridge England)* **2011**, *47*, 8028–8030.

[207] J.-Y. Yue *et al.*, "Simultaneous construction of two linkages for the on-surface synthesis of imine-boroxine hybrid covalent organic frameworks", *Chemical Science* **2017**, *8*, 2169–2174.

[208] J. Plas *et al.*, "Nanopatterning of a covalent organic framework host-guest system", *Chemical Communications* **2016**, *52*, 68–71.

[209] C. Liu *et al.*, "Room-Temperature Synthesis of Covalent Organic Frameworks with a Boronic Ester Linkage at the Liquid/Solid Interface", *Chemistry - A European Journal* **2016**, *22*, 18412–18418.

[210] H. Shi *et al.*, "On-Surface Synthesis of Self-Assembled Monolayers of Benzothiazole Derivatives Studied by STM and XPS", *Langmuir* **2017**, *33*, 4216–4223.

[211] A. C. Marele *et al.*, "Formation of a surface covalent organic framework based on polyester condensation", *Chemical Communications* **2012**, *48*, 6779.

[212] Z. Gong *et al.*, "Structural Variation in Surface-Supported Synthesis by Adjusting the Stoichiometric Ratio of the Reactants", *ACS Nano* **2016**, *10*, 4228–4235.

[213] S. Weigelt *et al.*, "Surface synthesis of 2D branched polymer nanostructures", *Angewandte Chemie - International Edition* **2008**, *47*, 4406–4410.

[214] S. Weigelt *et al.*, "Covalent interlinking of an aldehyde and an amine on a Au(111) surface in ultrahigh vacuum", *Angewandte Chemie - International Edition* **2007**, *46*, 9227–9230.

[215] Y. Yu *et al.*, "Room temperature on-surface synthesis of two-dimensional imine polymers at the solid/liquid interface: concentration takes control", *Chemical Communications* **2016**, *52*, 6609–6612.

[216] Y. Li *et al.*, "Transformation of self-assembled structure by the addition of active reactant", *Journal of Physical Chemistry C* **2011**, *115*, 6540–6544.

[217] X.-L. Sun *et al.*, "Synthesis of One-Dimensional Schiff Base Polymers that Contain an Oligothiophene Building Block on the Graphite Surface", *Chemistry - A European Journal* **2015**, *21*, 6898–6905.

[218] L. Xu *et al.*, "On-surface synthesis of two-dimensional imine polymers with a tunable band gap: a combined STM, DFT and Monte Carlo investigation", *Nanoscale* **2016**, *8*, 8568–8574.

[219] X.-H. Liu *et al.*, "Organic Frameworks via Solid-Vapor Interface Reactions On-surface Synthesis of Single-layered 2D Covalent Organic Frameworks via Solid-Vapor Interface Reactions", *Journal of the American Chemical Society* **2013**, *135*, 10470–10474.

[220] Y. Yu, Y. Zheng, S. Lei, "From a two-dimensional supramolecular network to one-dimensional covalent polymer at the liquid/solid interface: Insight into the role of the stoichiometric ratio of the precursors", *Journal of Physical Chemistry C* **2017**, *121*, 593–599.

[221] L. Jiang *et al.*, "Synthesis of pyrene-fused pyrazaacenes on metal surfaces: Toward one-dimensional conjugated nanostructures", *ACS Nano* **2016**, *10*, 1033–1041.

[222] C. Schmitz, M. Schmid, "Surface polymerization of poly (p-phenylene-terephthalamide) on Ag (111) investigated by X-ray photoelectron spectroscopy and scanning tunneling microscopy", *The Journal of Physical Chemistry C* **2011**, 18186–18194.

[223] C. H. Schmitz, J. Ikonomov, M. Sokolowski, "Two-dimensional polyamide networks with a broad pore size distribution on the Ag(111) surface", *Journal of Physical Chemistry C* **2011**, *115*, 7270–7278.

[224] S. Jensen, H. Früchtl, C. J. Baddeley, "Coupling of triamines with diisocyanates on Au(111) leads to the formation of polyurea networks", *Journal of the American Chemical Society* **2009**, *131*, 16706–16713.

[225] S. Boz *et al.*, "Protecting-group-controlled surface chemistry-organization and heat-induced coupling of 4,4-di(tert-butoxycarbonylamino)biphenyl on metal surfaces", *Angewandte Chemie - International Edition* **2009**, *48*, 3179–3183.

[226] A. Basagni *et al.*, "Stereoselective Photopolymerization of Tetraphenylporphyrin Derivatives on Ag(110) at the Sub-Monolayer Level", *Chemistry - A European Journal* **2014**, *20*, 14296–14304.

[227] M. Matena *et al.*, "On-surface synthesis of a two-dimensional porous coordination network: Unraveling adsorbate interactions", *Physical Review B* **2014**, *90*, 125408.

[228] Y. P. Lin *et al.*, "Self-assembled melamine monolayer on Cu(111)", *Journal of Physical Chemistry C* **2013**, *117*, 9895–9902.

[229] L. Y. O. Yang *et al.*, "Direct visualization of an aniline admolecule and its electropolymerization on au (111) with in situ scanning tunneling microscope", *Journal of the American Chemical Society* **2007**, *129*, 8076–8077.

[230] A. Rastgoo-Lahrood *et al.*, "From Au-Thiolate Chains to Thioether Sierpiński Triangles: The Versatile Surface Chemistry of 1,3,5-Tris(4-mercaptophenyl)benzene on Au(111)", *ACS Nano* **2016**, *10*, 10901–10911.

[231] C. Bombis *et al.*, "Hydrogen-bonded molecular networks of melamine and cyanuric acid on thin films of naCl on au(111)", *Small* **2009**, *5*, 2177–2182.

[232] N. Pavliček, L. Gross, "Generation, manipulation and characterization of molecules by atomic force microscopy", *Nature Reviews Chemistry1* **2017**.

[233] P. Rahe *et al.*, "Tuning molecular self-assembly on bulk insulator surfaces by anchoring of the organic building blocks", *Advanced Materials* **2013**, *25*, 3948–3956.

[234] P. Rahe *et al.*, "From dewetting to wetting molecular layers: C60 on CaCO3(101ÌĎ4) as a case study", *Physical Chemistry Chemical Physics* **2012**, *14*, 6544.

[235] R. Kristensen, S. L. Stipp, K. Refson, "Modeling steps and kinks on the surface of calcite", *Journal of Chemical Physics* **2004**, *121*, 8511–8523.

[236] C. Paris *et al.*, "Increasing the Templating Effect on a Bulk Insulator Surface: From a Kinetically Trapped to a Thermodynamically More Stable Structure", *Journal of Physical Chemistry C* **2016**, *120*, 17546–17554.

[237] J. Maglic, "Desorption of Benzene, Pyridine and Aniline from Calcite (10.4)", Bachelor thesis, Johannes Gutenberg-Universität, **2017**.

[238] E. Ataman *et al.*, "Functional Group Adsorption on Calcite: II. Nitrogen and Sulfur Containing Organic Molecules", *Journal of Physical Chemistry C* **2016**, *120*, 16597–16607.

[239] E. Ataman *et al.*, "Functional Group Adsorption on Calcite: I. Oxygen Containing and Nonpolar Organic Molecules", *Journal of Physical Chemistry C* **2016**, *120*, 16586–16596.

[240] J. Enns, "Syn-Eliminierung: Ist der Carboxylanker aktivierbar?", Bachelor thesis, Johannes Gutenberg-Universität, **2017**.

[241] J. L. Neff, "The Influence of Functional Groups on the Molecular Self-Assembly on Calcite", PhD thesis, Johannes Gutenberg-Universität, **2014**.

[242] M. J. Kittelmann, "On-Surface Chemical Reactions on an Insulating Substrate", PhD thesis, Johannes Gutenberg-Universität, **2013**.

[243] M. Kittelmann, P. Rahe, A. Kühnle, "Molecular self-assembly on an insulating surface: interplay between substrate templating and intermolecular interactions", *Journal of Physics: Condensed Matter* **2012**, *24*, 354007.

[244] A rough estimate of the temperature necessary for this reaction to occur can be obtained by assuming a simple Arrhenius law. Taking an attempt frequency of 1012 s-1, the energy barrier of 3 eV corresponds to a temperature of nearly 1000 K when one assumes that one-half of the molecules are dissociated after 30 min. This is surely way more than the experimentally required temperature.

[245] Fanta, Paul E., "The Ullmann Synthesis of Biaryls", *Chemical Review* **1946**, 139–196.

[246] J. W. Lauher, F. W. Fowler, N. S. Goroff, "Single-crystal-to-single-crystal topochemical polymerizations by design", *Accounts of Chemical Research* **2008**, *41*, 1215–1229.

[247] R. Medishetty *et al.*, "Solid-state polymerisation via [2+2] cycloaddition reaction involving coordination polymers", *Chem. Commun.* **2016**, *52*, 3989–4001.

[248] V. Ramamurthy, K. Venkatesan, "Photochemical Reactions of Organic Crystals", *Chemical Reviews* **1987**, *87*, 433–481.

[249] M. Núñez-Regueiro *et al.*, "Polymerized fullerite structures", *Physical Review Letters* **1995**, *74*, 278–281.

[250] S. Park *et al.*, "The phototransformation of C60 thin films on GaAs(100) studied by in situ Raman spectroscopy", *Journal of Applied Physics* **1998**, *84*, 1340.

[251] J. Onoe *et al.*, "In Situ FTIR, XPS, and STM Studies of the Nano-Structure of a Photopolymerized C60 Film", *Molecular Crystals and Liquid Crystals* **2000**, *340*, 689–694.

[252] M. Nakaya, T. Nakayama, M. Aono, "Fabrication and electron-beam-induced polymerization of C60 nanoribbon", *Thin Solid Films* **2004**, *464-465*, 327–330.

[253] L. Tröger *et al.*, "Concept for support and cleavage of brittle crystals", *Review of Scientific Instruments* **2009**, *80*, 063703.

[254] J. C. Schütte, "Abbildung organischer Moleküle auf dielektrischen Oberlächen", PhD thesis, Universität Osnabrück, **2009**.

[255] R. Bechstein, "Pristine and Doped Titanium Dioxide Studied by NC-AFM", PhD thesis, Universität Osnabrück, **2009**.

[256] S. Kuhn, "Revealing atomic-scale details in the force fields above carbonate surfaces", PhD thesis, Johannes Gutenberg-Universität, **2015**.

[257] L. Schüller, "Untersuchung der Möglichkeiten von metall-organischen Koordinationsnetzwerken auf Calcit(10.4)", Bachelor thesis, Johannes Gutenberg-Universität, **2014**.

[258] L. Schüller, "Further Examining the BPDCA-Iron Metal-Organic Coordination Network on $CaCO_3$(10.4)", Module Report, Johannes Gutenberg-Universität, **2016**.

[259] L. Schüller *et al.*, "Deposition order controls the first stages of a metal-organic coordination network on an insulator surface", *Journal of Physical Chemistry C* **2016**, *120*, 14730–14735.

[260] F. H. Kling, "Diffusion and structure formation of molecules on calcite (104)", PhD thesis, Johannes Gutenberg-Universität, **2016**.

[261] A. Roth, "Inaktivierung von Escherichia coli Bakterien aus DIN 5031 Teil 10", *Application Center Heraeus Noblelight GmbH Germany* **2014**.

[262] D. Nečas, P. Klapetek, "Gwyddion: an open-source software for SPM data analysis", *Open Physics* **2012**, *10*, 2391–5471.

[263] J. Fu *et al.*, "Three-dimensional image correction of tilted samples through coordinate transformation", *Scanning* **2008**, *30*, 41–46.

[264] F. Loske, P. Rahe, A. Kühnle, "Contrast inversion in non-contact atomic force microscopy imaging of C60 molecules", *Nanotechnology* **2009**, *20*, 264010.

[265] Y. Okawa *et al.*, "Controlled chain polymerisation and chemical soldering for single-molecule electronics.", *Nanoscale* **2012**, *4*, 3013–28.

[266] G. Wegner, "Polymerisation von Derivaten des 2.4-Hexadiin-1.6-diols im kristallinen Zustand", *Zeitschrift für Naturforschung* **1969**, *24 B*, 824–832.

[267] K. Fahsi *et al.*, "Stability and solid-state polymerization reactivity of imidazolyl- and benzimidazolyl-substituted diacetylenes: pivotal role of lattice water", *CrystEngComm* **2013**, *15*, 4261.

[268] W. Neumann, H. Sixl, "The mechanism of the low temperature polymerization reaction in diacetylene crystals", *Chemical Physics* **1981**, *58*, 303–312.

[269] C. Kollmar, "Electronic structure of diradical and dicarbene intermediates in short-chain polydiacetylene oligomers", *The Journal of Chemical Physics* **1993**, *98*, 7210–7228.

[270] P. C. M. Grim *et al.*, "Submolecularly Resolved Polymerization of Diacetylene Molecules on the Graphite Surface Observed with Scanning Tunneling Microscopy", *Angewandte Chemie International Edition* **1997**, *36*, 2601–2603.

[271] Y. Okawa *et al.*, "Chemical wiring and soldering toward all-molecule electronic circuitry", *Journal of the American Chemical Society* **2011**, *133*, 8227–8233.

[272] T. Takami *et al.*, "Periodic structure of a single sheet of a cloth-like macromolecule (atomic cloth) studied by scanning tunneling microscopy", *Angewandte Chemie International Edition* **1997**, *36*, 2755–2757.

[273] D. Takajo, A. Inaba, K. Sudoh, "Two-dimensional solid-state topochemical reactions of 10,12-pentacosadiyn-1-ol adsorbed on graphite", *Langmuir* **2014**, *30*, 2738–2744.

[274] Y. Okawa *et al.*, "Atomic force microscopy and theoretical investigation of the lifted-up conformation of polydiacetylene on a graphite substrate", *Soft Matter* **2008**, *4*, 1041.

[275] A. Miura *et al.*, "Light- and STM-Tip-Induced Formation of One-Dimensional and Two-Dimensional Organic", *Langmuir* **2003**, *19*, 6474–6482.

[276] O. Endo *et al.*, "Phase transition of a single sheet of sashlike polydiacetylene atomic sash on a solid surface", *Journal of the American Chemical Society* **2004**, *126*, 9894–9895.

[277] A. Richter *et al.*, "Electronic Supplementary Information (ESI) to "Diacetylene polymerization on a bulk insulator surface", *Physical Chemistry Chemical Physics* **2017**.

[278] M. A. Mueller, G. Wegner, "Photoinitiated degradation of poly(diacetylene)s in solution by random chain scission", *Makromolekulare Chemie* **1984**, *185*, 1727–1737.

[279] A. Kühnle, A. Richter, R. Bechstein, "PAMS - Planar Atomic and Molecular Scale devices", *Project Periodic Report - WP4* **2017**.

[280] C. Glaser, "Beiträge zur Kenntniss des Acetenylbenzols", *Berichte der deutschen chemischen Gesellschaft* **1869**, *2*, 422–424.

[281] P. Siemsen, R. C. Livingston, F. Diederich, "Acetylenkupplungen : eine leistungsfähige Methode für den Aufbau von Molekülen", *Angewandte Chemie* **2000**, *112*, 2740–2767.

[282] J. Eichhorn, W. M. Heckl, M. Lackinger, "On-surface polymerization of 1,4-diethynylbenzene on Cu(111).", *Chemical Communications* **2013**, *49*, 2900–2.

[283] F. Bohlmann *et al.*, "Über den Mechanismus der oxydativen Dimerisierung von Acetylenverbindungen", *Chemische Berichte* **1963**, *97*, 794–800.

[284] G. Natta, G Mazzanti, P. Corraddini, "Polimerizzazione stereospecifica dell´acetilene.", *Atti Accad. Naz. Lincei Rend. Cl. Sci. Fis. Mat. Nat.* **1958**, *25*, 3–12.

[285] J. Liu, J. W. Y. Lam, B. Z. Tang, "Acetylenic Polymers: Syntheses, Structures, and Functions", *Chemical Reviews* **2009**, *109*, 5799–5867.

[286] J. W. Y. Lam, B. Z. Tang, "Functional Polyacetylenes", *Accounts of Chemical Research* **2005**, *38*, 745–754.

[287] S. E. James C. W. Chien, *Polyacetylene - Chemistry, Physics and Material Science*, **1984**, p. 634.

[288] J. M. Njus, D. J. Sandman, "Thermal Solid State Polymerization of p-Ethynylbenzoic Acid", *Macromolecules* **2005**, *38*, 7645–7652.

[289] A. P. Melissaris, M. H. Litt, "High Modulus and High Tg Thermally Stable Polymers from Di-p-ethynylbenzoyl Ester Monomers: Synthesis, Solid State Polymerization, Processing, and Thermal Properties", *Macromolecules* **1994**, *27*, 2675–2684.

[290] L. Colazzo *et al.*, "Solid State Polymerization of Acetylene at High Pressure and Low Temperature", *Journal of Physical Chemistry A* **2000**, *104*, 8142–8145.

[291] C. I. Simionescu, V. Percec, "Polyacetylenes: Structure and Properties", *Journal of Polymer Science: Polymer Symposia* **1980**, *67*, 43–71.

[292] D. J. Sandman, J. M. Njus, B. Tran, "Approaches to Conjugated Polymers *via* New Solid State Polymerizations", *Macromolecular Symposium* **2004**, *216*, 77–85.

[293] A. P. Melissaris, M. H. Litt, "On the Polymerization of Crystalline 1,4-Diethynylnaphthalene, 2 - The Reaction Mechanism", *Macromolecular Chemistry* **1978**, *179*, 2013–2029.

[294] M. Hagihara *et al.*, "Radiation-Induced Polymerization of Crystalline Diethynylbenzene Derivatives", *Radiation Physics and Chemistry* **1986**, *28*, 165–167.

[295] G. Wegner, "Solid-State Polymerization Mechanisms", *Pure and Applied Chemistry* **1977**, *49*, 443–454.

[296] M. Bernasconi *et al.*, "Solid-State Polymerization of Acetylene under Pressure: Ab Initio Simulation", *Physical Review Letters* **1997**, *78*, 2008–2011.

[297] K. Aoki *et al.*, "Raman study of the solid-state polymerization of acetylene at high pressure", *The Journal of Chemical Physics* **1988**, *89*, 529–534.

[298] M. Nakamura *et al.*, "Photoinduced cis-to-trans isomerization of poly(2-ethynylthiophene) prepared with a [Rh(norbornadiene)Cl]$_2$ catalyst. 1H NMR, UV, and ESR studies", *Macromolecules* **2002**, *35*, 2000–2004.

[299] P. P.-S. Lee *et al.*, "Ultrasound-induced isomerization of stereoregular poly(phenylacetylene) ", *Polymer Preprints* **1999**, *40*, 659–660.

[300] C. Venturini, ""On-surface coupling reactions on calcium carbonate."", *PhD thesis* **2015**.

[301] "Computational Details: DFT calculations (T=0 K) comparable to calculations on 3-BBA)".

[302] E. Merkul, D. Urselmann, T. J. J. Müller, "Consecutive one-pot sonogashira-glaser coupling sequence- Direct preparation of symmetrical diynes by sequential Pd/Cu catalysis", *European Journal of Organic Chemistry* **2011**, 238–242.

[303] M. H. Vilhelmsen *et al.*, "The Glaser-Hay reaction: Optimization and scope based on 13C NMR kinetics experiments", *European Journal of Organic Chemistry* **2013**, *3*, 701–711.

[304] H. Matsubara *et al.*, "Synthesis of novel Fullerene Tweezers and Their Supramolecular Inclusion Complex C60", *Chemistry Letters* **1998**, 1099.

[305] J. Vandevondele *et al.*, "Quickstep: Fast and accurate density functional calculations using a mixed Gaussian and plane waves approach", *Computer Physics Communications* **2005**, *167*, 103–128.

[306] J. P. Perdew, K. Burke, M. Ernzerhof, "Generalized Gradient Approximation Made Simple", *Physical Review Letters* **1996**, *77*, 3865–3868.

[307] S. Grimme *et al.*, "A consistent and accurate ab initio parametrization of density functional dispersion correction (DFT-D) for the 94 elements H-Pu", *Journal of Chemical Physics* **2010**, *132*, 154104.

[308] B. G. Lippert, J. H. Parrinello, Michele, "A hybrid Gaussian and plane wave density functional scheme", *Molecular Physics* **1997**, *92*, 477–488.

[309] S. Goedecker, M. Teter, J. Hutter, "Separable Dual-Space Gaussian Pseudopotentials", *Physical Review B* **1996**, *54*, 1703–1710.

[310] J. VandeVondele, J. Hutter, "Gaussian basis sets for accurate calculations on molecular systems in gas and condensed phases", *Journal of Chemical Physics* **2007**, *127*, 114105.

List of Figures

List of Tables

List of Acronyms

2D-FFT two-dimensional fast Fourier transform

AFM atomic force microscope

AM amplitude modulation

3-BBA 3,3′-(1,3-butadiyne-1,4-diyl)bisbenzoic acid

3-EBA 3-ethynylbenzoic acid

4-EBA 4-ethynylbenzoic acid

4-BBA 4,4′-(1,3-butadiyne-1,4-diyl)bisbenzoic acid

BPDCA biphenyl-4,4′-dicarboxylic acid

CE-FM constant excitation frequency modulation

DETDCA 4,4′′-diethynyl-[1,1′:4′,1′′-terphenyl]-2′,5′-dicarboxylic acid

DFT density functional theory

DHBA 2,5-dihydroxybenzoic acid

DIBA 2,5-diiodobenzoic acid

DISA 3,5-diiodosalicylic acid

FM frequency modulation

FM-AFM frequency-modulation atomic force microscopy

FPMD first-principles molecular dynamics

HOPG highly oriented pyrolytic graphite

IBA 4-iodobenzoic acid

ICPs intrinsically conducting polymers

KPFM Kelvin probe force microscopy

MBE molecular beam epitaxy

MD molecular dynamic

MFM magnetic force microscopy

ML monolayer

NSOM near-field scanning optical microscopy

OSS on-surface synthesis

PAMS Planar Atomic and Molecular Scale devices

PBN pyrolytic boron nitride

PLL phase-locked loop

PM phase modulation

PREP preparation chamber

PSD position sensitive detector

QCM quartz-controlled micro-balance

RT room temperature

SPM scanning probe microscopy

STM scanning tunneling microscopy

TC	thermo couple
TEB	1,3,5-triethynyl-benzene
NTCN	2,3,6,7-naphtalene tetra carbonitrile
UHV	ultra-high vacuum
UV	ultraviolet
VT-AFM	variable temperature atomic force microscope

Publication list

- **Theoretical Study of Twin Polymerization - From Chemical Reactivity to Structure Formation**
  A. A. Auer, A. Richter, A. V. Berezkin, D. V. Guseva and S. Spange
  Macromol. Theory Simul. **21**, 615 (2012)

- **Diacetylene polymerization on a bulk insulator surface**
  A. Richter, V. Haapasilta, C. Venturini, R. Bechstein, A. Gourdon, A. Foster and A. Kühnle
  Phys. Chem. Chem. Phys. **19**, 15172 (2017)

- **Homocoupling of Terminal Alkynes on Calcite (10.4)**
  A. Richter, M. Vilas-Varela, D. Peña, R. Bechstein, A. Kühnle
  Surface Science (2017)

- **Generic Nature of Long-Range Repulsion Mechanism on a Bulk Insulator?**
  J. L. Neff, A. Richter, H. Söngen, C. Venturini, A. Gourdon, R. Bechstein, A. Kühnle
  Faraday Discuss. **204**, 419 (2017)

- **Reversible and Efficient Light-Induced Molecular Switching on an Insulator Surface**
  S. Jaekel, A. Richter, R. Lindner, R. Bechstein, C. Nacci, S. Hecht, A. Kühnle, and L. Grill.
  Faraday Discuss. **12**, 1821 (2018)

- **On-surface synthesis on a bulk insulator surface**
  A. Richter, A. Floris, R. Bechstein, L. Kantorovich and A. Kühnle
  J. Phys.: Condens. Matter **30**, 133001 (2018)

- **Acetylene polymerization on a bulk insulator surface**
  A. Richter, T. Rahman, V. Haapasilta, C. Venturini, R. Bechstein, A. Gourdon, A. Foster and A. Kühnle
  in preparation

Talks

(presenting author underlined)

- **On-Surface Coupling of Alkynes on the (10.4) Surface of Calcite**
  A. Richter, R. Lindner and A. Kühnle
  (PAMS - Project Meeting 2016, Mainz, Germany)

- **On-Surface Preparation of Molecular Devices**
  A. Richter, R. Lindner and A. Kühnle
  (PAMS - Second Review Meeting 2015, Brussels, Belgium)

- **On-Surface Coupling of Alkynes on the (10.4) Surface of Calcite**
  A. Richter, R. Lindner, R. Bechstein and A. Kühnle
  (On Surface Synthesis Workshop 2016, San Sebastián, Spain)

- **Progress in on-Surface Synthesis on Calcite (10.4)**
  A. Richter, J. Enns, J. Neff, R. Lindner, T. Rahman and A. Kühnle
  (PAMS-Project Meeting 2017, Kraków, Poland)

Poster Presentations

(presenting author underlined)

- **Diacetylene Polymerization on a Bulk Insulator Surface**
  A. Richter, T. Rahman, V. Haapasilta, C. Venturini, R. Bechstein, A. Gourdon, A. S. Foster and A. Kühnle
  (Zürich Instruments Users Meeting 2017, Mainz, Germany)

Acknowledgement

An dieser Stelle möchte ich allen danken, die zum Gelingen der Arbeit beigetragen haben.

Mein besonderer Dank gilt

- ... [redacted] für die Möglichkeit in einem hervorragend ausgestattetem Arbeitskreis meine Doktorarbeit machen zu dürfen, für stete Diskussionsbereitschaft und sehr hilfreiche Korrekturvorschläge zu dieser Arbeit.
- ... [redacted] für die Übernahme des Zweitgutachtens.
- ... [redacted] für die freundliche und unkomplizierte Übernahme des Prüfungsvorsitz.

Außerdem möchte ich hervorheben

- ... [redacted] für die ausführlichen Besprechungen von Messungen und Hilfe bei Problemen, sowie eine unkomplizierte Zusammenarbeit.
- ... [redacted] für die ausführliche Einarbeitung, viele hilfreiche Diskussionen und die angenehme Büroatmosphäre
- ... [redacted] für die nützlichen Programme zur Driftkorrektur und fr die Sublimationsversuche an der MBE-Kammer ohne die die Messung der zahlreichen Moleküle nicht möglich gewesen wäre, viele hilfreiche Diskussionen und seine LaTeX-Vorlage, mit der diese Doktorarbeit verfasst wurde.
- ... [redacted] für die Rettung mancher Probenhalter, die angenehme Büroatmosphäre und immer ein offenes Ohr bei UHV-Problemen.
- ... [redacted] für viele hilfreichen Diskussionen, das Korrekturlesen der Arbeit, die tollen Wandertips und seine positive Einstellung.

- ... [redacted] für erheiternde und witzige Kommentare und die Protokollführung.
- ... [redacted] für die Hilfe bei Technikfragen und PC-Problemen.

und natürlich auch

- ... [redacted] für interessante Gespräche, Hilfe bei Messwidrigkeiten und ein schönes Arbeitsgruppenklima.

Großer Dank gilt ebenfalls

- ... [redacted] insbesondere [redacted] für die Erstellung der DSC Daten und [redacted] für die Hilfe bei den TGA-Messungen.

Of course, I want to thank our collaborators, especially

- ... [redacted] for interesting discussions, the nice and straightforward collaboration of the 3-BBA and 3-EBA project and the fast sending of xyz-files and other images of the DFT calculations.
- ... [redacted] for inspiring discussions of molecular reactions, the fast synthesis and sending of new molecules and the measurement of TGA and DSC data.
- ... [redacted] for fruitful discussions and the synthesis of 3-BBA, 3-EBA and 4-EBA.

Ganz besonderer Dank gilt

- ... [redacted] für die großartige Unterstützung, die Geduld und das Korrekturlesen dieser Arbeit.
- ... [redacted] für die Unterstützung in allen Lebenslagen.
- ... [redacted] für die amüsanten Zeiten jenseits des UHV-Tellerrandes.

Finally, I want to thank the programmers of the free software used in this thesis, especially the developers of *Gwyddion* and *Inkscape*.

Curriculum vitae

Antje Richter
born on January 14th 1987 in Karl-Marx-Stadt

Academic education

1/2015	-	**6/2018**	Doctoral studies supervised by Prof. Dr. Angelika Kühnle Johannes Gutenberg University Mainz
		8/2010	Graduation with degree "Diplom Chemikerin" Diploma thesis supervised by Jun.-Prof. Dr. A. A. Auer and Prof. S. Spange
2005	-	**2010**	Studies of chemistry Chemnitz University of Technology

Professional Experience

1/2011	-	**12/2014**	Atotech Deutschland GmbH development engineer

School Education

2000	-	**2005**	Carl von Bach Gymnasium, Stollberg (Sachsen)
1997	-	**2000**	Werner-Heisenberg-Gymnasium, Chemnitz

Colophon

This thesis was typeset with LaTeX 2_ε. It uses the *Clean Thesis* style developed by Ricardo Langner. The design of the *Clean Thesis* style is inspired by user guide documents from Apple Inc.

Download the *Clean Thesis* style at `http://cleanthesis.der-ric.de/`.